1 **Progress in understanding of Indian Ocean circulation, variability, air-sea exchange and impacts on biogeochemistry**

2 Helen E. Phillips[1,2], Amit Tandon[3], Ryo Furue[4], Raleigh Hood[5], Caroline Ummenhofer[6,7], Jessica Benthuysen[8], Viviane

3 Menezes[6], Shijian Hu[9], Ben Webber[10], Alejandra Sanchez-Franks[11], Deepak Cherian[12], Emily Shroyer[13], Ming Feng[14,15],

4 Hemantha Wijeskera[16], Abhisek Chatterjee[17], Lisan Yu[6], Juliet Hermes[18], Raghu Murtugudde[19], Tomoki Tozuka[20,4],

5 Danielle Su[21], Arvind Singh[22], Luca Centurioni[23], Satya Prakash[17], Jerry Wiggert[24]

7 [1]Institute for Marine and Antarctic Studies, University of Tasmania, Hobart, 7005, Australia

8 [2]Australian Antarctic Program Partnership, University of Tasmania, Hobart, 7005, Australia

9 [3]Department of Mechanical Engineering, College of Engineering, University of Massachusetts Dartmouth, 02747, USA

10 [4]APL/JAMSTEC, Yokohama, Japan

11 [5]University of Maryland Center for Environmental Science, Horn Point Laboratory, Cambridge, 21613, USA

12 [6]Department of Physical Oceanography, Woods Hole Oceanographic Institution, Woods Hole, 02543, USA

13 [7]ARC Centre of Excellence for Climate Extremes, University of New South Wales, Sydney, Australia

14 [8]Australian Institute of Marine Science, Indian Ocean Marine Research Centre, Crawley, Australia

15 [9]Institute of Oceanology, Chinese Academy of Sciences, Qingdao, China

16 [10]School of Environmental Sciences, University of East Anglia, Norwich, NR4 7TJ, UK

17 [11]National Oceanography Centre, Southampton, UK

18 [12]National Center for Atmospheric Research, Boulder, USA

19 [13]College of Earth, Ocean and Atmospheric Sciences, Oregon State University, Corvallis, 97331, USA

20 [14]CSIRO Oceans and Atmosphere, Indian Ocean Marine Research Centre, Crawley, Australia

21 [15]Centre for Southern Hemisphere Oceans Research, Hobart, Australia

22 [16]U.S. Naval Research Laboratory, Washington, 20032, USA

23 [17]Indian National Centre for Ocean Information Services, Ministry of Earth Sciences, Hyderabad, India

24 [18]South African Environmental Observation Network, Cape Town, South Africa

25 [19]Department of Atmospheric and Oceanic Science, University of Maryland, College Park, 20742, USA

26 [20]Department of Earth and Planetary Science, Graduate School of Science, The University of Tokyo, Tokyo, Japan

27 [21]Sorbonne Universités, UPMC Université Paris 06, CNRS, UMR 7159 LOCEAN-IPSL, Paris, France

28 [22]Physical Research Laboratory, Ahmedabad, India

29 [23]Scripps Institution of Oceanography, University of California San Diego, La Jolla, 92093, USA

30 [24]University of Southern Mississippi, Hattiesburg, 399406, USA

33   *Correspondence to*: Helen E. Phillips (h.e.phillips@utas.edu.au)

36   **Abstract.** Over the past decade, our understanding of the Indian Ocean has advanced through concerted efforts toward

37   measuring the ocean circulation and its water properties, detecting changes in water masses, and linking physical processes

38   to ecologically important variables. New circulation pathways and mechanisms have been discovered, which control

39   atmospheric and oceanic mean state and variability. This review brings together new understanding of the ocean-atmosphere

40   system in the Indian Ocean since the last comprehensive review, describing the Indian Ocean circulation patterns, air-sea

41   interactions and climate variability. The second International Indian Ocean Expedition (IIOE-2) and related efforts have

42   motivated the application of new technologies to deliver higher-resolution observations and models of Indian Ocean

43   processes. As a result we are discovering the importance of small scale processes in setting the large-scale gradients and

44   circulation, interactions between physical and biogeochemical processes, interactions between boundary currents and the

45   interior, and between the surface and the deep ocean. In the last decade we have seen rapid warming of the Indian Ocean

46   overlaid with extremes in the form of marine heatwaves. These events have motivated studies that have delivered new

47   insight into the variability in ocean heat content and exchanges in the Indian Ocean, and climate variability on interannual

48   to decadal timescales.This synthesis paper reviews the advances in these areas in the last decade.

1. Introduction

49   **1. Introduction**

50   The physical processes taking place in the Indian Ocean and overlying atmosphere underpin the variability evident in

51   monsoons, extreme events, marine biogeochemical cycles, ecosystems, and ultimately human experience. The Indian Ocean

52   rim countries, accounting for one third of the Earth's human population, depend on this ocean for food and resources, and

53   are dramatically impacted by its variability (Hermes et al., 2019). Increasing our understanding of interactions between

54   geologic, oceanic and atmospheric processes that control the complex physical dynamics of the Indian Ocean region is a

55   priority for the second International Indian Ocean Expedition (IIOE-2). The questions about the Indian Ocean circulation,

56   climate variability and change that IIOE-2 seeks to address are: 1) how have the atmospheric and oceanic circulation of the

57   Indian Ocean changed in the past and how will they change in the future; 2) how do these changes relate to topography and

58   connectivity with the Pacific, Atlantic and Southern oceans; and 3) what impact does the circulation, variability, and change

59   have on biological productivity and fisheries.

60   This focus on the Indian Ocean has motivated new international efforts in field campaigns and modelling studies, and

61   leveraged advances in global observations that contribute to the Indian Ocean Observing System (IndOOS; Beal et al.,

2020). The Argo profiling float array (Roemmich et al., 2012) reached full coverage in the Indian Ocean in 2006, the RAMA moored buoy array (McPhaden et al., 2009) has now delivered multi-year time series of tropical oceanic and atmospheric variability, with some sites dating back to 2000. Satellite observing continues to provide observations vital to interpreting spatial and temporal variability in the *in situ* observations, and new technology is now enabling high resolution observations of boundary current variability and small scale processes. Thus, since the reviews of Schott and McCreary (2001) and Schott et al. (2009), the spatial coverage of observations and length of time series have increased substantially such that the signals of many previously unresolved processes are now able to be observed.

These new higher-resolution observations and companion improvements in model simulations have highlighted the importance of small scale processes in setting the large-scale gradients and circulation, interactions between physical and biogeochemical processes, interactions between boundary currents and the interior, and between the surface and the deep ocean. Overlaid on these interior Indian Ocean processes, ocean warming due to increasing greenhouse gas concentrations has been shown to be pervasive and relentless (Wijffels et al., 2016), and extending to abyssal depths (Johnson et al., 2008a; Desbruyeres et al., 2017). The Indian Ocean plays a key role in the global climate system, enabling upwelling of the Meridional Overturning Circulation lower cell through strong diffusive mixing (Lumpkin and Speer, 2007; MacDonald et al., 2009; Talley, 2013) and exporting the largest poleward heat flux of all Southern Hemisphere basins (Roxy et al., 2014). In recent decades, the upper 700 m of the entire Indian Ocean has warmed rapidly (Desbruyères et al, 2017) . In the southern Indian Ocean, the warming was directly linked primarily to heat advection from a strengthened ITF and, secondarily, to a decrease in mean air-sea flux cooling (Li et al., 2017b; Zhang et al., 2018a). This coupling shifted the balance of global warming between the ocean and atmosphere, accelerating ocean warming and causing a hiatus in the warming of Earth's surface atmosphere (Section 6). Marine heatwaves have emerged as an increasing threat to marine ecosystems as ocean temperatures warm (e.g. Oliver et al., 2018). Increasingly vulnerable populations need more reliable monsoon predictions, a task complicated by variability across timescales from intraseasonal to interannual, decadal and beyond in a tightly coupled ocean-atmosphere system (Hazra et al., 2017).

The starting point for this synthesis report are the reviews by Schott and McCreary (2001) and Schott et al. (2009), describing the circulation patterns, air-sea interactions and climate variability on timescales from intraseasonal to interannual, and relatively large spatial scales. We begin with a description of the large scale setting that has been well established since Schott et al. (2009) (Section 2). We then consider the structure and propagation of variability in air-sea interactions at seasonal and intra-seasonal scales, including the contribution of the mesoscale and the ocean's role in air-sea interaction (Section 3).

Section 4 discusses new advances in understanding of the upper ocean circulation, organised by region (southern basin, equatorial and northern basin). This section includes an update of the near-surface circulation maps of Talley et al. (2011),

96   including recent work on boundary currents around Australia and Madagascar, and a discussion of the biogeochemical
97   variability observed in each region. The interocean connections with the Pacific, Atlantic and Southern Oceans are discussed
98   in Section 5. Section 6 describes the variability of the Indian Ocean circulation with the recent advances in understanding
99   the warming across the basin, climate modes - such as the Indian Ocean Dipole, connection with the El Nino-Southern
100 Oscillation (ENSO), and Indian ocean marine heatwaves (Section 6.4). Section 7 focuses on multiscale processes in the Bay
101 of Bengal as an "ocean laboratory", since there have been multiple international programs in this Bay in the last decade.
102 Recent advances from the large scales (>100 km) down to sub-mesoscales (100 m to 10 km) and further down to mixing
103 scales (mm) are discussed. We then link back from mixing to large scales via salinity budgets and coupled phenomena such
104 as the Madden-Julian Oscillation (MJO) to understand the complexity of these processes across multiple scales. We end
105 with a short summary and open questions that will need to be addressed over the next decade.

106 **2 Large-scale setting**

107 The oceanic and atmospheric circulation of the Indian Ocean are unlike those in the Pacific and Atlantic oceans, largely due
108 to geography. The Asian landmass limits the northern extent of the Indian Ocean to around 25°N so that there is no high-
109 latitude cooling of the ocean, and consequently no dense water formation such as that seen in the North Atlantic and, to
110 some extent, the North Pacific. The intense seasonal variation in temperature over Asia drives the seasonal monsoons: the
111 southwest monsoon in boreal summer, and northeast monsoon in boreal winter. The timing of the onset of the monsoon, and
112 associated wet and dry periods in the Indian Ocean rim countries, varies considerably depending on a range of large-scale
113 climate modes and smaller-scale coupled ocean-atmosphere interactions. The seasonally-reversing winds drive seasonally-
114 reversing ocean currents in the northern Indian Ocean (Section 4.4), e.g. the southwest/northeast monsoon current and the
115 Somali Current. Equatorial currents in the Indian Ocean, eastward near the surface above westward undercurrents (Section
116 4.3), provide rapid connection between the western and eastern basin and are also subject to monsoon dynamics.

117 In the southern Indian Ocean (Section 4.2), the connection of the Indian and Pacific Oceans through the Indonesian Seas
118 also contributes to the unique circulation patterns. The very warm and fresh ITF water is funneled into the tropical southern
119 Indian Ocean and carried westward by the South Equatorial Current. The warm, fresh waters are much lighter than those
120 further south, creating a north-south density (pressure) gradient that drives near-surface broad, eastward geostrophic currents
121 between 16°S and 32°S and between Madagascar and Australia (Niiler et al., 2003). This pressure gradient also generates
122 the Leeuwin Current, a unique poleward-flowing eastern boundary current (Godfrey and Ridgway, 1985) that is a
123 downwelling region but is also, counter-intuitively, highly productive (Waite et al., 2007). These two features are not found
124 in the southeastern Atlantic and Pacific oceans. There, the eastern basin currents are characterised by a clear subtropical
125 gyre circulation with weak, equatorward flow and upwelling against the coast.

126   The tropical Indian Ocean (Section 4.3) is home to the largest fraction of sea surface temperature (SST) warmer than 28°C

127   (the tropical warm pool), and is therefore a key region for deep atmospheric convection: the upward part of the Walker

128   Circulation that drives cloud formation and precipitation over the tropical Indo-Pacific. Variation in SST is the primary

129   driver of variation in exchanges between the ocean and atmosphere and is thus a key focus in this paper. Sea surface salinity

130   effects on ocean-atmosphere exchanges have become better understood and are discussed throughout and in particular in

131   Section 7.

132   The tropical Indian Ocean sea surface temperature (SST) has warmed faster over the period 1950–2010 than either the

133   tropical Pacific or Atlantic (Han et al., 2014). Most of this warming (1.2°C over 1901–2012) has occurred in the western

134   Indian Ocean, which has been the largest contributor to the overall global SST trend, with implications for primary

135   productivity (Roxy et al., 2014, 2016). The Indian Ocean accounts for 50-70% of the total anthropogenic warming in the

136   global upper (700 m) ocean, (Lee et al., 2015; Desbruyères et al., 2017). The deeper ocean (700-2000 m) is warming across

137   the globe with a robust signature of anthropogenic warming evident even in the short Argo record since 2005 (Wijffels et

138   al. 2016, Rathore et al. 2020). Warming in the abyss is detectable and widespread, communicated from the surface of the

139   ocean along pathways from Antarctic Bottom Water formation regions (Purkey and Johnson, 2012). Considerable variability

140   in the Indian Ocean climate system exists on the backdrop of this strong, long-term warming trend.

141   Variability in the oceanic and atmospheric circulation of the Indian Ocean is the result of complex interactions that are both

142   internal and external to the Indian Ocean. The recent review of the IndOOS plan (Beal et al., 2020) summarises the major

143   scientific drivers, of which we still have limited understanding (Fig. 1). Anthropogenic climate change causes a background

144   trend of ocean warming and increasing acidity due to uptake of heat and carbon dioxide and affects the nature of large and

145   small scale variability mechanisms.

146
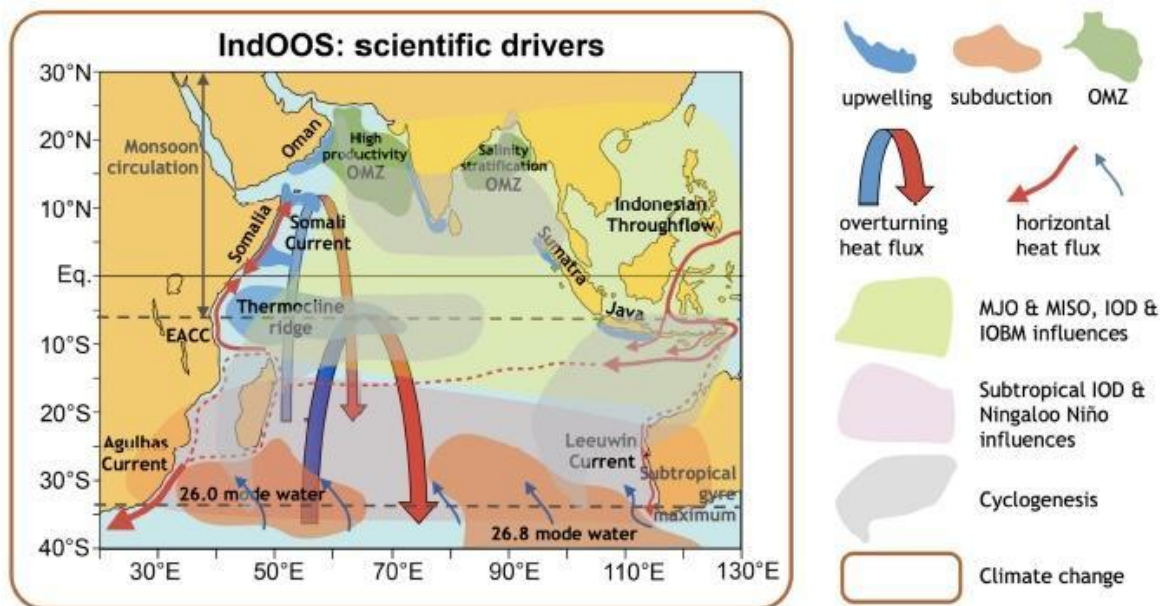
**Figure 1: Schematic view of key phenomena in the Indian Ocean (from Hermes et al. 2019). The main scientific
drivers of the Indian Ocean Observing System, including the Oxygen Minimum Zones (OMZs), upwelling and
subduction zones, major heat flux components, the tropical modes of the Madden-Julian Oscillation (MJO), the
Monsoon Intra-Seasonal Oscillation (MISO), the Indian Ocean Dipole (IOD) and Indian Ocean Basin Mode (IOBM),
the subtropical modes of Ningaloo Niño and subtropical IOD, cyclogenesis, and climate change.**

A net poleward flow of heat out of the Indian Ocean is accomplished by a combination of the horizontal circulation along
the boundaries, coupled with the vertical meridional overturning circulation (MOC). The ITF delivers heat from the Pacific
into the Indian Ocean. The Agulhas Current moves heat rapidly southward at surface and intermediate depths (Bryden and
Beal, 2001), with 30% of Indian Ocean heat export thought to be carried across 32°S by this gyre circulation (Talley, 2008).
The shallow Leeuwin Current makes a smaller direct contribution to the poleward flow of heat (Smith et al., 1991; Feng et
al., 2003; Furue et al., 2017) but generates a rich field of mesoscale eddies that carry heat and momentum into the Indian
Ocean interior, contributing to heat export across 32°S (Domingues et al. 2006, Feng et al., 2007; Dilmahamod et al. 2018).

At intermediate depths (500-2000 m), mode waters of varying density enter the Indian Ocean from the Southern Ocean.
Along their northward path they mix with lighter waters above, progressively upwelling to the sea surface in a range of
locations north of 10°S to then return south in a widespread southward Ekman transport of near-surface waters (Schott et
al., 2009). The lower part of the mode water layer mixes with denser waters below and joins the southward flowing deep
waters (2000-4000 m). This southward flow also has a contribution from transformed abyssal waters: Antarctic Bottom
Water moves northward at abyssal depths, mixing with lighter waters above, progressively upwelling along its path from

165 the Southern Ocean to the Indian Ocean to return southward at shallower depths (Talley, 2013). Cross-equatorial flow is

166 accomplished both at abyssal levels and via the East Africa Coastal Current, seasonally reversing Somali Current and broad

167 southward flow near the surface (Schott et al. 2009).

168 The remaining elements of Fig. 1 refer to oxygen minimum zones (OMZ) in the Arabian Sea and Bay of Bengal and the

169 range of mechanisms that drive strong variations in sea surface temperature leading to shifts in atmospheric convection and

170 precipitation with major effects on rim countries. These mechanisms include: Madden-Julian oscillation (MJO) and

171 Monsoon Intraseasonal Oscillation (MISO), Indian Ocean Dipole (IOD), Indian Ocean Basin Mode, Subtropical IOD, and

172 Ningaloo Niño which are discussed further in Section 7. Cyclogenesis is not discussed in this synthesis.

173 Extreme precipitation in the Bay of Bengal and evaporation in the Red Sea and Arabian Sea lead to strong variability in

174 ocean salinity that in turn impacts ocean circulation and air-sea interaction. The surface salinity gradient in the northern

175 Indian Ocean decreases from the Arabian Sea in the west to the Bay of Bengal in the east. Strong evaporation over the

176 Arabian Sea results in highly saline surface waters (Antonov et al., 2010; Chaterjee et al., 2012), while surface waters in the

177 Bay of Bengal are comparatively fresh and highly stratified as a result of monsoon precipitation and outflow from river

178 systems such as the Ganges-Brahmaputra (Shetye et al., 1996; Vinayachandran et al., 2002). The surface forcing is balanced

179 by the seasonally reversing monsoon currents to maintain the climatological distribution of salinity.

180 **3 Air-sea interactions**

181 The tropical Indian Ocean is highly variable across multiple scales, from intense tropical cyclones to decadal modes of

182 variability and strong warming due to climate change. Variability at all scales involves a degree of atmosphere-ocean

183 interaction, such as locally intense heat and moisture fluxes driven by cyclones, large-scale convection in the ascending

184 branch of the Hadley circulation, and basin scale ocean heat transport carried by overturning cells that contribute to decadal

185 variability and trends. At intermediate time scales, the intraseasonal oscillations involve strong air-sea coupling (e.g., Demott

186 et al., 2015). The Indian Ocean Dipole (IOD) is an example of an inherently coupled mode of variability (Saji et al., 1999,

187 Webster et al. 1999, Murtugudde et al. 2000). The monsoonal rainfall around the Indian Ocean is largely fuelled by warm

188 SSTs and strong sea-to-air moisture fluxes. These phenomena emphasise the need to understand the mechanisms of air-sea

189 interaction within the Indian Ocean, with a particular focus on how these processes can be better represented in models to

190 aid predictions of variability in the Earth system.

191 **3.1 Seasonal cycle and the monsoons**

192 In the open ocean south of 10°S, the wind pattern throughout the year is southeasterly trade winds across the tropics and

193 subtropics and westerlies south of 35°S (Fig. 2). The evaporative cooling of the ocean surface by the trade winds leads to

194 high salinity throughout the subtropics.The curl of the wind stress drives year-round Ekman pumping (downwelling) south

195 of around 15°S (Fig. 2). Downwelling of these denser, high salinity surface waters supplies the downward limb of a shallow

196 overturning circulation (Schott et al., 2002; Schott et al., 2009; Lee 2004). The subsurface path of the shallow overturning

197 is not well known, and the return to the surface is in any of a number of upwelling zones including the Seychelles-Chagos

198 Thermocline Ridge, along Somalia and Oman and the west coast of India. North of around 10°S, the winds over the Indian

199 Ocean are characterised by seasonal reversals due to the monsoons (Fig. 2), which in turn cause most of the near-surface

200 currents in these regions to seasonally reverse (Schott et al., 2009; Shankar et al., 2002, Section 4.4).
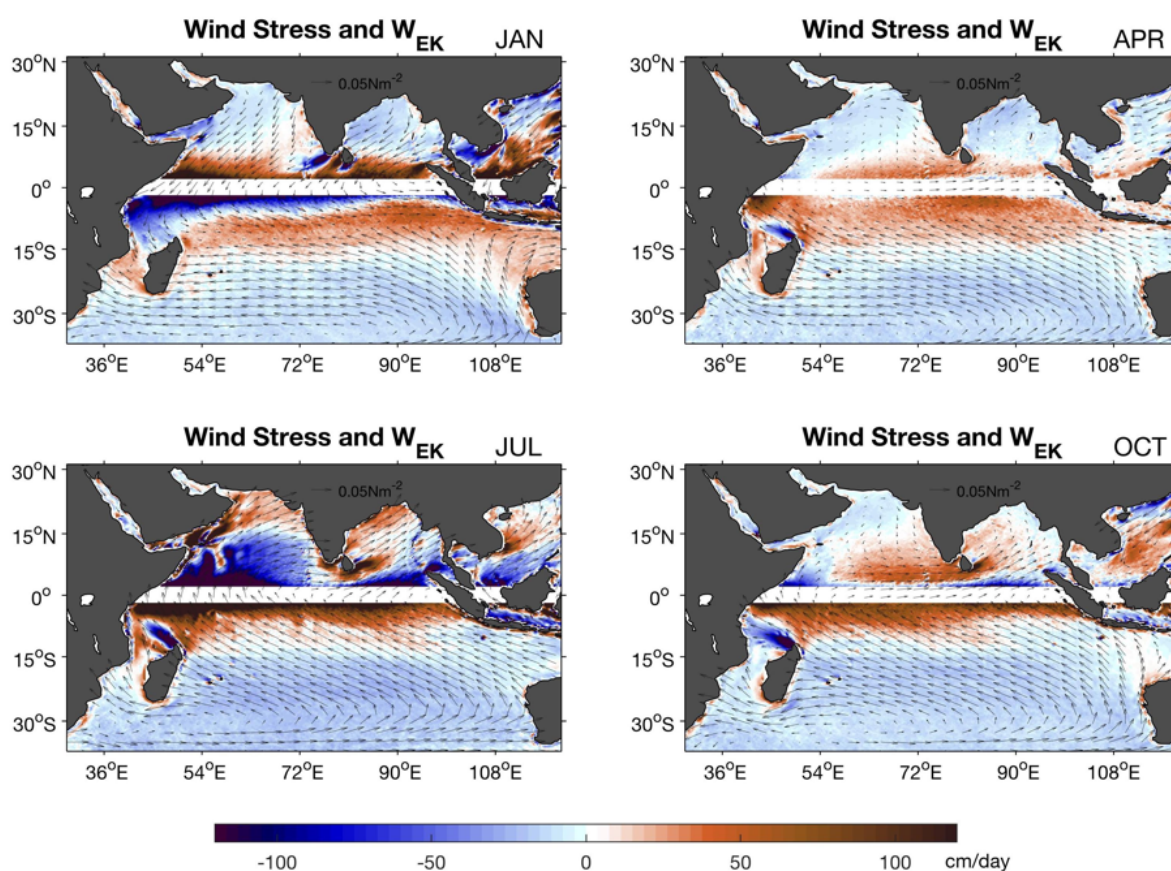
201

202 **Figure 2: Climatology (2001–2018) of monsoon wind stress (vectors) and Ekman pumping rate (colour shaded) with**

203 **positive values denoting Ekman suction (upwelling) and negative values Ekman pumping (downwelling) for (a)**

204 **January - NE monsoon, (b) April, (c) July - SW monsoon, and (d) October. The climatology was constructed by the**

205 **Objectively Analyzed air-sea Flux High-Resolution (OAFlux-HR) analysis (adapted from Yu 2019).**

206 A strong positive correlation between seasonal net heat fluxes into the ocean and SST variability (Fig. 3) suggests that the

207 seasonal cycle of SST is largely due to the seasonal cycle of winds and cloud cover (Yu et al., 2007). One prominent

208   exception is the Seychelles-Chagos thermocline ridge (located between 5°S and 10°S and east of 50°E), where upwelling
209   and horizontal advection exhibit substantial seasonal variations that in turn contribute to the seasonal cycle of SST (Hermes
210   and Reason, 2008; Foltz et al., 2010). On the equator and to the north, seasonally reversing winds drive complex patterns of
211   upwelling and downwelling that lead to complex SST variability.
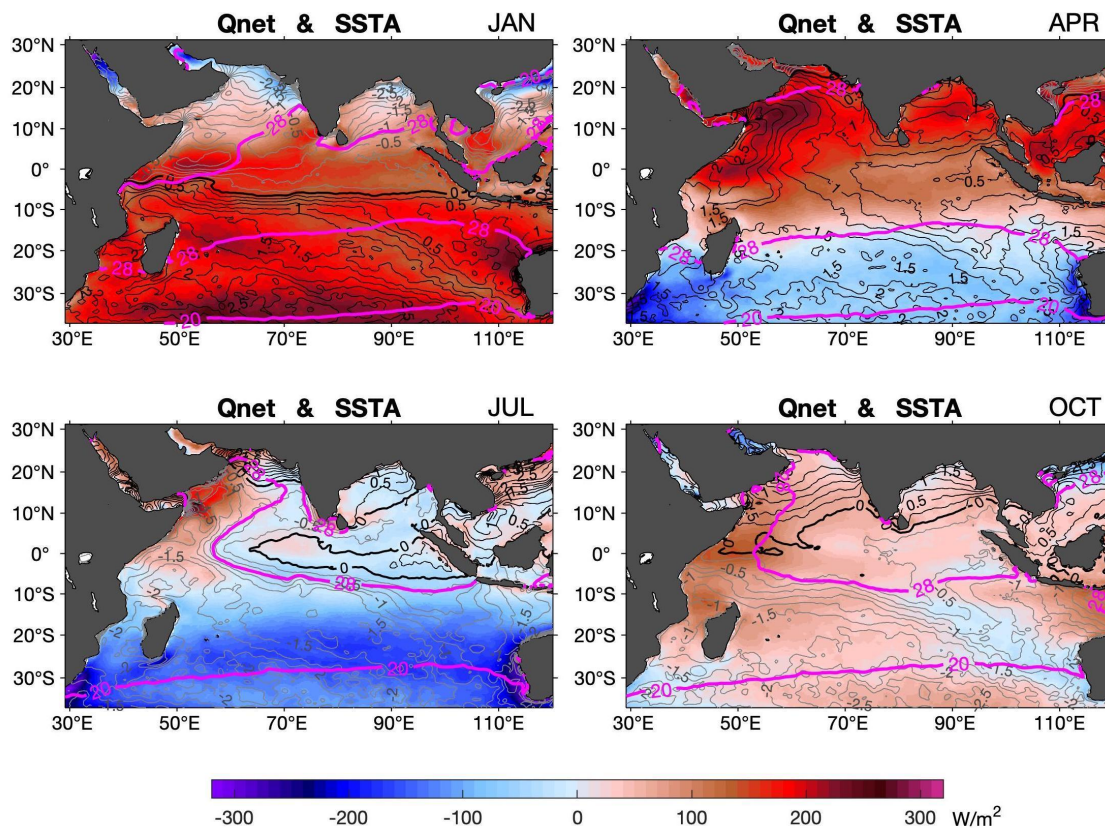
212

213   **Figure 3: Climatology (2001–2018) of ocean-surface net heat input (colour shaded; positive values denote ocean heat**
214   **gain and negative values ocean heat loss), SST anomaly (black contours) and 20°C, 28°C SST contours (pink) for (a)**
215   **January - NE monsoon, (b) April, (c) July - SW monsoon, and (d) October (adapted from Yu 2019). Net heat flux is**
216   **the sum of solar radiation, longwave radiation, and turbulent latent and sensible heat fluxes. The turbulent heat flux**
217   **climatology was constructed by the OAFlux-HR analysis and surface radiation climatology by the NASA CERES**
218   **EBAF (Kato et al., 2013).**

219   In the Bay of Bengal, surface heat fluxes dominate the seasonal cycle of SST, yet subsurface processes including barrier
220   layers created by the relatively strong salinity stratification compared to the weaker thermal stratification, vertical
221   entrainment causing warming and cooling of the mixed layer, variations in the depth of penetration of solar radiation and
222   zonal advection all contribute significantly to SST variability (Thangaprakash et al., 2016). In the Arabian Sea, surface heat

223   fluxes again dominate the variability in SST, with the exception of the upwelling zone along the western boundary
224   (Chowdary et al., 2015; Yu et al., 2007).

225   The variability in rainfall driven by the monsoons also creates near-surface salinity variability, most notably in the Bay of
226   Bengal where there is a pronounced annual cycle of sea surface salinity (SSS; Fig. 4, Akhil et al., 2014). Freshwater input
227   at the northern end of the Bay forms a shallow mixed layer stratified by low salinity and is advected southwards along the
228   east coast of India, where it is eventually eroded by vertical mixing (Akhil et al., 2014). The variability in freshwater input
229   contributes to the seasonal cycle of barrier layer thickness in the Bay of Bengal (Howden and Murtugudde, 2001; Thadathil
230   et al., 2007), which in turn modulates how strongly SST responds to surface forcing (Li et al., 2017). The seasonally
231   reversing currents that connect the salty Arabian Sea and fresh Bay of Bengal also strongly influence sea surface salinity
232   patterns (Section 4.1.3).
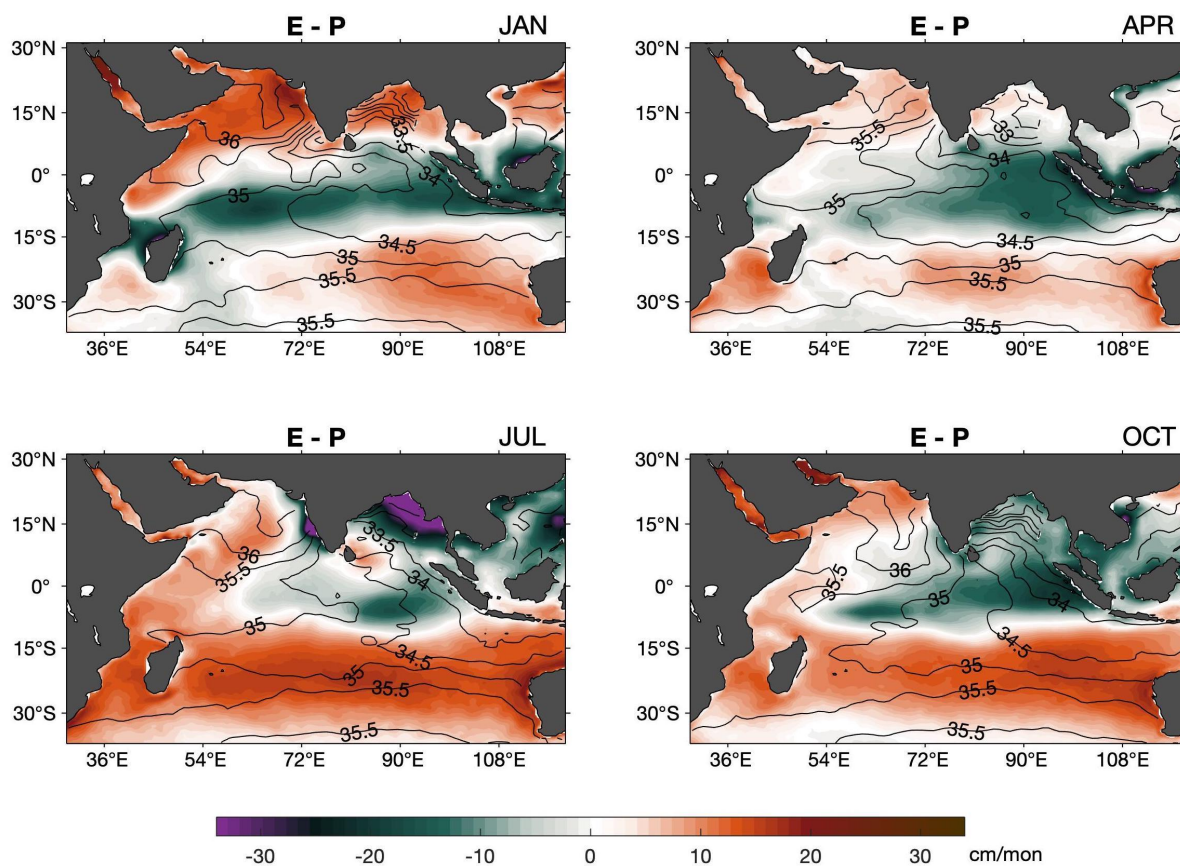
233

234   **Figure 4: Climatology (2001–2018) of evaporation minus precipitation (colour shaded; positive values denote**
235   **freshwater leaving the ocean and negative values addition of fresh water to the ocean) and sea surface salinity (black**
236   **contours) for (a) January - NE monsoon, (b) April, (c) July - SW monsoon, and (d) October (adapted from Yu 2019).**

237   The seasonal cycles in the atmosphere and ocean circulation strongly influence the biological productivity of the near-
238   surface Indian Ocean (Wiggert et al. 2006). Fig. 5 shows the seasonal cycle of satellite chlorophyll *a* and surface currents.
239   The dramatically low productivity in the subtropics, where wind stress curl drives large-scale downwelling (Fig. 2), and
240   highly productive coastal boundaries where wind-driven upwelling occurs, highlights the impact of the circulation and
241   atmosphere-ocean interaction on biological productivity. In turn, the chlorophyll *a* distribution has important implications
242   for air-sea interaction, since higher concentrations of phytoplankton lead to increased absorption of solar radiation (e.g.,
243   Morel and Antoine, 1994; Murtugudde et al. 2002). Organisation of chlorophyll *a* at intraseasonal timescales has also been
244   reported (Section 3.2.1).
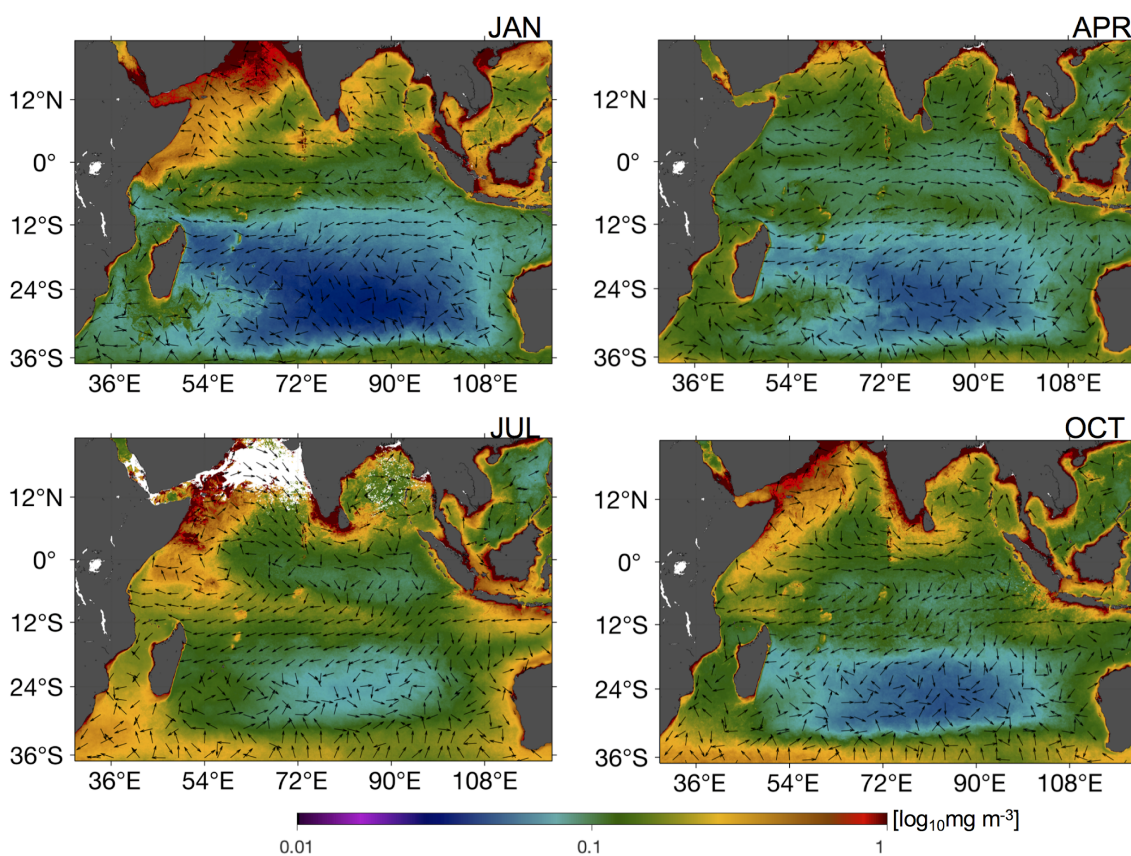
245

246   **Figure 5: Climatology (2002-2018) of chlorophyll-a concentrations (colourmap) and current velocities (arrows) for**
247   **(a) January (b) April (c) July (d) October. Chlorophyll a climatology was obtained from the MODIS-Aqua product**
248   **and current velocities were obtained from the third-degree Ocean Surface Current Analysis Real-time (OSCAR)**
249   **product.**

3.2 Intraseasonal air-sea interaction

3.2.1 Madden-Julian Oscillation - MJO

The Madden-Julian Oscillation (MJO; Madden and Julian, 1972, 1971) is the dominant mode of variability in the Indian Ocean at subseasonal time scales. The MJO (Fig. 6) is characterised by eastward-propagating features of enhanced and reduced convection over distances of more than 10,000 km and with a periodicity of around 30–60 days (Zhang, 2005). The MJO propagates slowly (~5 m s^{-1}) through the portion of the Indian and Pacific Oceans where the sea surface is warm, constantly interacting with the underlying ocean and influencing many weather and climate systems. Within the large-scale envelopes of enhanced convection, smaller-scale clusters of clouds propagate westward, and can produce local extremes in rainfall. Air-sea interaction is believed to sustain, and perhaps amplify, the patterns of enhanced and reduced convection as the MJO propagates eastward (Demott et al., 2015).
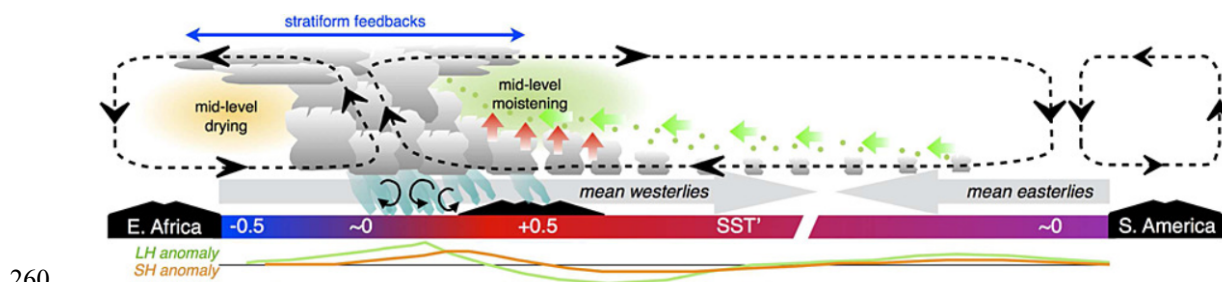
Figure 6: Schematic depiction of Indian and Pacific Ocean feedbacks to the MJO when convection (gray cloud elements) is maximized in the eastern Indian Ocean. Rainfall (aquamarine), circulation anomalies (black dashed cells), convective downdrafts (black rotor arrows), mean winds (faint gray arrows), and moistening by convective detrainment (small green dots) and horizontal and vertical advection (thick green and red arrows, respectively) are overlaid. Net moistening (drying) is shaded green (orange). Positive (red) and negative (blue) SST anomalies for a strong event are shaded, while latent (sensible) heat flux anomalies are shown with green (orange) curves. Central and East Pacific spatial scale is compressed relative to the Warm Pool. Adapted from DeMott et al. (2015).

The MJO-related pattern of winds results in anomalous westerly (easterly) winds to the west (east) of the region of convergence, convection and enhanced rainfall (Fig. 6). These winds generate Kelvin and Rossby waves along the Equator. The Kelvin waves generated by the MJO have been hypothesised (Bergman et al. 2001) to trigger ENSO events in the Pacific. In the Indian Ocean, there is a distinctive sequence of basin-scale ocean waves generated by the MJO. Eastward-propagating equatorial ocean Kelvin waves strike the coast of Sumatra, where they generate coastally-trapped Kelvin waves that propagate northward and southward away from the generation site. Westward-propagating equatorial ocean Rossby waves are also formed (Oliver and Thompson, 2010; Webber et al., 2010). These waves influence local upwelling and

275 currents; they have been linked to variability in coastal currents around the Bay of Bengal (Vialard et al., 2009), to
276 enhancement of the spring Wyrtki jets in the eastern equatorial Indian Ocean (Prerna et al., 2019), to changes in subsurface
277 equatorial currents in the central Indian Ocean (Iskandar and McPhaden, 2011) and to changes in upwelling and chlorophyll
278 a concentration in the off-equatorial central Indian Ocean (Webber et al., 2014). Downwelling Rossby waves in the western
279 Indian Ocean create positive SST anomalies through a combination of reduced entrainment of cooler water from below and
280 zonal advection (Rydbeck et al., 2017; Webber et al., 2012b). These waves therefore act as a triggering mechanism for new
281 MJO events (Rydbeck and Jensen, 2017; Webber et al., 2010, 2012b, 2012a), and may also play a role in amplifying existing
282 MJO events.

283 MJO-related winds also lead to variability in mixing within and at the bottom of the mixed layer. Westerly wind bursts
284 generate zonal currents that create strong vertical current shear (Moum et al., 2014). These currents and the associated
285 mixing persist after the passage of the atmospheric disturbance. Cooler waters from below the surface are mixed with surface
286 waters, leading to a reduction in available ocean heat content for the next MJO event and thus reducing its potential
287 amplitude (Moum et al., 2016). By examining the causes of SST variability in two separate MJO events, McPhaden and
288 Foltz (2013) showed that the presence or absence of barrier layers may play a crucial role in determining how strongly
289 mixing and vertical entrainment influence SST. They also found that zonal advection plays a relatively stronger role when
290 a barrier layer is present. Chi et al. (2014) confirmed the importance of barrier layers in influencing the turbulent heat flux,
291 but found that thin barrier layers can be eroded by strong current shear that occurs during active phases of the MJO. Wind
292 mixing and surface heat and freshwater fluxes both contribute in roughly equal proportions to intraseasonal variability in
293 mixed layer depth (Keerthi et al., 2016).

294 Various studies have investigated the relative importance of surface heat fluxes and subsurface ocean processes for the
295 evolution of SST at intraseasonal time scales. Several observational studies have concluded that the SST variability is
296 predominantly generated by variability in surface heat fluxes in the Seychelles-Chagos Thermocline Ridge (SCTR,
297 Jayakumar et al., 2011; Vialard et al., 2008), while Drushka et al. (2012) suggest this finding applies across most of the
298 tropical Indian Ocean. Such studies, however, typically exhibit large uncertainty in the subsurface ocean terms. Modelling
299 studies have shown that ocean dynamics play an important role in generating SST variability (Halkides et al., 2015; Han et
300 al., 2007). For example, Fig. 7 from the study of Halkides et al. (2015) shows the relative contribution of modelled ocean
301 dynamical processes and thermodynamical processes (i.e., surface heat fluxes) in forcing intraseasonal SST variability. Fig.
302 7a shows that ocean dynamical processes (green shading), including horizontal and vertical advection, are the dominant
303 source of intraseasonal SST variability on the equator and in upwelling regions off Indonesia, Sri Lanka and along the
304 western boundary. The ocean dynamical processes are in turn dominated by horizontal advection along the equator and
305 tropical coastlines (Fig. 7b, pink shading), and vertical advection (blue shading) in the off-equatorial ocean interior.

306
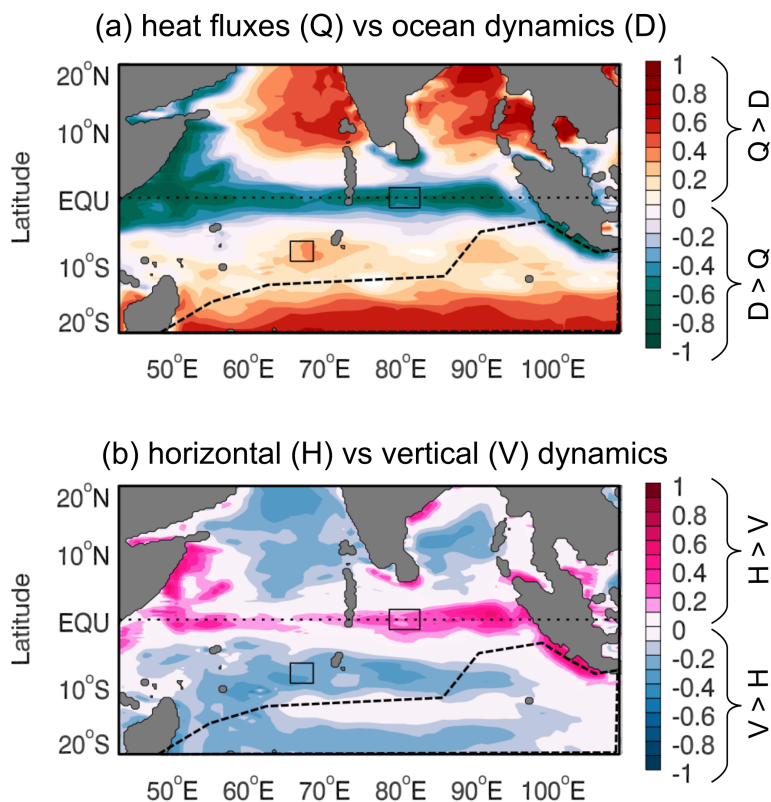
Figure 7: Modelled balance of processes driving intraseasonal SST variability (M_B). (a) Relative role of heat fluxes (Q) and ocean dynamics (D) in driving SST variability, with red (green) colours implying Q (D) dominates forcing, (b) Relative role of horizontal (H) and vertical (V) processes in the dynamical forcing, with pink (blue) colours implying that H (V) processes dominate. All fields are derived from the ECCO-JPL ocean state estimate. The dotted line marks the Equator, dashed line in the southern hemisphere outlines a region in which the model does not fully resolve the ocean heat budget , and the boxes on the Equator and at 10°S mark regions for further analysis not described here. Modified from Halkides et al. (2015).

Organisation of chlorophyll a at intraseasonal timescales has also been reported, with model studies indicating potential biophysical feedbacks due to the variability of penetrative radiation into the water column (Waliser et al. 2005, Jin et al. 2013a). In the Bay of Bengal, the proportion of incoming solar radiation absorbed within the mixed layer varies between 60% and 97% due to a combination of variability in chlorophyll a concentration and mixed layer depth (Lotliker et al., 2016). Representing the seasonal cycle of chlorophyll a concentration in the Arabian Sea in a coupled model led to substantial changes in the simulated SST and monsoon rainfall over India (Turner et al., 2012), suggesting that incorporating this process into coupled models may be important to improve simulation of monsoon rainfall and circulation around the Indian Ocean.

322   Figure 8 illustrates propagation of surface patterns in an MJO composite constructed by Jin et al. (2013a). In each panel the

323   peak in outgoing longwave radiation (OLR, a proxy for convection) is indicated by a red diagonal line. The MJO generates

324   substantial surface heat flux anomalies that create a pattern of surface heat fluxes and SST anomalies such that warm (cool)

325   SSTs lead enhanced (reduced) convection by a quarter of a phase (e.g., Shinoda et al., 1998). The MJO also leads to low-

326   frequency rectifications in the mean state of physical and ecosystem responses (Fig. 8, Waliser et al. 2003, Jin et al. 2013a,b).

327
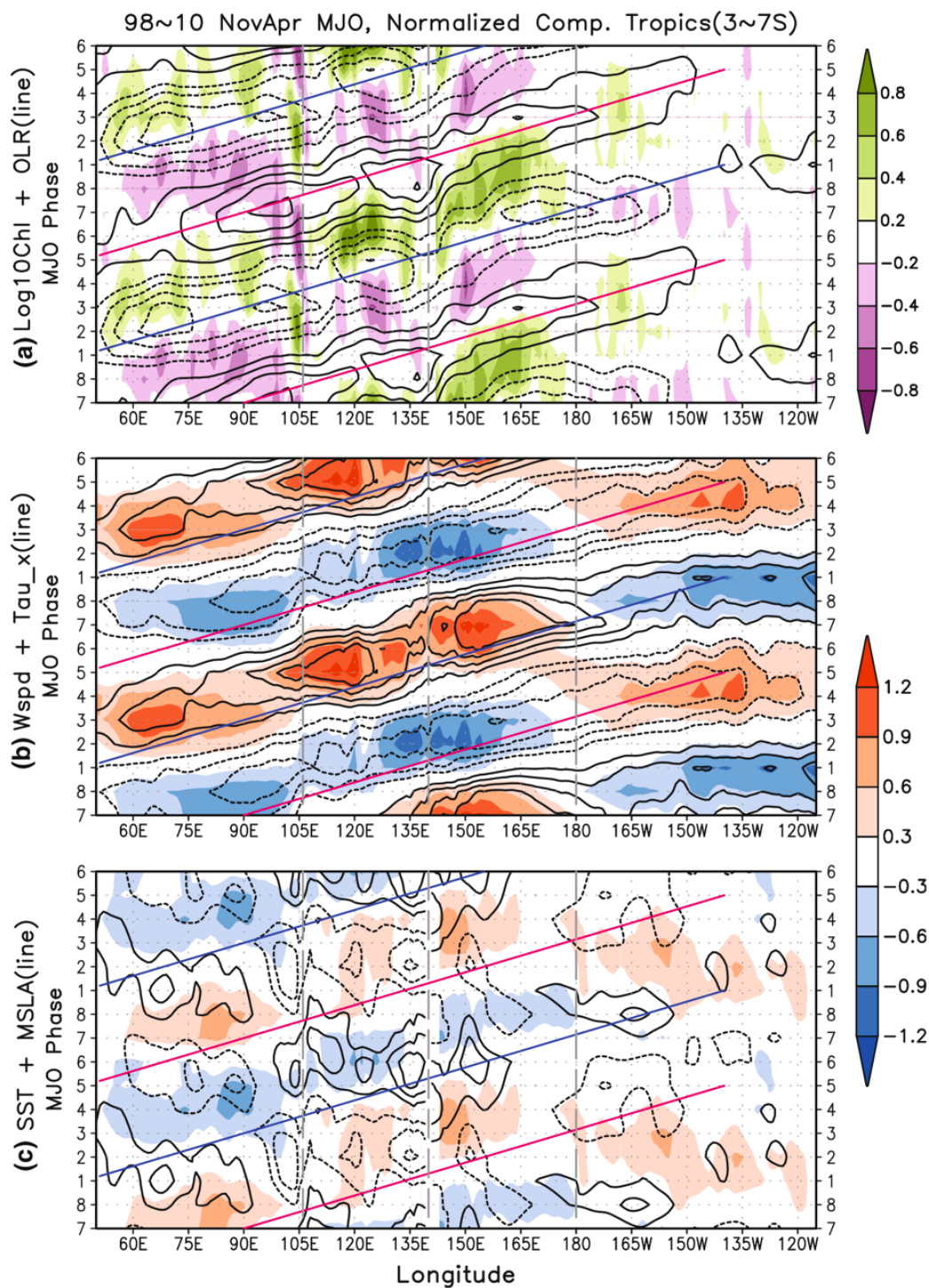
Figure 8: MJO composite evolution for the Boreal winter (Nov-Apr) averaged over latitudes 3°–7°S for the period of November 1st, 1997 to October 31st, 2010, of a) Log$_{10}$Chl from SeaWIFS satellite observations (shaded) and satellite-derived outgoing longwave radiation (contour), b) wind speed (shaded) and zonal wind stress (contour), both from the cross-calibrated multi-platform (CCMP) dataset, and c) NOAA-OI satellite SST anomalies (shaded) and AVISO mean sea level anomaly (contour). All contour intervals match shading levels in (c), and solid (dash) line indicates positive (negative) values. All variables are normalised, and the same MJO composite is repeated for two cycles for convenience. There are between 127--227 events composited for each MJO phase. Red diagonal lines indicate peak signals of positive OLR, and blue lines indicate negative OLR peak, so these are guides for the MJO propagation. The relative location of each propagation line in all panels is the same. Left and center gray vertical dashed line indicates west and east boundary of the Maritime Continent, and the right gray line is on the Dateline, where Chl a propagation stops. From Jin et al. (2013a).

3.2.2 Monsoon Intraseasonal Oscillation - MISO

While the MJO dominates intraseasonal variability during October to April, during May to September (boreal summer, southwest monsoon), the Monsoon Intraseasonal Oscillation (MISO; Goswami, 2012; Suhas et al., 2013) dominates. MISOs can be seen as low pressure systems laden with moisture which deliver rain from atmospheric instabilities (Fig. 9). The MISO is also known as the Boreal Summer Intraseasonal Oscillation (BSISO; Lau and Waliser, 2012; Lee et al., 2013). The MISO oscillations are dynamically linked to the equatorial MJO (e.g., Sperber and Annamalai, 2008), but exhibit northeastward and northwestward propagating features, with the main centre of action being the Bay of Bengal. These northward-propagating bands of enhanced and reduced rainfall exhibit a similar relationship with SST to the MJO: warm SST leading increased rainfall (cool SST leading reduced rainfall) that then determine the wet/dry (or active/break) cycles of the South Asian monsoon (Vecchi and Harrison, 2002; Roxy et al., 2013; Suhas et al., 2013; Zhang et al., 2018). These SST anomalies are primarily forced by variations in surface heat fluxes in the Bay of Bengal (Girishkumar et al., 2017; Vialard et al., 2012), while variations in wind-induced mixing, Ekman pumping and entrainment drive SST variability in the Arabian Sea (Duncan and Han, 2012; Vialard et al., 2012).

352
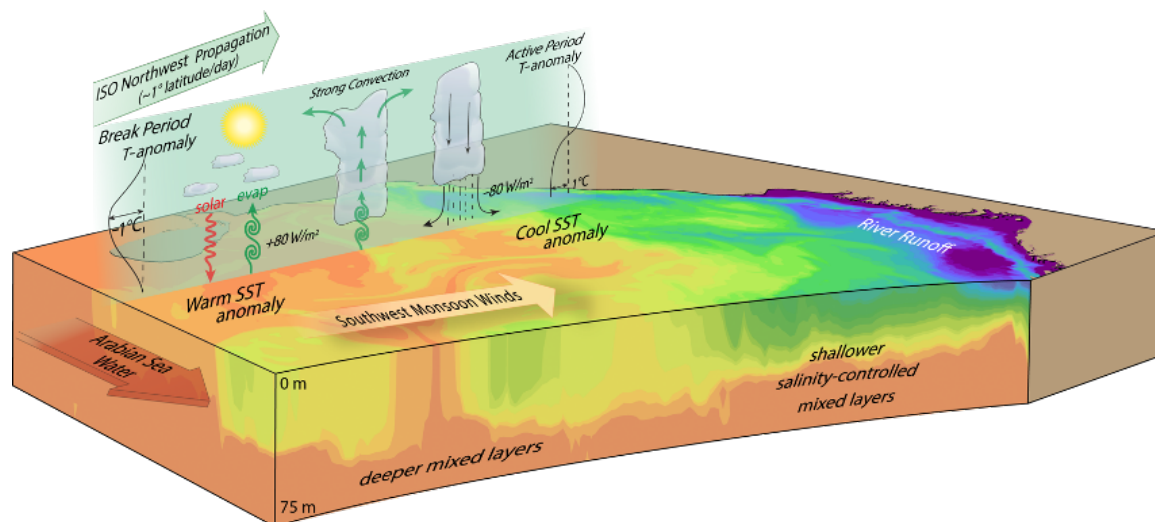
Figure 9: A schematic of the Monsoon Intraseasonal Oscillation (MISO) in the Bay of Bengal, showing the coupled ocean-atmosphere 30–60 day mode northwestward propagation and associated processes in the atmosphere and the ocean. (From Mahadevan et al., 2016a).

356   Simulations of the MISO are still generally poor in state-of-the-art coupled models (e.g., Goswami et al., 2013; Jayakumar
357   et al., 2017; Sabeerali et al., 2013; Sharmila et al., 2013) and re-analysis products (e.g. Sanchez-Franks et al., 2018).
358   Evidence exists from observations of low-level convergence and OLR, as well as forced atmospheric and coupled ocean-
359   atmospheric model experiments, that both MJOs and MISOs are phenomena that require coupling between the ocean and
360   atmosphere to exist. This is even though the scales of SST anomalies tend to be an order of magnitude smaller than the
361   scales of the propagating atmospheric systems (Waliser et al., 1999; Zhou and Murtugudde, 2009). Including air-sea
362   coupling in simulations of the MISO has been identified as key to improving simulation of this oscillation in some models
363   (e.g., Jayakumar et al., 2017; Li et al., 2018; Roxy et al., 2013; Sharmila et al., 2013), and has been shown to improve aspects
364   of simulation in others (e.g., Bellon et al., 2008; Peatman and Klingaman, 2018).

365   While new theories continue to be proposed for MJOs (e.g., Wang et al., 2016), MISOs have not received similar attention
366   likely due to their more local nature compared to the global impacts of MJOs (e.g. their impact on ENSO). The mechanism
367   that causes the northward propagation of the MISO is still a topic of research. The most recent theory for MISOs proposed
368   by Zhou et al. (2017a, b) invokes an explicit coupling between the ocean and the atmosphere in a so-called Central Indian
369   Ocean (CIO) mode. Zonal winds at intraseasonal timescales over the Indian Ocean are argued to be coupled to SSTs to
370   produce a barotropic instability in the meridional gradient of the zonal winds. The horizontal atmospheric eddy fluxes
371   generated by the barotropic instability are argued to explain the northward propagation and the advection of momentum and
372   moisture as a coupled phenomenon. Key questions remain about the oceanic and air-sea interaction processes that reorganise

373   the SSTs in the CIO mode as well as the role of the vertical vs. horizontal shears in driving northward propagation of

374   MISOs.

375   Observations and models indicate that MISOs may be slowing down because of the warming in the Indian Ocean (Sabeerali

376   et al., 2013), which needs to be understood better for providing reliable monsoon predictions and projections in this climate

377   vulnerable region. This is underscored by the observational evidence that climate variability and change are increasing the

378   frequency of dry spells and the intensity of wet spells in the Indian summer monsoon, which are directly related to MISO

379   (Singh et al., 2014).

380   **3.2.3 Intraseasonal drivers of heavy rainfall**

381   As the MJO season begins to wind down in April, northward propagating MISOs begin to become dominant in the northern

382   Indian Ocean, north of around 5°N. While the southwesterlies produce some of the strongest coastal upwelling off Somalia

383   and cool the Arabian Sea, the Bay of Bengal remains warm and largely above the convective threshold (28°C) thanks to the

384   freshwater input from rainfall as well as rivers discharging into the Bay (Roxy and Tanimoto, 2007). The freshwater input

385   creates a shallow density stratification (barrier layer) within the temperature mixed layer and thereby weakens the upwelling

386   of cold water from the thermocline. MISOs deliver rain from atmospheric instabilities, but what controls the rainfall at

387   intraseasonal timescales during the summer can be expected to be region specific with moisture supply determining the

388   rainfall variability over land (Pathak et al., 2017).

389   Over the ocean, the largely evaporative Arabian Sea is relatively cool but the southwesterlies begin to slow down as they

390   approach the Western Ghats mountain range on the west coast of India, leading to maximum rainfall there during the boreal

391   summer monsoon season (Xi et al., 2015). Rather counterintuitively, the warm SST in the Bay of Bengal remains above the

392   convective threshold (Gadgil et al., 1984; Roxy, 2013) and yet, the ocean is not in direct control of the intraseasonal rainfall

393   events. Once the SSTs are organised to be warm enough to support atmospheric convection, baroclinic instabilities, and not

394   static instabilities induced by warm SSTs, drive the majority of rainfall over the Bay of Bengal (Xi et al., 2015). These

395   findings should provide a proper paradigm for understanding the role of SST in monsoon and MISO in terms of the ocean

396   dynamics and air-sea interaction processes that matter most.

397   **3.3 Ocean internal variability impacts on air-sea interaction**

398   Mesoscale eddies are ubiquitous in the world ocean. In the Pacific and Atlantic, the tropical instability waves are known to

399   have air-sea coupling and to impact on low frequency variability such as ENSO (Jochum et al., 2004; Jochum and

400   Murtugudde, 2004; An, 2008). The tropical Indian Ocean is, however, dominated by linear dynamics and the impacts of

401   eddies are (or seem) small. Even though the Indian Ocean has the largest SST variability occurring at seasonal timescales,

402   strong mesoscale variability is also observed along the Somali coast where the western boundary current crosses the Equator.

403   The slope of the East African coastline and the equatorial crossing of the low-latitude jet produce multiple eddies (Nof and
404   Olson, 1993), which are shown to generate strong air-sea coupling at mesoscales (Schott and McCreary, 2001; Schott et al.,
405   2009; Vecchi et al., 2004; Seo et al., 2008). Some intraseasonal oscillations in the ocean were reported in the southwestern
406   tropical Indian Ocean (Kindle and Thompson, 1989) but generally, the impact of ocean internal variability on SSTs in the
407   tropics has not been widely studied.

408   Low-frequency internal variability is also possible. Jochum and Murtugudde (2004) performed forced ocean model
409   experiments with climatological forcing alone to demonstrate that significant low-frequency variability at interannual
410   timescales is generated in the Indian Ocean due internal variability such as mesoscale eddies and other types of nonlinearity.
411   The role of internal variability in regional coupled climate variability as well as ecosystem and biogeochemistry remain
412   interesting problems for this already warm ocean, which is continuing to warm rapidly and monotonically. In this warm
413   ocean, even small SST anomalies can be important for generating large-scale ocean atmosphere interactions (Palmer and
414   Mansfield, 1994).

4 Upper Ocean Circulation and Biogeochemical Variability

4.1 Overview

417   The near surface circulation in the Indian Ocean consists of the monsoon-dominated, seasonally reversing currents north of
418   around 10°S, and the steady currents to the south, as illustrated in Fig. 10a for the southwest monsoon (July-August) and
419   Fig. 10b for the northeast monsoon (January-February). This figure has been updated from Talley et al. (2011) to recognise
420   recent advances in understanding of circulation patterns. In the northern Indian Ocean, additions are a revision of the Red
421   Sea circulation (Menezes et al., 2019). In the southern Indian Ocean, moving in an anti-clockwise direction from the
422   Maritime Continent, additions are: 1) seasonally reversing flows in the Java Sea; 2) the Holloway Current along Australia's
423   Northwest Shelf (Holloway and Nye, 1985; Holloway, 1995; Brahmanpour et al., 2016); 3) revised position of the the
424   salinity-driven Eastern Gyral Current that flows eastward from around 90°E along approximately 15°S, recirculating
425   Indonesian Throughflow Water from the South Equatorial Current to supply the poleward-flowing Leeuwin Current (Meyers
426   et al., 1995; Domingues et al., 2007; Menezes et al., 2013, 2014); 4) the South Indian Countercurrent with 3 distinct branches,
427   northern, central and southern, flowing from the southern tip of Madagascar to Australia where they merge with the
428   poleward-flowing Leeuwin Current (Menezes et al., 2014); and 5) the splitting of the Flinders Current near 110°E, with
429   one branch recirculating back toward Australia, and the other a westward continuation of the Flinders Current, previously
430   not shown (Duran et al., 2020).

431

432
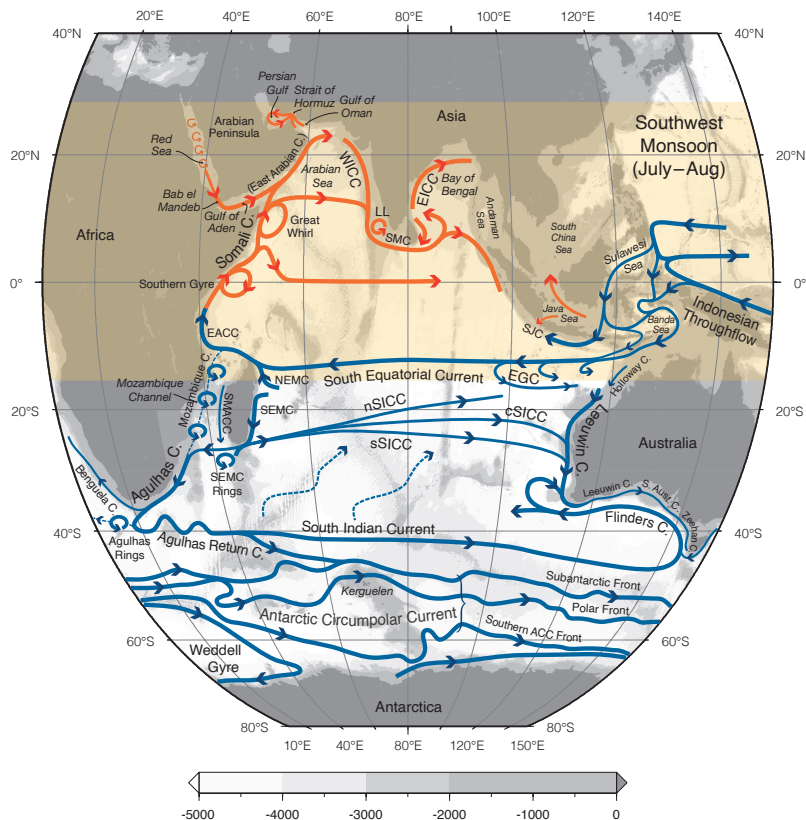
Figure 10a: Schematic near-surface circulation during the Southwest Monsoon (July-August). Blue: year-round mean flows with no seasonal reversals. Orange: monsoonally reversing circulation (after Schott & McCreary, 2001). The ACC fronts are taken directly from Orsi, Whitworth, and Nowlin (1995). Acronyms: EACC, East African Coastal Current; NEMC, Northeast Madagascar Current; SEMC, Southeast Madagascar Current; SMACC, Southwest MAdagascar Coastal Current; WICC, West Indian Coastal Current; EICC, East Indian Coastal Current; LH and LL, Lakshwadeep high and low; SJC, South Java Current; EGC, Eastern Gyral Current; SICC, South Indian Countercurrent (south, central and southern branches); NEC, Northeast Monsoon Current; . Updated from Talley et al. (2011), originally based on Schott and McCreary (2001). The light gray shading shows seafloor bathymetry.

442
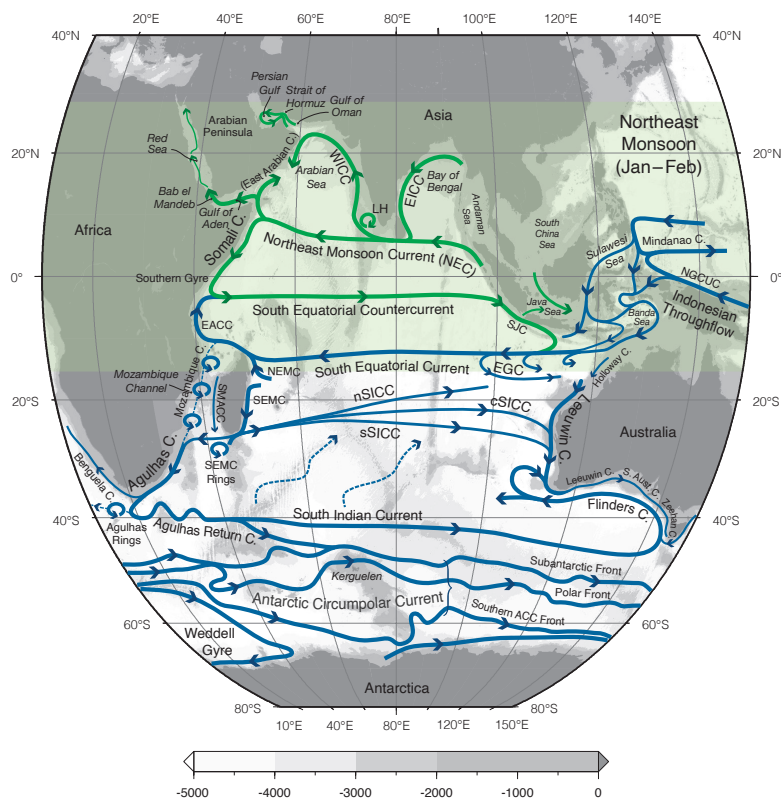
Figure 10b: Schematic near-surface circulation during the Northeast Monsoon (January-February). Details as for Fig. 10a.

The intermediate and deep circulation of the Indian Ocean, and overturning cells will not be examined in this synthesis. The reader is referred to Talley et al. (2011) and references therein.

4.2 Southern Indian Ocean

4.2.1 South Equatorial Current

4.2.1.1 Circulation

The South Equatorial Current (SEC) carries Indonesian Throughflow (ITF) waters into the interior Indian Ocean, flowing westward between 10–20°S (Fig. 10a and 10b). Upon reaching the northern tip of eastern Madagascar, it bifurcates and supplies the Northeast Madagascar Current (NEMC; Schott and McCreary, 2001; Song et al., 2004; Valsala and Ikeda,

454 2007) and the Southeast Madagascar Current (SEMC) and contributes to the development of Mozambique Channel eddies.

455 The mean flow through the Mozambique Channel is weak (Song et al., 2004), although there is an indication from ocean

456 model results that the eddy-dominated flow contributes on the order of 20Sv southward (Durgadoo et al., 2013). The

457 Mozambique Channel eddies, eddies from the SEMC and recirculation combine to feed into the Agulhas Current (Schott

458 and McCreary, 2001).

459

460 The SEC experiences intraseasonal, seasonal and interannual variability. In the eastern IO, the intraseasonal variation of the

461 SEC is mostly attributed to the baroclinic instability of the mean current (Feng and Wijffels, 2002), which is important for

462 the meridional heat transport in the region and contributes to the demise of Indian Ocean Dipole events (Ogata and

463 Masumoto, 2011; Yang et al. 2015). Barotropic instability of the SEC has also been proposed to be a key mechanism for

464 generating intraseasonal variability (Yu and Potemra, 2006). These intraseasonal signals propagate westward as Rossby

465 Waves, influencing the SEC variability in the western Indian Ocean (Zhou and Murtugudde, 2008).

466

467 Interannual variability of the SEC in the eastern Indian Ocean conveys the ENSO and IOD influences on the ITF transport

468 variability into the western Indian Ocean. Geostrophic transport variability in the long-time repeat XBT line IX1 (Liu et al.,

469 2015) shows that the SEC is stronger during La Niña and Indian Ocean Dipole events.

470 The SEC also conveys the Pacific Decadal Oscillation influences on the ITF on decadal time scales (Section 6.1.2). During

471 the climate change hiatus period of 2000-2011, the enhanced heat transport of the SEC/ITF was a key mechanism for the

472 fast warming trend in the southern subtropical Indian Ocean (Section 6.1).

473

474 **4.2.1.2 Biogeochemical Variability**

475 The ITF impacts both ocean currents and basin-scale biogeochemistry (Talley and Sprintall, 2005; George et al., 2013; van

476 Sebille et al., 2014). Talley and Sprintall (2005) mapped silicate on the 31.96 potential density surface, revealing a striking

477 silicate maximum associated with the SEC that extends westward to at least 60ºE, highlighting the broad reach of ITF

478 nutrient influence into the Indian Ocean. Ayers et al. (2014) estimated the depth- and time-resolved nitrate, phosphate, and

479 silicate fluxes at the three main exit passages of the ITF that feed into the SEC: Lombok Strait, Ombai Strait, and Timor

480 Passage. They found that the nutrient flux is significant relative to basin wide new production, and that the majority of ITF

481 nutrient supply to the Indian Ocean via the SEC is to thermocline waters, where it is likely to support primary production

482 and significantly impact biogeochemical cycling.

483

484 Satellite chlorophyll and primary production estimates suggest that values in the SEC are considerably higher than those

485 found in the southern hemisphere subtropical gyre to the south, with Chla from ~0.10 to 1.0 mg/m^3 and primary production

486   from ~400 to 1000 mgC m⁻² d⁻¹ (Fig. 5 and see Figs. 5 and 6 in Hood et al., 2017) The highest concentrations and rates in

487   the SEC are observed in the Eastern Indian Ocean in July and August during austral winter, associated with the

488   aforementioned ITF nutrient sources and upwelling off Java. The lowest chlorophyll concentrations and rates are observed

489   in January (austral summer).

490

491   Between 50 and 80ºE the SEC is coincident with the southern half of the Seychelles-Chagos Thermocline Ridge (SCTR,

492   Vialard et al., 2009). The SCTR is characterized by a relatively shallow thermocline and thin mixed layer (~30m) across

493   the south tropical Indian Ocean in the latitude band 5-15ºS. Between 50 and 80ºE the SCTR/SEC is a region of significant

494   upwelling (Hermes and Reason, 2008; Vialard et al., 2009; Resplandy et al., 2009; Dilmahamod, 2014), which affects

495   biogeochemistry, and even fisheries (Resplandy et al., 2009; Robinson et al., 2010; Dilmahamod, 2014). Model results and

496   satellite observations show that the SEC/SCTR region exhibits an annual cycle in surface chla concentration and primary

497   production, with the highest values in austral winter (June-August; > 0.20 mg/m³ and >600 mgC m⁻² d⁻¹, respectively) due

498   to the strong southeasterly winds that increase wind stirring and induce upwelling (Resplandy et al., 2009; Dilmahamod,

499   2014; Fig. 5 ; see alsoFigs. 5 and 6 in Hood et al., 2017).

500

501   Vertical sections of the SEC/SCTR region also reveal a deep chla maximum (George et al., 2013). Along 65ºE this

502   maximum shoals from > 100 m at 16ºS to ~50 m at 10ºS due to upwelling. Vertical sections of the SCTR also show that the

503   increases in surface Chl-a concentrations in austral winter are associated with decreases in the subsurface chla maximum

504   (Resplandy et al., 2009; Dilmahamod, 2014). Surface freshening associated with the core of the SEC also influences the

505   chla distribution in the SCTR region by modulating the static stability and mixed layer depth (George et al. (2013).

506

507   The SEC provides relatively oligotrophic (low nutrient, low chlorophyll and low primary production) tropical source waters

508   that feed into the EACC, NEMC, SEMC and the Mozambique channel.

4.2.2 Western Boundary

4.2.2.1 Circulation

511   The Agulhas Current (Fig. 10) has long been known as one of the strongest western boundary currents in the global oceans,

512   with an average transport of 70 Sverdrups and current speeds in excess of 2 m s⁻¹ (Beal et al., 2011). The Agulhus Current

513   plays a vital role in the global thermohaline circulation, advecting warm, salty, subtropical water southwards, following the

514   continental shelf of South Africa and meandering less than 150 km offshore (Gründlingh, 1983; Lutjeharms 2006). The

515   strength and warmth of the Agulhas Current influences atmospheric storm tracks and storm development. The large moisture

516   source of the warm Agulhas Current region contributes significantly to the frequency and strength of African precipitation,

517   which significantly impacts rain-fed subsistence farming (Hermes et al. 2019 and references therein).

518

519   South of the tip of Africa, the Agulhas Current retroflects eastwards into the South Indian Ocean (Fig. 10). This retroflection

520   area is highly variable, occluding rings that propagate into the South Atlantic Ocean. The Agulhas variability is linked

521   upstream to the IOD, SIOD and ENSO and downstream with the Atlantic meridional overturning circulation, providing an

522   essential link between the Pacific, Indian and Atlantic Oceans. Estimates of the rate of mass and heat exchange carried by

523   Agulhas leakage south of Africa (and the number of rings shed per year) vary and are difficult to verify reliably (Weijer et

524   al., 2014). Temporal variations in the Agulhas Current have been shown to have a significant effect on inter-ocean exchange

525   between the South Indian and South Atlantic oceans, primarily by influencing the frequency of ring shedding at the Agulhas

526   retroflection (van Sebille et al., 2011; le Bars et al., 2014). Seasonal changes in the Agulhas retroflection region (Lutjeharms

527   and van Ballegooyen, 1988; Quartly and Srokosz, 1993) and in the southwest Indian Ocean (Ffield et al., 1997) have been

528   suggested from hydrographic and satellite data (Krug et al., 2012), but with weak statistical significance due to a lack of

529   sufficiently   long   time   series.

530

531   Although long term observations in this region are limited there are numerous recent studies that have further elucidated our

532   understanding of the Agulhas Current. Beal and Elipot (2016) used 3 years of in situ data to show that, contrary to

533   expectations, the Agulhas Current has not intensified since the early 1990s. Instead, it has broadened as a result of more

534   eddy activity, driven by intensifying winds. Variability in the path and strength of the Agulhas Current has mostly been

535   attributed to solitary Agulhas meanders within the Current system (also known as Natal pulses) which drive upwelling and

536   cross-shelf transports, affecting marine productivity, fisheries and recruitment over the Agulhas Bank (Beal and Bryden,

537   1999; Roberts et al., 2010, Elipot and Beal, 2015). Recent work has highlighted the importance of submesocale eddies in

538   the AC frontal region driving an inshore edge flow reversal which can have important consequences on fisheries (Krug et

539   al., 2017).

540

541   The advance in models has also helped improve our understanding of the Agulhas Current, which is generally not well

542   represented in global ocean models. Hutchinson et al. (2018) used idealized models to expose a link between the seasonality

543   of the Agulhas Current and propagation of first baroclinic mode Rossby waves communicating the wind stress signal across

544   the western portion of the Southern Indian Ocean, with the signal from winds further east having little effect.

545   **4.2.2.2 Biogeochemical Variability**

546   Chlorophyll *a* concentrations and production rates in Mozambique Channel surface waters are generally low (< 0.4 mg/m^{-3}

547   and < 700 gC m^{-2} d^{-1}, Fig. 5), and not significantly different in cyclonic and anticyclonic eddies (Lamont et al., 2014; Barlow

548   et al., 2014; see also Figs. 5, 6 and 20 in Hood et al., 2017). Deep chlorophyll maxima are also observed between 25 and

549   125 m depth depending on the proximity to the shelf and the influence of mesoscale eddies (Barlow et al., 2014; Lamont et

550 al., 2014). Eddies in the Mozambique Channel also have a strong influence on the lateral transport of nutrients and
551 chlorophyll from the coasts of Madagascar and Africa. Indeed, enhanced phytoplankton production within both cyclonic
552 and anticyclonic eddies in the Mozambique Channel often occurs in response to lateral nutrient inputs into the euphotic zone
553 by horizontal advection from the coasts of Madagascar and Africa rather than eddy induced upwelling and downwelling
554 (José et al., 2014; Lamont et al., 2014; Roberts et al., 2014). In contrast, in the Southeast Madagascar Current,
555 topographically-induced coastal upwelling brings cold, nutrient-rich water up to the surface, which supports high rates of
556 primary production (Lutjeharms and Machu, 2000; Ho et al., 2004; Quartly and Srokosz, 2004). This upwelling and its
557 impacts are observed in both the austral summer and winter (Ho et al., 2004).

558

559 The Agulhas Current itself is warm and oligotrophic with sources derived from low nutrient and low chlorophyll surface
560 waters from the Mozambique Channel, Southeast Madagascar Current and the southwestern tropical Indian Ocean (Fig. 5;
561 Lutjeharms, 2006). Chlorophyll a concentrations and production rates in Agulhas Current surface waters are particularly
562 low during austral summer (< 0.2 mg/m^{-3} and < 500 mgC m^{-2} d^{-1}) with higher concentrations and rates in the austral winter
563 (Machu and Garcon, 2001; see Figs. 5, 6 and 20 in Hood et al., 2017). The Agulhas Current can drive upwelling and elevate
564 primary production in the coastal zone through meandering and topographic interactions, but it can also dramatically
565 suppress primary production when it impinges onto the shelf (Schumann et al., 2005).

566

567 In general, chlorophyll concentrations and primary production are elevated in the coastal zone of southeast Africa along the
568 inshore side of the Agulhas Current (Fig. 5; Machu and Garcon, 2001; Goschen et al., 2012; see Figs. 5, 6 and 20 in Hood
569 et al., 2017). This enhancement is most pronounced in austral summer and further southward downstream, and it is
570 associated with upwelling favourable (easterly) winds and the aforementioned topographically-induced upwelling.

571 **4.2.3 Interior flows**

572 **4.2.3.1 Circulation**

573 In the central-eastern South Indian Ocean between 20°S and 30°S, the surface geostrophic flow is generally eastward,
574 opposite to the prediction both of the Ekman and Sverdrup theories (Sharma 1976; Sharma et al., 1978; Godfrey and
575 Ridgway, 1985; Schott et al., 2009). This flow is driven by the large-scale, poleward drop in the dynamic height (steric
576 height) near the surface (Godfrey and Ridgway, 1985; Schott et al., 2009) related to the meridional transition from the very
577 fresh and warm SEC waters to the increasingly cooler, saltier and denser waters to the south. The flow generally extends
578 from the sea surface to ~200–300 m (Domingues et al., 2007; Palastanga et al., 2007; Divakaran and Brassington, 2011;
579 Menezes et al., 2014).

580

581   Embedded in this general eastward flow are narrower eastward jets (Maximenko et al., 2009; Divakaran and Brassington,

582   2011; Menezes et al., 2014), collectively known as the South Indian (Ocean) Countercurrent (SICC; Palastanga et al. 2007;

583   Siedler et al. 2006; Menezes et al., 2014). They start out as a single jet emanating from the southern tip of Madagascar

584   around 25°S, possibly fed by a partial retroflection of the SEMC (Palastanga et al., 2007; Siedler et al., 2006, 2009).

585   Numerical particle tracking experiments conducted by Siedler et al. (2009) show that about 40% of the SICC transport

586   originates from the SEMC region. The SICC flow divides into separate jets around the Central Indian Ridge (65°E–68°E),

587   and continues to the west coast of Australia

588   (Menezes et al., 2014). Eastward flows exist in similar latitude bands in the North and South Pacific and North and South

589   Atlantic (Yoshida and Kidokoro, 1967; Merle et al., 1969; Takeuchi, 1984; Kubokawa, 1999; Qiu and Chen, 2004; Kobashi

590   and Kubokawa, 2012). However, the jets in these basins are weaker and shallower than the SICCs and do not extend all the

591   way to the eastern boundary (Menezes, 2015).

592

593   Three main jets (Fig. 10a) are evident in geostrophic velocity calculated from both altimetric sea surface height and

594   hydrography and are captured in OGCMs (Maximenko et al., 2009; Divakaran and Brassington, 2011; Menezes et al., 2014).

595   The stronger southern jet (3–4 Sv) crosses the basin around 26°S and has an associated thermal front at depths around 100–

596   200 m (Sharma 1976; Siedler et al., 2006; Menezes et al., 2014; Palastanga et al., 2007). This front suggests that the southern

597   SICC has physics similar to the Subtropical Countercurrents (STCCs) of the Pacific Ocean (Kubokawa, 1999; Kobashi and

598   Kubokawa, 2012, Menezes et al., 2014). The STCC mechanism, however, does not explain the central and northern

599   branches (Menezes et al., 2014).

600

601   The central branch of the SICC is found east of 75°–80°E, between 22° S and 24°S, and has a volume transport between 0.5

602   Sv and 3–5 Sv (Menezes et al., 2014). The shallowest and weakest northern SICC jet (1 Sv) has an equatorward orientation

603   and flows on the southern flank of the northern cell of the subtropical gyre (Palastanga et al., 2007; Menezes et al., 2014).

604   Part of the northern SICC merges with the Eastern Gyral Current (EGC) around 15°S, 100°E (Fig. 10a). The eastward

605   flowing EGC is part of an anticyclonic recirculation centred at the Indonesian-Australian basin (5°S–20°S and 100°E–

606   125°E) (Domingues et al., 2007; Menezes et al., 2013, and references therein). Both the SICC and the EGC supply water

607   to the Leeuwin Current (LC) and are an essential component of the LC dynamics (Domingues et al., 2007; Benthuysen et

608   al., 2014; Lambert et al., 2016; Furue et al., 2013, 2017; Yit Sen Bull and van Sebille, 2016).

609

610   The EGC and the SICC are dynamically distinct, however. In the EGC region, salinity overwhelms the temperature

611   contribution to density gradients to generate near-surface eastward geostrophic vertical shear (Menezes et al., 2013). This

612   salinity front is formed by the encounter of the fresh Indonesian Throughflow Water carried westward by the SEC-and the

613   salty subtropical underwater (SUW) formed at the Southern Indian Ocean subtropical salinity maximum. The seasonal

614   cycles of the EGC and the SICC are also distinct: the EGC is stronger in austral winter (3–5 Sv) and weaker (<0.5 Sv) in

615   summer with the cycle in phase with the Leeuwin Current (Feng et al., 2003; Menezes et al., 2013; Furue et al., 2017). The

616   SICC, is overall stronger in spring-summer and weaker in winter (Palastanga et al., 2007; Jia et al., 2011a; Menezes et al.,

617   2014). It experiences strong interannual variability, which peaks at biennial timescales and is decadally modulated (Menezes

618   et al., 2016).

619

620   The multiple jets of the SICC are embedded in a zone of high eddy kinetic energy, with eddies generated by instabilities of

621   the Leeuwin Current and of the SICC itself (Palastanga et al., 2007; Divakaran and Brassington, 2011; Huhn et al., 2012;

622   Jia et al., 2011a, 2011b; Menezes et al., 2014, 2016; Siedler et al., 2006). By co-locating Argo floats and satellite data,

623   Dilmahamod et al. (2018) described the passage of surface and subsurface South Indian Ocean eddies (SIDDIES). These

624   westward-propagating, long-lived features (>3 months) originate in areas of high evaporation in the eastern Indian Ocean

625   and prevail over a preferential latitudinal band, forming a permanent structure linking the eastern to the western Indian

626   Ocean (the "SIDDIES Corridor"). This corridor of eddy passage allows the advection of water masses and biogeochemical

627   properties across the basin (Dilmahamod et al., 2018).

628

629   The location and strength of the SICC vary between studies, from well-defined jets (Siedler et al. 2006, Palastanga et al.

630   2007, Divakaran and Brassington 2011, Menezes et al. 2014) to a mean velocity structure (Jia et al., 2011a), or even absence

631   of the SICC (Srokosz et al. 2015). Depending on the region and time in which its characteristics were determined, the SICC

632   varies from a weak mean current of 2–3 cm/s (Jia et al., 2011a) to a strong jet of 50 cm/s eastward flow(Siedler et al., 2006).

633

634   **4.2.3.2 Biogeochemical Variability**

635   The near-surface eastward flows are generally associated with very low (oligotrophic) nutrient and chlorophyll-*a* (Chl-*a*)

636   concentrations (< 0.1 mg/m^{-3}) and also very low primary production (< 500 mgC m^{-2} d^{-1}; Fig. 5 and see Figs. 5 and 6 in

637   Hood et al., 2017). A well-defined deep Chl-*a* maximum is observed between 50 and 150 m during the austral fall along

638   55ºE between 20 and 30ºS (Coles et al., unpublished data). An exception to this, however, is the South-East Madagascar

639   bloom (SMB). The SMB occurs in near-surface waters off the southeastern coast of Madagascar in the late austral

640   summer/fall (Jan-April). It was first described as a dendroid bloom by Longhurst (2001), owing to its branching shape that

641   projects eastward (Fig. 11). The bloom can extend over a 2,500 km^2 area with Chl-*a* concentrations reaching 2-3 mg/m^3

642   (Longhurst, 2001), making it a 'hot spot' for primary production in an otherwise oligotrophic region. Fig. 11 illustrates the

643   bloom's large spatial variability, with high Chl-*a* filaments apparently co-occurring and being transported with mesoscale

644   and submesoscale eddies and jets.
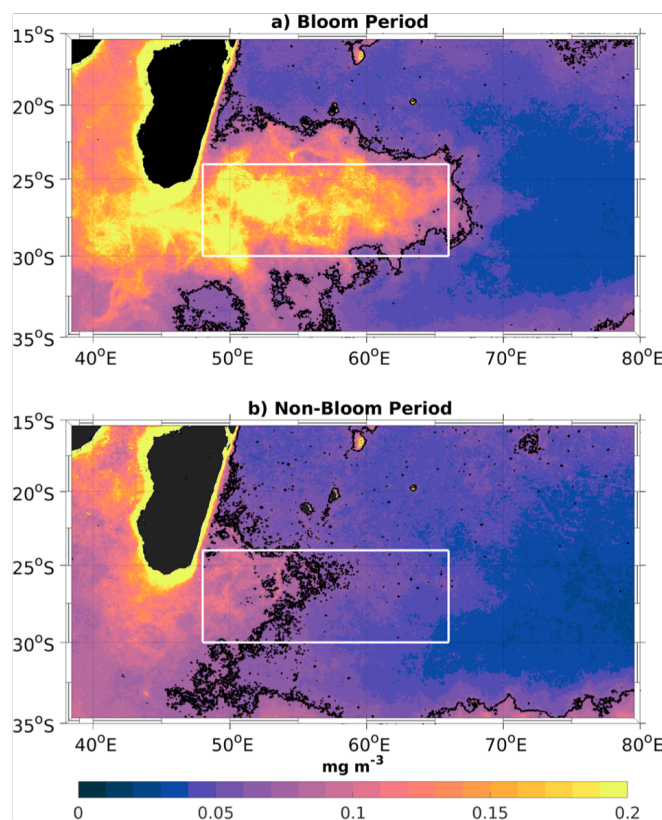
Figure 11: (a) Spatial maps of mean Chl-a concentration (mg/m3) during months of maximum austral summer bloom. (b) Same as (a) but during January of minimum Chl-a concentration in austral summer. The black contour denotes the 0.07 mg/m3 threshold used to distinguish between bloom and non-bloom years. From Dilmahamod et al. (2019).

Why the SMB flourishes in late austral summer is unclear. Longhurst (2001) attributed SMB development to mixed layer deepening and entrainment of nutrients by the vigorous mesoscale eddy field. These nutrients could stimulate phytoplankton growth in the photic zone, with the eddies shaping the eastward propagation of the enhanced surface Chl-*a* concentrations. However, Uz (2007), Srokosz and Quartly (2013), and Dilmahamod et al. (2019) subsequently showed that the bloom occurs within a warm (> 26.5°C), shallow mixed layer (~30 m) overlying a strong pycnocline. Furthermore, they suggested that diazotrophs known to inhabit the region (Poulton et al., 2009) might introduce new nitrogen (N) from N_2 fixation that could support the enhanced Chl-*a* concentration as observed elsewhere (Mulholland et al., 2014; Hood et al. 2004; Coles et al., 2004). Subsequent studies also highlight the role of mesoscale eddies (Fig. 11), that could advect, disperse and co-mingle

658   nutrients and/or phytoplankton biomass (Dilmahamod et al. 2019; Huhn et al., 2012; Raj et al., 2010; Srokosz and Quartly,

659   2013; Srokosz et al., 2004, 2015; Uz, 2007).

660   A different explanation of the SMB and its eastward projection was proposed by Srokosz et al. (2004). In their proposed

661   mechanism, the bloom initiates off Madagascar due to coastal processes that bring limiting nutrients to the photic zone and

662   phytoplankton are transported horizontally by mesoscale eddies, resulting in an eastward propagation of the bloom.

663   Dilmahamod et al. (2020) extend this further using a model to suggest that, from a nutrient flux analysis, horizontal advection

664   of low-salinity nutrient-rich Madagascan coastal waters can indeed trigger a phytoplankton bloom. Alternatively, the

665   apparent eastward propagation of the SMB has recently been attributed to advection by the SICC (Fig. 10; Dilmahamod et

666   al., 2019; Huhn et al., 2012; Wilson and Qiu, 2008). Indeed, Huhn et al. (2012) further suggested that the bloom is shaped

667   by a meridional barrier of jet-like Lagrangian coherent structures associated with the SICC.

668   **4.2.4 Eastern Boundary**

669   **4.2.4.1 Circulation**

670   Unlike any other eastern boundary current, the Leeuwin Current (LC; Figs. 10 and 12a) flows poleward, along the shelf

671   break of the west coast of Australia (Smith et al., 1991). Figure 12a presents the long-term average volume transport of the

672   LC System from an observational climatology (Furue et al., 2017). The LC system includes the Leeuwin Undercurrent and

673   exchanges with the interior zonal flows, where near-surface eastward flow enters the LC, flows poleward and at the same

674   time sinks to the Leeuwin Undercurrent depths, flows equatorward, and finally moves westward out of the LC System. The

675   primary source waters for the LC are the interior eastward flows (Section 4.2.3.1) that turn southeastward as they approach

676   the coast and merge with the LC (Fig. 12a; Domingues et al., 2007; D'Adamo et al., 2009; Menezes et al., 2013, 2014; Furue

677   et al., 2017, 2019). The LC carries 0.3 Sv southward at 22°S, gains 4.7 Sv from the Indian Ocean interior, loses 3.5 Sv

678   through downwelling to the layer beneath, and carries 1.5 Sv at its southern limit. The LC is approximately 200–300 m

679   deep, extends from 22°S (North West Cape) to 34°S (Cape Leeuwin) and exists throughout the year despite significant

680   seasonality (Feng et al., 2003; Ridgway and Godfrey, 2015; Furue et al., 2017). The Holloway Current, which flows

681   southwestward on the North West Shelf (D'Adamo et al., 2009; Bahmanpour et al., 2016), is another weaker source to the

682   LC from the north. Inshore of the LC, there exist seasonal equatorward flows that recirculate waters of distinct watermass

683   properties influenced by air-sea interaction over the continental shelf (Woo et al., 2006).

684

685
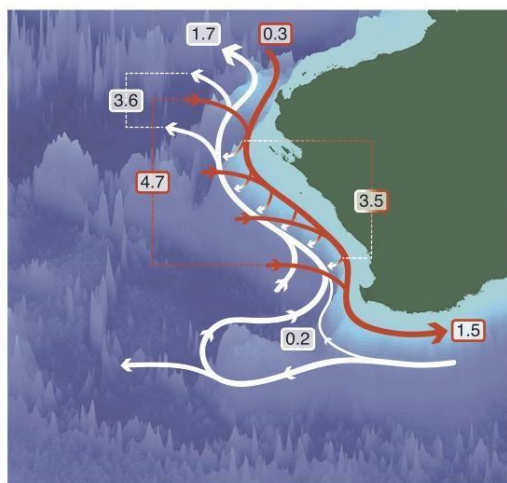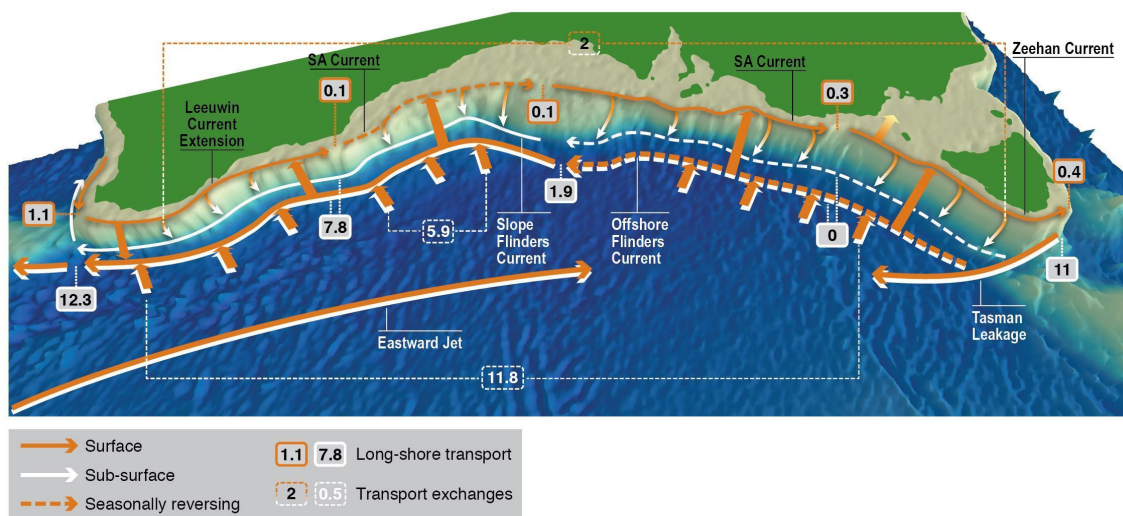
Figure 12: a) Schematic summary of Australia's Leeuwin Current System three-dimensional transports (Sv). The red arrows and red-outline numbers represent the upper-layer (0–200 m) meridional transport of the poleward Leeuwin Current and meridionally-integrated zonal transport of the shallow eastward flows. The white arrows represent the lower-layer (200–900 m) flows of the Leeuwin Undercurrent. Taken from Furue et al. (2017). © American Meteorological Society. Used with permission. b) Schematic summary of the Southern Australia Current System three-dimensional transports (Sv). Long-shore transport for the Shelf Break Currents and Flinders Current in grey box with orange and white outlines, respectively. Integrated vertical and onshore flow transport in dashed outline box. Reprinted from Duran et al. (2020), with permission from Elsevier, Progress in Oceanography. Both schematics are based on a geostrophic calculation in the CARS ⅛-degree climatology.

695

696   Beneath the LC, the Leeuwin Undercurrent exists in a depth range of 200-900 m, just offshore of the LC (Furue et al., 2017).

697   It is fed in the south by a weak northward deflection of the Flinders Current, and a stronger northeastward recirculation of

698   the Flinders Current around topography. The Leeuwin Undercurrent carries 0.2 Sv northward at its southern end, receives

699   3.5 Sv downwelled from the layer above, loses 3.6 Sv to westward flow into the Indian Ocean interior, and carries 1.7 Sv

700   northward at its northern end near 22°S (Furue et al., 2017)

701

702   The LC flows around the southwestern corner of Australia and continues to flow eastward along the shelf break of the south

703   coast of Australia to reach the southern tip of Tasmania near 42°S, 140°E (Fig. 12b, Oliver et al., 2016; Oke et al., 2018;

704   Duran et al., 2020). This 5500-km long boundary current was first documented as a continuous flow by Ridgway and

705   Condie (2004). When the longshore current is weak, however, it tends to be somewhat fragmentary (Oke et al., 2018; Duran

706   et al., 2020) and sometimes even reverses in places (Duran et al., 2020). For this reason, and additionally because of the

707   scarcity of observational sampling, the current is not traditionally regarded as a single current. Along southern Australia,

708   the boundary currents can be described following Ridgway and Condie's (2004) naming convention. The current's western

709   sector is called the Leeuwin Current Extension, the central part, to the south of the Great Australian Bight, is called the

710   South Australian Current, and the easternmost part along Tasmania is called the Zeehan Current. They are collectively

711   known as the Shelf-Break Currents (SBCs) of the Southern Australia Current System (Duran et al., 2020).

712

713   As a poleward boundary current, the LC waters are relatively fresh and warm from tropical origins (Rochford, 1969;

714   Andrews, 1977; Legeckis and Cresswell 1981; Domingues et al., 2007; Woo and Pattiaratchi, 2008). As the LC flows

715   poleward, the saltier Indian Central Water, the surface water of the Subtropical South Indian Ocean, joins the LC

716   (Section 4.2.3.1). At the same time, the mean density of the LC becomes higher as it flows poleward, partly because of the

717   continual eastward inflow joining the LC and partly because of surface cooling (Woo and Pattiaratchi, 2008; Furue, 2019).

718   The SBCs also carry warmer water eastward along the south coast of Australia (Ridgway and Condie, 2004).

719

720   The LC's mean state is driven by the meridional pressure gradient in the upper ocean (e.g., Godfrey and Ridgway, 1985;

721   Godfrey and Weaver, 1989, 1991), evident as a large poleward decrease in SSH balanced by an eastward surface geostrophic

722   current (Section 4.2.3.1). The eastward flow approaches the eastern boundary, inducing downwelling and a surface poleward

723   current (Fig. 12; Godfrey and Ridgway, 1985; McCreary et al., 1986; Thompson, 1987; Weaver and Middleton, 1989, 1990;

724   Furue et al., 2013; Benthuysen et al., 2014), in opposition to the southerly winds. The mechanisms that determine the vertical

725   extent of the interior eastward flow remains unclear. Offshore of the LC, this eastward flow exists over the upper 200 m in

726   OGCMs and below that level the flow is weakly westward (Domingues et al., 2007; Furue et al., 2017). This depth coincides

727   with the depth of the shelf break and the bottom of the LC; this correspondence may be achieved by the westward

728   propagation of baroclinic Rossby waves (Weaver and Middleton, 1989; Furue et al., 2013).

729

730   It is not clear whether the SBCs along the south coast of Australia are, dynamically, an extension of the LC. The SBCs are

731   at least consistent with the local northward Ekman drift (Ridgway and Condie, 2004; Duran et al., 2020) and hence would

732   exist without the LC.

733

734   On seasonal timescales, the LC transport generally tends to be strongest in austral autumn and weakest in austral summer

735   (McCreary et al., 1986; Smith et al., 1991; Feng et al., 2003; Furue et al., 2017). There are two theories to explain this

736   seasonality. In one, the local winds, which generally induce an offshore Ekman drift and therefore tend to weaken the LC,

737   reach their annual maximum or minimum when the LC transport reaches its minimum or maximum, respectively (McCreary

738   et al., 1986; Furue et al., 2013). In the other, a seasonal pressure anomaly originates in the Gulf of Carpentaria and propagates

739   counterclockwise along the shelf break, driving the seasonality of the LC and of the SBCs to the south of Australia (Ridgway

740   and Godfrey, 2015). Like the LC, the SBCs tend to be strongest in austral autumn and weakest in austral summer (Ridgway

741   and Condie, 2004; Oke et al., 2018; Duran et al., 2020). In particular, the eastern part of the South Australian Current is seen

742   to reverse in summer in Duran et al.'s (2020) analysis. This variability is consistent with the counterclockwise propagation

743   of pressure anomaly shown by Ridgway and Godfrey (2015) and also with the seasonality of the wind stress along the south

744   coast of Australia, with onshore (offshore) Ekman drift tending to drive eastward (westward) shelf-break flow (Duran et al.

745   2020). Again it is not clear which mechanism dominates the seasonality of the SBCs.

746

747   On interannual time scales, the LC is modulated by the El Niño Southern Oscillation owing to the steric height anomalies

748   in the western equatorial Pacific Ocean propagating through the Indonesian Seas and along Western Australia (Feng et al.,

749   2003). During El Niño and La Niña periods, the LC transport weakens and strengthens, respectively, and is correlated with

750   Fremantle sea level (Feng et al., 2003). During the strong 2010–2011 La Niña event, the LC reached record strength speeds

751   (Feng et al., 2013) and the consequences of this event are described in Section 7.4. On multidecadal timescales, the major

752   boundary currents around Australia, including the LC, are reported to have strengthened during 1979–2014 in an eddy-

753   resolving OGCM, consistent also with observations (Feng et al., 2016; see Section 6.1.2 for associated changes). At

754   intraseasonal timescales, winds or heat anomalies on the North West Shelf region due to MJO events lead to intraseasonal

755   variability of the Holloway Current on the North West Shelf and then of the LC (Marshall and Hendon, 2014; Marin and

756   Feng, 2019).

757

758   The LC is accompanied by mesoscale eddies that cause the LC to meander energetically (Pearce and Griffiths, 1991; Feng

759   et al., 2005; Waite et al., 2007; Meuleners et al., 2008). Those eddies are, at least partially, generated by barotropic,

760   baroclinic, or mixed instability of the LC itself (Pearce and Griffiths, 1991; Feng et al., 2005; Meuleners et al., 2008). The

761   eddy kinetic energy is greatest when the LC transport is strongest, in May–June (Fang and Morrow, 2003; Feng et al.,

762   2005). Some of these eddies cause a large meander of the LC: a large anti-cyclonic eddy often forms at 28°–29°S and at

763   31°–32°S (Feng et al., 2003; Feng et al., 2007) and in this case, the LC leaves the continental shelf and flows offshore around

764   this eddy before coming back to the continental shelf. This state typically starts during May–June and ends in July–August

765   (Feng et al., 2007). Similarly, it is suggested that the eastern part of the SBCs becomes unstable in boreal autumn and winter,

766   generating eddies, which subsequently propagate westward south of Australia (Oke et al., 2018).

767

768   Just below the Leeuwin Current is the equatorward Leeuwin Undercurrent (LUC; Thompson, 1984; Church et al., 1989;

769   Smith et al., 1991; Fig. 12a). The LUC hugs the continental slope and extends from 200 m to 800 m (Furue et al., 2017).

770   The LUC begins at Cape Leeuwin (34°S, 114°E) and is fed by a northward bend of a small fraction of the Flinders Current

771   (FC; Furue et al., 2017; see Fig. 10 for the pathway of FC). The remaining part of the FC keeps flowing westward but

772   another small fraction of it appears to retroflect eastward and join and augment the LUC (Duran, 2015; Furue et al., 2017).

773   Near 22°S, most of the LUC volume leaves the continental slope and flows offshore (Duran, 2015), apparently following

774   the southern flank of the Exmouth Plateau although its bottom at 900 m is much shallower than the topographic feature.

775

776   To the south of Australia, an undercurrent has been recently identified below the Zeehan Current in a numerical simulation

777   (Oke et al., 2018) and in a geostrophic calculation based on a gridded T–S climatology (Duran et al., 2020). Traditionally

778   this flow was identified as a branch of the FC (Cirano and Middleton, 2004; Rosell-Fieschi et al., 2013; Feng et al., 2016)

779   because the former flows in the same direction as the latter, but the FC as the northern boundary current of the Subtropical

780   Gyre cannot exist on an eastern boundary (Anderson and Gill, 1975; Philander and Yoon, 1982; McCreary et al., 1992) and

781   it does not have a vertical structure of an undercurrent (Duran et al., 2020). This northwestward- or westward-flowing

782   undercurrent appears to exist all the way from the west coast of Tasmania to Cape Leeuwin (the southwestern tip of

783   Australia) but its separation from the FC is less clear to the south of the Great Australian Bight and further west, where the

784   FC starts to accelerate and tends to overwhelm the undercurrent (Duran et al., 2020). Below, we call this current "slope FC"

785   following Duran et al. (2020).

786

787   The mechanisms responsible for the undercurrents off Western Australia remain an open question, although models have

788   been developed to investigate potential processes. The linear, continuously stratified models of McCreary et al. (1986) and

789   Kundu and McCreary (1986) produce a surface poleward and a subsurface equatorward current, resembling the LC and

790   LUC, along the eastern boundary. This class of model, however, requires large vertical diffusivity to produce realistic LC

791   and LUC (McCreary, 2013, personal communication). Along a continental slope, alongshore and cross-shelf buoyancy

792   advection cause a shelf break front, forming a surface intensified poleward current, like the LC, and an equatorward

793   undercurrent by thermal wind shear (Benthuysen et al., 2014). Analytical shelf models have been extended to include cross-

794   shelf buoyancy gradients to derive a poleward undercurrent like the LUC (Schloesser, 2014). These process-based analytical

795   theories have not been tested in an eddy-resolving model.

796

797   The LUC and the slope FC are connected to the LC and the SBCs, respectively, by downwelling (Fig. 12; Furue et al., 2017;

798   Duran et al., 2020), suggesting a common, but as yet unexplained, dynamics. Note, however, that for the LC–LUC pair, the

799   mean downwelling appears to occur along isopycnal surfaces, and hence he LC water mass is not found in the LUC (Furue,

800   2019). For the SBCs and the slope FC, the nature of the downwelling is not known. The seasonality of these undercurrents

801   are not well known. No systematic seasonal variability of the LUC was evident in a hydrographic climatology and ocean

802   general circulation model (Furue et al., 2017).

803

804   4.2.4.2 Biogeochemical Variability

805   The tropical source waters and downwelling tendency of the Leeuwin Current combine to create a warm, oligotrophic

806   current with low productivity. Chl-*a* concentrations are usually < 30 mgChla m^{-2} and rates of primary production rates

807   generally do not exceed 500 mgC m^{-2} d^{-1} (Koslow et al., 2008; Lourey et al., 2006; Lourey et al., 2013). Productivity in the

808   Leeuwin Current is lowest during austral summer, when the water column is stratified. During summer, subsurface

809   chlorophyll maxima are found between 50 and 120 m depth (Hanson et al., 2007) as observed in open ocean subtropical

810   oligotrophic waters (e.g., Venrick, 1991). However, rates of primary production in near shore upwelling regions (e.g., off

811   of the North West Cape during summer) can sometimes attain very high levels (3000–8000 mgC m^{-2} day^{-1}) as observed

812   in other eastern boundary upwelling zones (Furnas, 2007).

813   In all seasons, meanders in the Leeuwin Current give rise to warm core, anticyclonic eddies that carry moderately high

814   chlorophyll coastal water offshore. The elevated chlorophyll concentrations in these eddies is due to the presence of coastal

815   diatom communities. These diatoms are transported offshore into cooler oligotrophic waters that are dominated by much

816   smaller open ocean phytoplankton species (Waite et al., 2007a; Paterson et al., 2008; Waite et al., 2016). These eddies,

817   which can extend to more than 2000 m depth, are unusual because they are downwelling (anticyclonic) circulations that

818   should inhibit the input of new nutrients from depth. Nonetheless, these eddies, and the elevated chlorophyll concentrations

819   that are associated with them, persist for months (Feng et al., 2007; Moore et al., 2007; du Fois et al., 2014). It has been

820   hypothesized that the diatom communities in these eddies are supported by internal nutrient recycling and/or lateral supply

821   (Waite et al., 2007a; Paterson et al., 2013; Thompson et al., 2007).

822   Generation of these warm (and cold) core eddies by the Leeuwin Current is prolific between 20º and 35º S (Gaube et al.,

823   2013). Most of these eddies move directly westward and some may be very long-lived (Feng et al., 2005; Feng et al., 2007;

824   Moore et al., 2007; Gaube et al., 2013; du Fois et al., 2014). The persistence and potential biogeochemical/ecological

825   impacts of these eddies in the open ocean have not been investigated fully.

4.3 Equatorial regime

4.3.1 Wyrtki Jets

Owing to the seasonally reversing monsoon winds, the equatorial Indian Ocean (EIO) exhibits unique characteristics and is in contrast with the equatorial Atlantic and Pacific Oceans. Unlike the other basins, the annual winds along the EIO are very weak and mostly meridionally oriented except during the two intermonsoon seasons between boreal winter (April-May) and summer (Oct-Nov) when strong westerly wind bursts prevail along the EIO (see Schott and McCreary, 2001 and references therein).These westerly winds force strong eastward jets in the top 100 m along the equator and are known as spring and fall Wyrtki Jets, respectively (Wyrtki, 1973). These surface jets are usually confined within the top 100 m of the water column (Han et al., 1999; Iskander et al., 2011) and deepen (shoal) the thermocline and elevate (lower) the sea level in the east (west) (Rao et al., 1989; Schott and McCreary, 2001; Nagura and McPhaden, 2010a). These jets play a major role in zonal redistribution of mass, heat, salt and other water properties at the Equator and in off-equatorial basins (Reppin et al., 1999; Murtugudde and Busalacchi, 1999; Han et al., 1999; McPhaden et al., 2015; Chatterjee et al., 2017). Long term ADCP observations from the RAMA equatorial mooring suggests that the fall jet in the central EIO is usually stronger with a maximum transport of ~19.7 Sv compared to the spring jet which shows maximum transport of ~14.9 Sv with comparable standard deviations (McPhaden et al., 2015).

These eastward surface zonal currents tend to propagate westward during spring and eastward during fall (Nagura and McPhaden, 2016). The westward phase propagation speed during spring is estimated to be on average between 0.7-1.5 m s^{-1} (Qiu et al., 2009; Nagura and McPhaden, 2010a) and driven primarily by the westward propagating surface zonal winds associated with atmospheric deep convection that moves from the Maritime Continent to the northern Bay of Bengal during Spring (Nagura and McPhaden, 2010b; Nagura and McPhaden, 2016). Equatorial Rossby waves may be also contributing to this westward propagation (Nagura and McPhaden, 2010a). In contrast, during fall, as the deep convection moves southeastward, the surface equatorial zonal winds, and thus surface currents, propagate eastward.

The spring and fall Wyrtki Jets also show considerable intraseasonal and interannual variability. While the intraseasonal variability of the Wyrtki Jets has been shown to be influenced by their own instability (Sengupta et al., 2001, 2007; Han et al., 2004) and local winds (Masumoto et al., 2005, Sengupta et al., 2007, Iskander et al., 2009; Prerna et al., 2019), the interannual variability of the Wyrtki Jets is mainly caused by the anomalous wind forcing along the EIO associated with ENSO (Murtugudde et al., 2000; Gnanaseelan et al., 2012; Joseph et al., 2012) and IOD (Nagura and McPhaden, 2010b; Prerna et al., 2019): IOD weakens (strengthens) the equatorial zonal winds during its positive (negative) phase. While IOD modulates the zonal winds along the entire equator, the influence of ENSO is primarily limited to the eastern part of the EIO (Gnanaseelan et al., 2012). Moreover, it has been shown that these climate modes affect the boreal fall jet more significantly than the boreal spring jet. Recent modelling studies suggest that MJO convection can lead to a stronger spring Wyrtki jet

857 particularly in the eastern EIO. The interannual variability of MJO, therefore, can contribute to the observed interannual

858 variability of this equatorial jet as well (Deshpande et al., 2017; Prerna et al., 2019).

4.3.2 Meridional Circulation

860 Meridional velocity along the equator shows prominent high frequency variability at all depths, but of higher frequencies in

861 the periodic band of 10-20 days with a peak at ~15 days (also referred to as biweekly variability) and in the 20-30 days band

862 with a peak at ~25 days.

863 The existence of the high frequency variability in the meridional velocity is observed all along the EIO and across the entire

864 depth range (Masumoto et al., 2005; David et al., 2011; Chatterjee et al., 2013; Smyth et al., 2014) and is attributed to Yanai

865 waves (also referred to as mixed Rossby-Gravity waves). Unlike Kelvin and Rossby waves, Yanai wave phases can

866 propagate westward or eastward depending upon their frequency, but their group velocity is always eastward. The spatial

867 structure of these waves resembles that of the Tropical Instability Waves (TIWs) of the equatorial Pacific and Atlantic and

868 hence, exhibits convergent meridional heat flux into the equatorial regime (Shinoda, 2010; Smyth et al., 2014). While these

869 waves were first observed in the late 1990s, the establishment of the equatorial RAMA moorings (McPhaden et al., 2009)

870 over the last two decades has provided more insight into these processes. Bi-weekly (10-20 day) is shown to be forced by

871 the direct meridional wind stress (Sengupta et al., 2004) and to some extent by the meridional gradient of the zonal wind

872 stress (Miyama et al., 2006). The 20–30-day band can be excited by off-equatorial barotropic/baroclinic instabilities in

873 addition to direct wind forcing. A detailed review of the biweekly variability is provided in Schott et al. (2009) and hence,

874 in this review, we mainly focus on the 20-30 day variability.

875 While the 20-30-day oscillation in meridional velocity is reported near the surface in the central EIO (David et al., 2011),

876 in the eastern EIO these variabilities are seen only in subsurface layers (100-200 m depth) of the water column (Masumoto

877 et al., 2005). This indicates a possible downward energy propagation of a vertical beam that carries energy to deeper depths.

878 In the central EIO these 20-30-day Yanai waves are excited by horizontal shear between the westward-flowing South

879 Equatorial Current and the eastward-flowing Southwest Monsoon Current during IOD events (Fig. 10a; David et al., 2011).

880 In the western EIO, these waves are primarily driven by cross equatorial meridional winds (Chatterjee et al., 2013). During

881 early boreal summer (June/July), when the Somali current begins to cross the Equator along the western boundary of the

882 basin, it bends offshore to conserve potential vorticity (Schott and McCreary, 2001) and forms a gyral circulation known as

883 the Southern Gyre (Fig. 10a). Subsequently, these swift currents turn barotropically unstable and generate eddy flow that is

884 advected southward to the Equator near the western boundary i.e. at ~50-55°E. They generate a westward propagating cross

885 equatorial flow with a wavelength set by the eddy field which is similar to the wavelength of 20-30 days. Yanai waves and

886 thus excite these frequencies efficiently (Chatterjee et al., 2013).

4.3.4 Equatorial Undercurrents

Unlike in the Pacific and Atlantic Oceans, the Indian Ocean Equatorial Undercurrent (EUC) is a much weaker and seasonally varying transient feature driven by seasonally reversing monsoon winds (Reppin et al., 1999; Schott and McCreary, 2001). The equatorial RAMA moorings have recorded an eastward EUC with a core within the thermocline during boreal winter and spring (Chen et al., 2015, 2019) and occasionally in summer and fall at a depth of 90-170 m water column (Iskandar and McPhaden, 2011). During winter, the eastward EUC is forced by the upwelling Kelvin and Rossby waves that are in turn forced by the easterly winds along the equator; during summer the westward EUC is primarily forced by the eastward pressure gradient generated by the downwelling reflected Rossby waves off the eastern boundary of the basin. On intraseasonal timescales of 30-70-days, the EUC variability is dominated by that of Kelvin and Rossby waves of lower order baroclinic modes (Iskander and McPhaden, 2011).

4.3.4 Equatorial Upwelling

In the absence of persistent equatorial easterlies, the EIO does not show a permanent upwelling in the eastern part as is seen in the Pacific and Atlantic Oceans. In the Pacific and Atlantic Oceans, permanent easterlies drive permanent equatorial upwelling, but in the Indian Ocean, the mean easterlies are weak or absent and permanent upwelling does not exist. Instead, coastal upwelling along the coasts of Sumatra and Java is prominent. During June-October, south-easterly trade winds blow close to the Equator and drive the offshore Ekman transport away from the Sumatra-Java coast (Quadfasel and Cresswell, 1992; Sprintall et al., 1999; Susanto et al., 2001). The associated wind-driven upwelling intensifies as the monsoon progresses, reaching its peak by August and finally weakening by October as the monsoon winds wane. Recent studies suggest that when the easterly winds prevail during summer, upwelling favourable Kelvin waves also contribute to intensifying the equatorial upwelling (Iskander et al., 2009; Chen et al., 2016). During boreal winter-early spring (December-March), an intermittent/weaker subsurface thermocline shoaling is evident (Chen et al., 2016). Subsequently, the prevalence of westerly winds which drive downwelling Kelvin waves depress the thermocline in the east (Susanto et al., 2001; Prerna et al., 2019). Apart from this seasonal cycle, interannual climatic variability associated with ENSO and IOD events (Saji et al., 1999; Vinayachandran et al., 1999) also influences the upwelling intensity in this region (Section 7.2).

4.3.5 Biogeochemical Variability

Much of the current understanding of biogeochemical variability in the equatorial zone of the Indian Ocean is based on satellite ocean color observations and models, augmented by some additional, relatively sparse, in situ measurements. Seasonal climatologies of near-surface chlorophyll concentrations and primary production show a significant seasonality in equatorial waters that is clearly associated with monsoon forcing (Fig. 5[1], Wiggert et al., 2006; Strutton et al., 2015; and see Figs. 5 and 6 in Hood et al., 2017). In general, Chl-*a* concentrations and primary production increase northward from the equator with the lowest concentrations (< 0.1 mg m^{-3}) and rates (<800 mg C m^{-2} d^{-1}) occurring during boreal spring

918   intermonsoon period. During the southwest monsoon, Chl-*a* concentrations and rates of primary production increase in
919   western equatorial waters in response to monsoon-forced mixing and upwelling. However, concentrations and rates in the
920   central and eastern equatorial waters stay relatively low (< 0.5 mg m^{-3}, <800 mgC m^{-2} d^{-1}, respectively). Island wake effects
921   can be seen advecting high chlorophyll water (> 0.5 mg m^{-3}) along the equator from the Chagos-Laccadive ridge at 73°E
922   eastward during the autumn intermonsoon period and westward during spring (see Fig. 1 in Strutton et al., 2015).

923   Well-developed deep Chl-*a* maxima have been observed in the equatorial Indian Ocean along 65°E centered at about 50
924   meters in November-December (George et al., 2013) and along 80°E centered at about 75 meters in August-September
925   (Sorokin et al., 1985). It is unknown whether or not this subsurface Chl-*a* maximum exists along the equator throughout
926   the year, but it is probably present whenever the water column is stratified. Models predict the presence of a deep (60 m)
927   Chl-*a* maximum in eastern Indian Ocean equatorial waters along 87°E (Wiggert *et al*., 2006). This feature is present
928   throughout the year (in the model) except when high chlorophyll surface water is advected into the region during the
929   southwest monsoon.

930   As discussed above, the equatorial Indian Ocean is strongly influenced by physical processes at intraseasonal to interannual
931   time scales (i.e., Wyrtki Jets, MJO and IOD).
932   All of these physical processes influence biogeochemistry. For example, IOD events can significantly increase chlorophyll
933   concentrations and primary production in eastern Indian Ocean equatorial waters (Wiggert *et al*., 2009). In addition,
934   relaxation of an IOD can deplete upper ocean nutrients, decreasing biological productivity (Kumar *et al*., 2012).
935   Biogeochemical responses to the IOD also have significant higher trophic level impacts (Marsac and Le Blanc, 1999).
936
937   Resplandy *et al*. (2009) used a combination of satellite observations and biophysical model simulations to show how
938   chlorophyll concentrations and primary production just south of the equator, in the vicinity of the Seychelles-Chagos
939   thermocline ridge, can be increased by MJO-induced wind mixing and nutrient entrainment. They also concluded that IOD-
940   driven interannual variability of thermocline depth influences the biogeochemical response to MJO, i.e., following IOD
941   events, the deepened nutricline inhibits nutrient input into the mixed layer, and thus decreases the biogeochemical response
942   to MJO.

943   Based on model simulations Wiggert *et al*. (2006) argued that Wyrtki jets depress the thermocline and nitracline along the
944   equator on the eastern side of the basin and, as a result, lower equatorial primary production when they arrive in the spring
945   and autumn. This pattern was observed in a 25 day time series study on the equator at 80.5°E in late 2006 that showed a
946   deepening of the surface layer, nutracline and subsurface Chl-*a* maximum during the autumn Wyrtki jet period (Kumar *et*
947   *al*., 2012).
948

949   Finally, Strutton et al. (2015) examined time-series measurements of near-surface chlorophyll concentration from a mooring
950   that was deployed at 80.5 E on the equator in the Indian Ocean in 2010. These data revealed at least six spikes in chlorophyll
951   from October through December, separated by approximately 2-week intervals.   These events coincided with the
952   development of the fall Wyrtki jets. Measurements from the mooring revealed that the chlorophyll pulses were associated
953   with the increases in eastward surface winds and eastward currents in the mixed layer. Strutton et al. (2015) argued that
954   these observations are inconsistent with upwelling dynamics because eastward winds that cause intensification of the Wyrtki
955   jet should drive downwelling. They concluded that the chlorophyll spikes could be explained by two alternative mechanisms:
956   (1) turbulent entrainment of nutrients and/or chlorophyll from across the base of the mixed layer by wind stirring or Wyrtki
957   jet-induced shear instability or (2) enhanced southward advection of high chlorophyll concentrations into the equatorial zone
958   associated with wind-forced biweekly mixed Rossby-gravity waves.

4.4 Northern Indian Ocean

960   The two main basins of the northern Indian Ocean, the Bay of Bengal (BoB) and the Arabian Sea (AS), are characterized at
961   the surface by remarkably contrasting sea surface salinity with differences of the order of 3 psu (e.g. Chatterjee et al. 2012,
962   Gordon et al. 2016, Hormann et al. 2019) decreasing from west to east (Fig. 4). The fresh surface layer of the BoB is
963   maintained by large freshwater input deriving from direct rainfall over the ocean and river runoff, especially during the
964   South Asian monsoon. The salt balance of the BoB is maintained by the subsurface supply of salt water via the Southwest
965   Monsoon Current (Fig. 10, Vinayachandran et al., 2013). The saltier SSS of the AS is the consequence of an evaporative
966   regime (e.g., Rao & Sivakumar, 2003; Sengupta et al., 2006). A reversing monsoonal near-surface circulation (Fig. 10 a,b)
967   plays a central role in the exchanges of freshwater and heat between the BoB and the AS (McCreary et al. 1993, Hormann
968   et al. 2019).

969   Recent multi-year deployments of satellite tracked surface drifters drogued at 15 m depth (Wijesekera et. al, 2016,
970   Centurioni et al. 2018) have helped to better constrain the amplitude and structure of the circulation and the exchange
971   processes between the two basins, and to refine the findings reported by other authors (e.g. Schott and McCreary, 2001).
972   Additionally, implementation of a moored buoy network along the slope and shelf of the Indian coast has helped significantly
973   in enhancing our understanding of the east India Coastal Current (EICC) and west India Coastal Current (WICC) in the east
974   and west coast of India, respectively (Mukherjee et al., 2014; Amol et al., 2014; Mukhopadhyay et al., 2020; Anya et al.
975   2020).

4.4.1 Bay of Bengal

977   In a climatological sense, the main features of the near-surface circulation of the western BoB (Figs. 10a and 10b) are the
978   reversing EICC, the Southwest/Northeast Monsoon Current (SMC/NMC) and the seasonally variable Sri Lanka Dome. The
979   eastern side of the BoB, extending into the Andaman Sea, is characterised by a sluggish circulation.

4.4.1.1 Southwest/Northeast Monsoon Currents

During the boreal summer SW monsoon, the Southwest Monsoon Current (SMC, Fig. 10a) flows eastward around the Indian subcontinent supplying salty water from the Arabian Sea to the fresher Bay of Bengal (e.g., Jensen, 2001; Jensen et al., 2016; Vinayachandran et al., 2013; Wijesekera et al., 2015, 2016). During the winter monsoon, the Northeast Monsoon Current (NMC, Fig. 10b) reverses the flow carrying fresher water into the Arabian Sea. Figure 13 provides a snapshot from two operational forecast systems, the Coupled Ocean-Atmosphere Mesoscale Prediction System (COAMPS) and the 1/12° HYbrid Coordinate Ocean Model (HYCOM), of the NMC flow and route for freshwater to enter the Arabian Sea (Wijeskera et al., 2015).
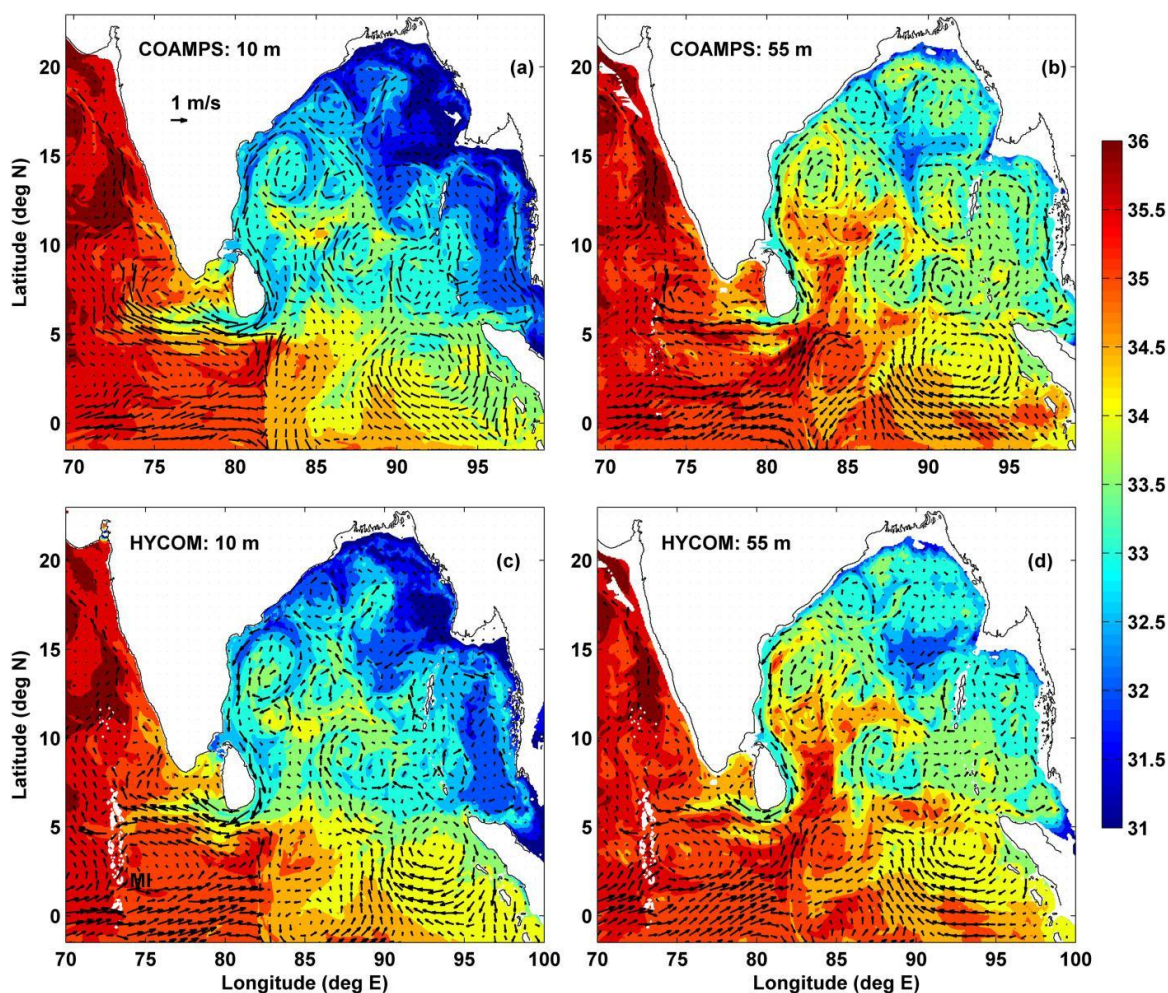
Figure 13: (top) COAMPS velocity vectors (arrows) and salinity (psu) (color shading) at (a) 10 m and (b) 55 m on 18 December 2013. (bottom) HYCOM velocity vectors (arrows) and salinity distribution (psu) (color shading) at (c) 10 m, and (d) 55 m. MI denotes Maldives Island chain. Taken from Wijeskera et al. (2015).

A more recent study has found that the origins of the Arabian Sea high salinity water are specifically from the western Arabian Sea and western Equatorial Indian Ocean, and they reach the Bay of Bengal via a combination of the Indian Ocean EUC and the SMC (Sanchez-Franks et al., 2019; Section 8.2). Changes in the supply of salty water to the Bay of Bengal varies interannually due to the strength in the equatorial currents, forced by the local wind field and ENSO (Sanchez-Franks et al., 2019), and is expected to influence the salinity budget of the Bay of Bengal (Vinayachandran et al., 2013) and thus modulate SST variability (Jensen et al., 2016; Li et al., 2017; Vinayachandran et al., 2013; Webber et al., 2018).

4.4.1.2 East Indian Coastal Currents (EICC)

The EICC forms the western boundary current of the Bay of Bengal and plays an important role in the basin-scale heat and salt budget of the Indian Ocean, and hence in determining the local climate (Shenoi et al, 2002), biological processes (Madhupratap et al, 2003; Vinayachandran et al, 2005; Naqvi et al, 2006; Dileepkumar, 2006; McCreary et al, 2009) and marine fisheries (Vivekananda and Krishnakumar, 2010) of this region. It reverses its direction seasonally north of 10°N in response to a combination of local alongshore winds, remote alongshore winds in the eastern BoB, remote forcing from the equatorial Indian Ocean and the interior Ekman pumping of the basin (Shankar et al., 1996; McCreary et al., 1996; Vinayachandran et al., 1996; Mukherjee et al., 2017). The EICC is generally equatorward south of 10°N throughout the year. While local winds dominate summer and winter, the remote forcing dominates during the inter-monsoon periods (Shankar et al., 1996; McCreary et al., 1996; Suresh et al., 2013).

Climatological ship-drift and hydrographic data suggest the EICC flows poleward during February-September (Shetye et al., 1993) and turns equatorward during November-January (Shetye et al., 1996) (Fig. 10). During boreal spring (March-May), the EICC is strongest with a magnitude exceeding 100 cm/s and shows unidirectional reasonably stronger currents even in the deeper depths to about 150 m. This is the time when it forms the western boundary current of a cyclonic basin-wide gyre of the BoB. At this time, the local alongshore winds are weakest and the stronger EICC is primarily forced by the interior anticyclonic Ekman pumping over the basin (McCreary et al., 1996; Shankar et al., 1996; Vinayachandran et al., 1996; Mukherjee et al., 2017). During summer, the EICC is weaker and is restricted to within the top 70 m of the water column. The poleward flow is generally limited to the central part of the coast between 10-18°N and often switches to short pulses of poleward currents along the coast (Mukherjee et al., 2018; Francis et al., 2020). The poleward flow is driven by local winds, but the response of the interior cyclonic Ekman pumping and equatorial winds driving an opposite flow along the coast causes a weaker poleward EICC than in spring (McCreary et al., 1996; Vinayachandran et al., 1996; Shankar et

1019   al., 2002). The basin-scale gyre also disappears in summer and the EICC then consists of several eddies along the coast. The

1020   EICC turns equatorward during November-January (Shetye et al., 1996).

1021   Along the east coast of India, ADCP observations reveal that variability in alongshore currents is dominated by seasonal

1022   timescales Mukhopadhyay et al. (2010a). While the annual cycle is driven by local alongshore winds and interior Ekman

1023   pumping, the semiannual cycle is the result of asymmetry in the monsoon and equatorial forcing (Mukherjee et al., 2018).

1024   The seasonal reversal of the EICC is apparent all along the east coast, suggesting that the canonical directions of the EICC

1025   are a robust feature and explaining their existence in ship-drift climatologies (Cutler and Swallow, 1984; Mariano et al.,

1026   1995). In the annual band, upward phase propagation is evident all along the coast, suggesting the dominance of remote

1027   forcing over local alongshore winds in driving the EICC.

1028   Near-surface alongshore currents also display significant 120 day and intraseasonal variability. The magnitude of the 120

1029   day variability is generally weaker than the semiannual period, particularly in the southern part of the coast. As for the

1030   annual period, upward phase propagation is also evident for the semiannual and 120 day period, except at Cuddalore where

1031   downward phase propagation is common during summer and winter months (Mukherjee et al., 2014; Mukhopadhyay et al.,

1032   2020). Further, unlike annual and semiannual periods, the 120 day and intraseasonal variability decorrelate along the coast

1033   indicating that these high frequencies are dominated by local responses rather than remote forcing (Mukherjee et al., 2018;

1034   Mukhopadhyay et al., 2020a).

1035   **4.4.1.3 Undercurrents**

1036   ADCP observations along the east coast of India suggest that during summer and winter, when the near-surface current is

1037   shallow, the EICC often exhibits undercurrents along the continental slope. As the EICC is deeper in the north, the

1038   undercurrent is observed at a depth of 100-150 m and can extend up to 700 m. However, in the south undercurrents are seen

1039   at relatively shallow depths of about 70-75 m (Francis et al., 2020). Moreover, while these undercurrents are observed

1040   throughout the coast, they are much more prominent and more frequent in the southernmost station of the coast, i.e. at

1041   Cuddalore (Fig. 14, Mukherjee et al., 2014; Mukhopashyay et al., 2020).
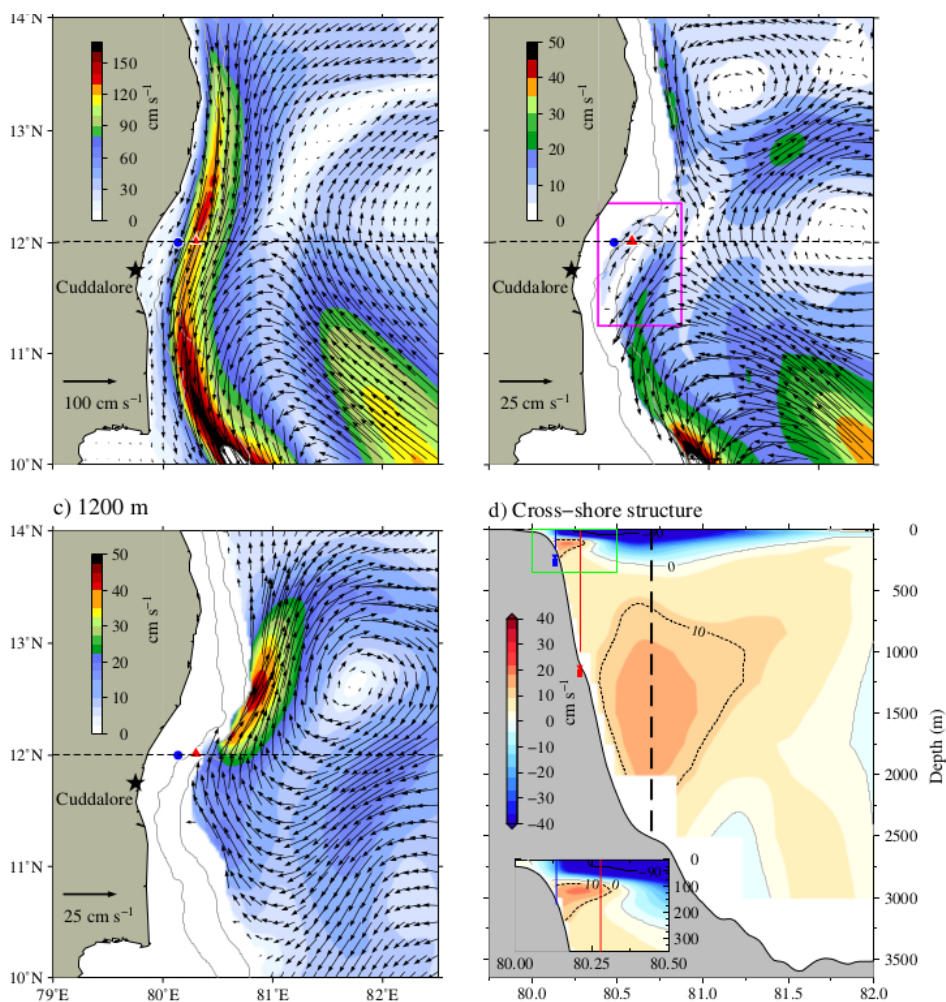
Figure 14: Circulation pattern in the southwestern Bay of Bengal at (a) surface (b) 200 m and (c) 1200 m on 15 November 2014. Vectors show the current direction, and overlaid is the current magnitude (cm s−1). Note that the scales of current vectors and color bar are different at each subplot. Blue circle (red triangle) represents the location of ADCP deployed on the shelf (slope) off Cuddalore. Dashed black line represents the 12°N latitude. Continuous gray lines represent the 100 m and 1000 m bathymetric contours. Rectangular box (magenta) indicates the subsurface eddy near the shelf break. (d) Cross-shore structure of alongshore currents across 12°N. Dashed black vertical line shows the core of the undercurrent, and red (blue) vertical lines shows the location of ADCP mooring on the slope (shelf). Inset plot is the zoomed view of shelf break region indicated by green box (Reproduced from Francis et al., 2020).

The prominent upward phase propagation of the annual signal in the subsurface layers, particularly in the southern stations, suggests downward propagation of energy and is thereby attributed as one of the main causes of the undercurrents

(Mukherjee et al., 2014). A recent modelling study suggests that the wintertime undercurrent off Cuddalore consists of two separate subsurface anticyclonic eddy circulations: a shallow small scale circulation at a depth range of 100-200 m and a broader and deep flow below 500 m depth off the continental slope (Francis et al., 2020). The shallow subsurface anticyclonic eddy was found to spin off from the zonal shear of the mean near-surface EICC along the shelf break (Fig. 14). These eddies exhibit high frequency fluctuations and have 20-30 km length scales. Since the zonal share of the EICC is primarily linked to the strength of the EICC itself, the variability and strength of this undercurrent is also linked with the EICC.

4.4.1.4 Role of EICC in salt transport

The EICC starts flowing southward north of 15°N as early as June (Fig. 10a) and eventually develops into a strong coastal current during the winter monsoon (November through January) that extends all the way south of Sri Lanka and connects the northernmost part of the bay, where large amounts of freshwater are discharged by the Indian river system, with the Arabian Sea (AS; Fig. 4, Fig. 13). For this reason, the EICC is regarded as one of the possible pathways responsible for the exchange of salt between the AS and the BoB (Hormann et al. 2019), along with the SMC (Fig. 10a; Jensen, 2001; Jensen et al., 2016; Vinayachandran et al., 2013, 2018; Webber et al., 2018), which transports saline water north into the BoB during June-September. Some of this saline water is transported directly around the tip of India (Fig. 10a), yet there is also a role for transport along the equator from the western tropical Indian Ocean and the western AS (Sanchez-Franks et al., 2019). In February, the off-shore current south of Sri Lanka is still flowing westward into the AS but the EICC north of 10°N starts flowing northward, reaches its maximum strength in April and stops south of 10°N by June, joining the offshore limb of a cyclonic circulation further north that fills the northern Bay from June through August.

4.4.1.5 Sri Lanka Dome

The Sri Lanka Dome (Vinayachandran et al. 1999; Schott and McCreary, 2001; Wijesekera et. al, 2016, Cullen and Shroyer, 2019) is mainly visible as a closed anticyclonic (clockwise) eddy in the near-surface geostrophic current velocity field starting in May and lasting through October (Fig. 15c). It is a recurring upwelling dome that forms east of Sri Lanka between 5-10°N, 83–87°E. The SLD is embedded within the Southwest Monsoon Current (SMC) system (Gadgil, 2003) enhances the SMC exchange from the Arabian Sea to the Bay of Bengal (Anutaliya et al., 2017). Upwelling associated with the SLD influences the vertical exchange of water properties, enhances biological productivity, and cools sea surface temperature (SST) which affects local atmospheric convection (Vinayachandran et al., 2004; de Vos et al., 2014).
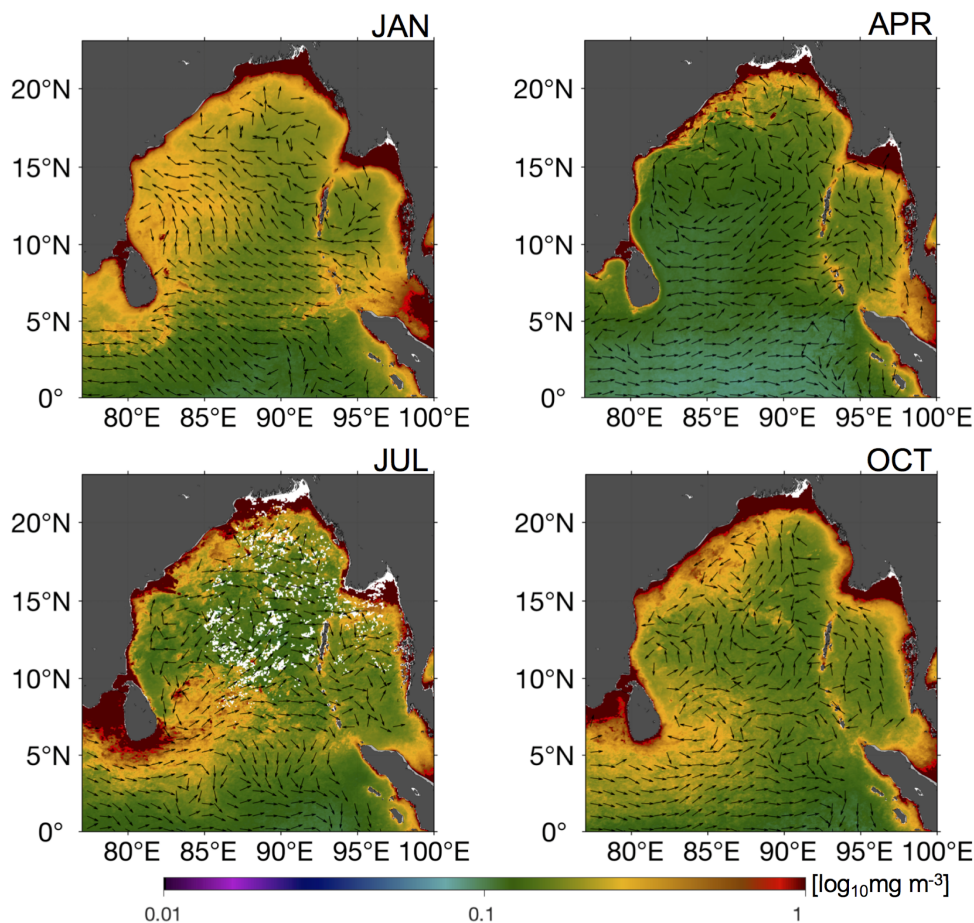
Figure 15: Climatology (2002-2018) of chlorophyll-a concentrations (colormap) and current velocities (arrows) in the Bay of Bengal for (a) January (b) April (c) July (d) October. Chlorophyll climatology was obtained from the MODIS-Aqua product and current velocities were obtained from the third-degree Ocean Surface Current Analysis Real-time (OSCAR) product.

4.4.1.6 Biogeochemical Variability

In the Bay of Bengal, large inputs of freshwater from rivers give rise to enhanced stratification that inhibits upwelling and wind-mixing and therefore nutrient enrichment of surface waters (Kumar et al., 2002; Vinayachandran et al., 2002; Madhupratap et al., 2003; Vinayachandran, 2009). Nonetheless, increased productivity is observed along the coast primarily in association with riverine nutrient inputs (Vinayachandran, 2009). These nutrients stimulate diatom blooms (Sasamal et al., 2005) that give rise to significant increases in Chl-*a* concentration (~ 30–100 mgChla m^{-2}) and production (~ 0.55–1 gC m^{-2} d^{-1}) near the coast (Gomes et al., 2000; Fig. 15). This high Chl-*a* river water flows either along the coast or offshore, up

1093 to several hundred kilometers, depending on the coastal current pattern (Vinayachandran, 2009). Along the Indian coast,

1094 the flow of Chl-*a*–rich water is determined by the EICC, which flows northward during the spring intermonsoon period and

1095 Southwest Monsoon and southward during the autumn intermonsoon and Northeast Monsoon (Fig. 15). When the EICC

1096 meanders seaward from the Indian coast, it leads to offshore increases in high chlorophyll water. It should also be noted

1097 that during the spring intermonsoon and Southwest Monsoon the northward-flowing EICC is upwelling favorable, which

1098 may contribute to increases in Chl-*a* concentration and primary production along the Indian coast (Hood et al., 2017)

1099

1100 In addition, elevated productivity is observed further offshore in the southwestern part of the Bay of Bengal during the

1101 Northeast Monsoon (Vinayachandran and Mathew, 2003; Vinayachandran, 2009). Modeling studies suggest that these

1102 elevated surface Chl-*a* concentrations are caused by wind-driven entrainment, not only of subsurface nutrients, but also of

1103 phytoplankton from the subsurface chla maximum that is present during the autumn intermonsoon period (Vinayachandran

1104 et al., 2005). In contrast, productivity near the coast is suppressed during the Northeast Monsoon when the EICC flows

1105 equatorward (Fig. 14). Presumably, this is due to a combination of the downwelling-favorable currents and winds. However,

1106 primary production over the shelf in the northern part of the Bay increases during the Northeast Monsoon (Gomes et al.,

1107 2000; Fig. 15), possibly due to river nutrient inputs (Vinayachandran, 2009) and / or wind-stress and buoyancy-driven

1108 nutrient entrainment as is observed in the northern Arabian Sea during the Northeast Monsoon (Wiggert et al., 2000; 2005;

1109 Hood et al., 2017).

1110

1111 Subsurface Chl-*a* maxima are observed in the Bay of Bengal developing during all seasons whenever and wherever wind

1112 forcing and/or currents are insufficiently strong to upwell or entrain them into the surface layer (Sarma and Aswanikumar,

1113 1991; Murty et al., 2000; Sarjini and Sarma, 2001; Kumar et al., 2007). During the intermonsoon periods the Bay of Bengal

1114 transitions to more oligotrophic conditions with relatively low surface chlorophyll concentrations (< 0.6 mg/m^3; Fig. 15)

1115 and production rates (< 700 mgC m^{-2} d^{-1}; see Fig. 6 in Hood et al., 2017). *Trichodesmium erythraeum* blooms have been

1116 observed during the intermonsoon periods along with high abundances of *Synechococcus* and heterotrophic dinoflagellates

1117 (Sarjini and Sarma, 2001; Jyothibabu et al., 2008). In offshore waters subsurface chlorophyll maxima are generally located

1118 between 40 and 70m in autumn and 60 and 90m in spring (Kumar et al., 2007). These deep Chl-*a* maxima tend to shoal

1119 near the coast (Sarma and Aswanikumar, 1991; Murty et al., 2000) and their depth and chlorophyll concentrations are

1120 strongly influenced by eddies (Kumar et al., 2007).

1121

1122 Strong upwelling also occurs along the southern coast of Sri Lanka during the Southwest Monsoon (Vinayachandran, 2004;

1123 2009; de Vos et al., 2014). Satellite SST and chlorophyll images reveal dramatic eastward advection of cool (< 28° C)

1124 chlorophyll rich upwelled water by the SMC (Vinayachandran, 2004; 2009; de Vos et al., 2014). Chlorophyll-rich waters

1125 from the southwestern coast of India are also advected by the SMC towards Sri Lanka during the Southwest Monsoon

1126 (Vinayachandran, 2004; 2009; Strutton et al., 2015). Surface chlorophyll concentrations and rates of primary production

1127   along the southern coast of Sri Lanka can exceed 10 mgChla m^{-3} (de Vos et al., 2014) and 1000 mgC m^{-2} d^{-1} (see Fig. 6 in

1128   Hood et al., 2017), respectively, during the Southwest Monsoon, compared to much lower concentrations and rates during

1129   the Northeast Monsoon when the NMC flows westward (de Vos et al., 2014; Hood et al., 2017). Vinayachandran (2004;

1130   2009) attribute the productivity response during the Southwest Monsoon to nutrient enrichment from coastal upwelling

1131   driven by monsoon winds. Presumably, these high chlorophyll concentrations and production rates are associated with

1132   diatom blooms. This elevated productivity extends to the east of Sri Lanka during the peak of the Southwest Monsoon

1133   (Vinayachandran et al., 1999; Vinayachandran, 2004; 2009). This eastward extension into the southern Bay of Bengal

1134   occurs along the path of the SMC (Vinayachandran et al., 1999) and is associated with upward Ekman pumping east of Sri

1135   Lanka. This Ekman pumping also leads to the formation of the aforementioned Sri Lanka Dome (Vinayachandran and

1136   Yamagata, 1998).

1137

1138   **4.4.2 Arabian Sea**

1139   As for the Bay of Bengal (BoB), the Arabian Sea (AS) near surface circulation is also driven primarily by the seasonally

1140   reversing monsoon winds. The AS is connected to the BoB through the passage between the southern tip of India and the

1141   equatorial wave guide, and to the southern hemisphere by the cross equatorial flow via the Somali current system. The

1142   Somali current (Fig. 10) forms one of the western boundary currents of the AS. Another major boundary current system is

1143   along the west coast of India, the WICC (Fig. 10), which transports heat and salt from the northern Arabian Sea to the BoB,

1144   and vice-versa. Recent observations (Chatterjee et al., 2012) and modelling studies (Shankar et al., 2015; Vijith et al., 2016)

1145   indicate that the northern extent of the WICC reaches up to 20ºN during the winter monsoon, carrying fresher BoB water to

1146   the northern latitudes and modulating the wintertime convection there. In this section we will first discuss some recent

1147   developments of the Somali current system and then the WICC.

1148   **4.4.2.1 Somali current System**

1149   The Somali Current is a seasonally reversing western boundary current and is often composed of discontinuous non-linear

1150   eddy driven flows. During summer it flows poleward and the upwelling here is nearly as large as for the eastern boundary

1151   upwelling regimes of the Pacific and Atlantic Oceans (See Schott and McCreary, 2001 for a detailed review). Unfortunately,

1152   owing to the piracy issue, direct in-situ observations are very rare in this region and mostly date back to the early 1960's

1153   and 1970's. Hence, the scientific community has mostly relied on numerical model simulations to enhance understanding

1154   of this region over the last few decades.

1155   Recent modelling studies suggest that during the summer monsoon, unlike other western boundary currents, the Somali

1156   Current system can be divided into three dynamically distinctive regions (Wang et al., 2018; Chatterjee et al., 2019): northern

1157   (north of 8ºN), central (3-8ºN) and the southern (south of 3ºN) part. The northern and southern parts are driven by the large

1158   anti-cyclonic gyres called the Great Whirl (GW) and the southern Gyre (SG), respectively (Fig. 10a). Local southwesterly
1159   alongshore winds known as the Findlater Jet (Findlater, 1969) drives Ekman transport all along the Somali coast (Schott
1160   and McCreary, 2001) with varied magnitude which is strongest in the southern part, and significantly weakens northward
1161   (Chatterjee et al., 2019). The wind stress forcing leads to Ekman Pumping in the central Arabian Sea, setting up a bowl-
1162   shaped mixed layer and warming at the 100 m level. Ekman downwelling velocities are strongest in the northern part and
1163   likely contributes to the formation of the Great Whirl front which upwells cold subsurface water in this part of the coast.
1164   The central part, in contrast, is mainly driven by the local winds and remotely forced Rossby waves. In fact, the annual
1165   Rossby waves radiated out of the southwestern coast of Sri Lanka seem to play a major role in the reversal of currents to
1166   poleward flow in the northern part of the Somalia coast as early as in mid April. This reversal likely initiates the generation
1167   of the Great Whirl (Beal and Donohue, 2013; Vic et al., 2014), a month in advance of the strong northeastward Findlater Jet
1168   commences along the Somali coast. As the monsoon progresses, these downwelling favourable Rossby waves oppose the
1169   coastal Ekman upwelling and thereby start to weaken the upwelling all along the coast. Moreover, as the alongshore winds
1170   peak, this favours enhanced mixing at the bottom of the mixed layer, which deepens the thermocline further. This process
1171   is more conspicuous in the central part of the coast, where the depth of the 22ºC isotherm deepens by about 30-40 m from
1172   June to August (Chatterjee et al., 2019). By this time, the upwelling becomes limited to the northern part of the coast along
1173   the Great Whirl front of the Somali region.

1174   **4.4.2.2 West India Coastal Current (WICC)**

1175   The WICC reverses its direction annually: flowing equatorward (upwelling favourable) during the summer monsoon (i.e.
1176   May to September; Fig. 10a) and poleward (downwelling favourable) during the winter monsoon (i.e. November to
1177   February; Fig. 10b). The equatorward flow during the summer characterises the WICC as a classical eastern boundary
1178   current (Shetye and Shenoi, 1988). Interestingly, as the monthly mean alongshore winds off the west coast of India are
1179   unidirectional (equatorward) throughout the year, the surface currents flow against the winds during the winter driven by
1180   coastally-trapped Kelvin waves forced remotely in the BoB and along the east coast of India (McCreary et al., 1993; Shankar
1181   and Shetye, 1997; Shankar et al., 2002; Suresh et al., 2016). Recent observations based on satellite data and alongshore
1182   ADCP moorings reveal strong interannual variability of this seasonal cycle. Vialard et al. (2009), based on a short ADCP
1183   record during 2006-2008, reported an absence of seasonal cycle off Goa and they attributed this absence to the radiation of
1184   Rossby waves south of the critical latitude. However, later as the longer record of ADCP data became available, a clear
1185   seasonal cycle in the WICC became evident with weaker amplitudes in the south, stronger poleward (Amol et al., 2014).

1186   The WICC also shows significant intraseasonal variability at times, particularly during boreal winter, exhibiting much
1187   stronger energy in the intraseasonal band than in the seasonal band (Vialard et al., 2009; Amol et al., 2014). Unlike the
1188   seasonal cycle, intraseasonal variability is stronger in the south and weakens poleward. Vialard et al. (2009) attributed this
1189   intraseasonal variability to the atmospheric MJO forcing. Recently, a modelling study suggested that interception of the

1190   intraseasonal equatorial Rossby waves by the southern tip of India and Sri Lanka excites coastal Kelvin waves which

1191   contribute significantly (~60–70%) to the intraseasonal variability along the west coast (Suresh et al., 2013). A satellite sea

1192   level study by Dhage and Sturb (2016) confirmed the model-based findings of Suresh et al. (2013) and revealed that large

1193   scale winds from the south of India and Sri Lanka also contribute to the coastal signals along the west coast of India.

1194   Another striking feature observed in these ADCP data is the clear signature of upward phase propagation in all timescales

1195   during both monsoon seasons. This upward phase propagation is more conspicuous for the seasonal period than for the

1196   intraseasonal. As a result, the phase of the surface currents often tends to be opposite that in the subsurface layers (Amol et

1197   al., 2014). Moreover, it is found that the strength of this undercurrent intensifies northward along the west coast with

1198   strongest undercurrent off Mumbai and the weakest off Kanyakumari (southernmost point of Indian mainland), indicating

1199   a possible downward propagation of energy along the ray path as suggested earlier by Nethery and Shankar (2007). Since

1200   the ray angle (θ) depends on the frequency (σ) and stratification (N_b) according to $\theta = \sigma / N_b$ (McCreary, 1984; Nethery and

1201   Shankar, 2007) the angle the beam makes from the horizontal is deeper for the intraseasonal band than for the seasonal. As

1202   a result, intraseasonal beams propagate energy deeper layers into the water column. Therefore, while the WICC shows some

1203   coherence along the coast in the seasonal time scale, it completely decorrelates horizontally for the intraseasonal period.

1204   **4.4.2.3 Biogeochemical Variability**

1205   During the southwest monsoon, the western side of the northern Indian Ocean transitions to a eutrophic coastal upwelling

1206   system in response to the upwelling favorable winds and currents (Wiggert et al., 2005; Hood et al., 2017 and references

1207   cited therein; Fig. 5[1] ; see also Figs. 5 and 6 in Hood et al., 2017). These changes can be seen in ocean color data as

1208   substantial increases in chla concentrations along the coasts of Somalia, Yemen and Oman (e.g., Brock and McClain, 1992;

1209   Banse and English, 2000; Kumar et al., 2000; Lierheimer and Banse, 2002; Wiggert et al., 2005; George et al., 2013; Hood

1210   et al., 2017). Chlorophyll-a concentrations in the western Arabian Sea can exceed 40 mgChla m^{-2} during the southwest

1211   monsoon with production rates > 2.5 gC m^{-2}d^{-1} (Marra et al. 1998; and see also Fig. 6 in Hood et al., 2017). However, the

1212   environmental conditions vary significantly between the eutrophic coastal zones to the west and the oligotrophic open ocean

1213   waters offshore that are influenced by wind-curl induced downwelling to the southwest of the Findlater Jet (Lee et al., 2000).

1214   The surface nitrate and Chl-a concentrations decline dramatically from > 10 to < 0.02 µM and from > 1.0 to < 0.2 mgChla

1215   m^{-3}, respectively, from the west coast to open ocean in the Arabian Sea (Brown et al., 1999; Wiggert et al., 2005; Hood et

1216   al., 2017). In general, the phytoplankton community structure transitions to larger cells (diatoms) during the southwest

1217   monsoon in the western Arabian Sea (Brown et al., 1999; Tarran et al., 1999; Shalapyonok et al., 2001). However, small

1218   primary producers remain important, even in areas strongly influenced by coastal upwelling (Brown et al., 1999). In

1219   contrast, during the oligotrophic spring and fall intermonsoon periods, surface waters in the western Arabian Sea are

1220   dominated by picoplankton (Garrison et al., 2000). Subsurface Chl-a maxima are observed between 40 and 140 meters in

1221   the central southeastern Arabian Sea during all seasons (Gunderson et al., 1998; Goericke et al., 2000; Ravichandran et al.,

1222   2012), at times occurring in layers below the oxyclines of the oxygen minimum zone (Georicke et al., 2000). These features

1223   are strongly influenced by mesoscale features (Gundersen et al., 1998).

1224

1225   During the southwest monsoon off Oman and Somalia, the presence of the topographically-locked eddies generate strong

1226   offshore flows that advect high nutrient, high Chl-*a* concentrations and coastal phytoplankton communities hundreds of

1227   kilometers offshore (Keen et al., 1997; Latasa and Bidigare, 1998; Manghnani et al., 1998; Gundersen et al., 1998; Hitchcock

1228   et al., 2000; Lee et al., 2000; Kim et al., 2001). These advective effects can be seen, for example, in association with the

1229   Great Whirl off the coast of northern Somalia (Hitchcock et al., 2000) and in the filaments that develop off the Arabian

1230   Peninsula during the southwest monsoon (Wiggert et al. 2005; Hood et al., 2017). In contrast, during the northeast monsoon,

1231   the circulation and winds transition to downwelling favourable. During the northeast monsoon, cold dry northeasterly winds

1232   from southern China and the Tibetan Plateau flow across the northern Arabian Sea. The sheer from these winds, combined

1233   with surface cooling and buoyancy-driven convection, drive mixing and entrainment of nutrients that, in turn, promote

1234   modest increases in chlorophyll and primary production over the northern Arabian Sea (Wiggert et al., 2000; Wiggert et al.,

1235   2005; Fig. 5[2] ; see also Figs. 5 and 6 in Hood et al., 2017). These increases in Chl-*a* have been associated with increased

1236   diatom abundance (Banse and McClain, 1986; Sawant and Madhupratap, 1996). In the last decade, however, there appears

1237   to have been a shift in the composition of winter phytoplankton blooms in the northern and central Arabian Sea from diatom

1238   dominance to blooms of a large, green mixotrophic dinoflagellate, *Noctiluca scintillans* (Gomes et al., 2014; Goes et al.,

1239   2020).

1240

1241   During the southwest monsoon, the upwelling-favorable WICC induces upwelling along the west coast of India, which

1242   increases Chl-*a* concentrations by more than 70% compared to the central Arabian Sea (Kumar et al., 2000; Naqvi et al.,

1243   2000; Luis and Kawamura, 2004; Hood et al., 2017). However, these increases in Chl-*a* and their offshore extent are modest

1244   compared to the western Arabian Sea (Fig. 5[3] and see also Fig. 5 in Hood et al., 2017). The increased Chl-*a* concentrations

1245   near the coast are associated with increases in diatom abundance (Sawant and Madhupratap, 1996). In contrast, during the

1246   northeast monsoon the WICC is downwelling-favorable and tends to suppress primary production off the southwestern coast

1247   of India. The depletion of nutrients in this region during the northeast monsoon coincides with blooms of *Trichodesmium*

1248   and dinoflagellate species (Parab et al., 2006; Matondkar et al., 2007) resulting in the extremely high rates of nitrogen

1249   fixation (Gandhi et al., 2011, Kumar et al., 2017). However, as discussed above, further north and offshore, nutrient

1250   entrainment enhances phytoplankton biomass and primary production during the northeast monsoon (Wiggert et al., 2000;

1251   McCreary et al., 2001; Luis and Kawamura, 2004; Gomes et al., 2014; Goes et al., 2020; Fig. 5[4]). Near-surface Chl-*a* and

1252   primary production off the west coast of India (estimated from satellite ocean color measurements) increases from ~9 to 24

1253   mgChla m^{-2} and from ~1 to 2.25 g C m^{-2} d^{-1}, respectively, from winter to the summer monsoon (Luis and Kawamura, 2004;

1254   Fig. 5[5] and see also Figs. 5 and 6 in Hood et al., 2017). The elevated productivity during the southwest monsoon is

1255   modulated by the aforementioned coastal Kelvin waves that originate from the Bay of Bengal and propagate along the West

1256   Indian Shelf, modifying circulation patterns and upwelling (Luis and Kawamura, 2004).

1257

1258   Satellite ocean color observations suggest that Chl-*a* concentrations remain low all year-round in the Laccadive Sea in spite

1259   of the transition from upwelling circulations (anti-cyclonic) during the southwest monsoon to downwelling circulations

1260   (cyclonic) during the northeast monsoon (Lierheimer and Banse, 2002; Fig. 5[6]). This suggests that the upwelling-

1261   enhanced productivity off the west coast of India during the southwest monsoon is largely restricted to the coastal zone.

1262   There are, however, sporadic zonal increases in Chl-*a* concentration that extend into the Laccadive Sea (Lierheimer and

1263   Banse, 2002). It is not known whether or not there are cryptic subsurface phytoplankton blooms during the southwest

1264   monsoon associated with the Laccadive Low.

1265   **5 Inter-ocean exchange**

1266   **5.1 Indonesian Throughflow**

1267   **5.1.1 General features**

1268   The Indonesian Throughflow (ITF) transfers low-salinity tropical waters from the Pacific to the Indian Ocean via the

1269   Indonesian seas (Fig. 10). The ITF is the only tropical oceanic pathway that links ocean basins and plays an important role

1270   in the global ocean circulation and climate system (Sprintall et al., 2014; 2019). The simultaneous measurements in the exit

1271   channels of the ITF from the International Nusantara Stratification and Transport (INSTANT) program during 2004-2006

1272   (Gordon et al., 2008; Sprintall et al., 2009) suggested that the ITF has a mean transport of 15 Sv into the Indian Ocean. The

1273   ITF pathway is composed of many narrow channels within the Indonesian seas, among which about 80% of the total ITF is

1274   through the Makassar Strait (Fig. 10, Gordon et al., 2008, 2010). The remaining passages include the Maluku Sea, Lifamatola

1275   Passage, Karimata Strait and Sibutu Passage (Fang et al., 2010; Gordon et al., 2012; Susanto et al., 2013).

1276   **5.1.2 Variability, dynamics and influence**

1277   The interannual variability of the ITF is mainly dictated by the ENSO-related wind forcing through the Pacific waveguide

1278   (e.g., Hu and Sprintall, 2016), but the IOD occasionally offsets the Pacific ENSO influences through the Indian Ocean wind

1279   variability and Indian Ocean waveguide (Sprintall and Révelard, 2014; Liu et al. 2015; Feng et al., 2018). Strong wind

1280   forcing over the equatorial Indian Ocean triggers equatorial Kelvin waves and influences the ITF variability on intraseasonal,

1281   semi-annual and interannual time scales (Drushka et al., 2010; Pujiana et al., 2013; Shinoda et al., 2012). Kelvin waves

1282   through the Indian Ocean waveguide are suggested to influence the interannual variability in the tropical Pacific Ocean

1283   (Yuan et al., 2013).

The ENSO cycle also influences the outflowing ITF transport through the salinity effect in the downstream buoyant pool, which contributes to about 36% of the total interannual variation (Hu and Sprintall, 2016). Fresh anomalies in the buoyant pool can be as large as 0.2 in practical salinity averaged over the upper 180 m of the water column (Phillips et al. 2005). Such salinity anomalies can further strengthen the volume transport of the LC (Feng et al., 2015a). The Inter-decadal Pacific Oscillation/Pacific Decadal Oscillation (IPO/PDO), through modulations of decadal wind stress in the tropical Pacific has also directly influenced the strength of the ITF (Feng et al., 2011; Hu et al., 2015; Mayer et al., 2018), as well as its heat and freshwater transports, causing changes in upper ocean heat content variations in the southern Indian Ocean (Feng et al., 2010; Schwarzkopf and Böning, 2011; Nidheesh et al., 2013; Sprintall, 2014; Lee et al., 2015; Nieves et al., 2015; Du et al., 2015; Ummenhofer et al., 2017). During, the negative IPO phase, such as the climate change hiatus period in 1998-2012, enhanced trade winds in the Pacific strengthened the ITF volume and heat transport into the Indian Ocean, driving a rapid warming trend in the Southern Indian Ocean (England et al., 2014; Nieves et al., 2015; Lee et al., 2015; Liu et al., 2015, Zhang et al., 2018). However, contributions from air-sea exchanges (Jin et al. 2018a,b) have also been suggested. Furthermore, using a combination of theory, ocean reanalyses, OGCM simulations, and coupled climate model simulations, Jin et al. (2018a,b) found eastern and western Indian Ocean heat content to be affected by remote Pacific forcing through two distinct mechanisms via oceanic influences transmitted through the ITF and through the atmospheric bridge, respectively. The intensified freshwater input within the Maritime Continent during the past decade is found to strengthen the ITF and its heat and freshwater transports into the Indian Ocean, causing significant warming and freshening trends and accelerated sea-level rise in the eastern Indian Ocean (Hu and Sprintall, 2017a, 2017b; Zhang et al., 2018; Jyoti et al., 2019). The decadal enhancement of the ITF transport has built up upper ocean heat content anomalies in the southeast Indian Ocean and increased the likelihood of marine heatwaves off the west coast of Australia (Feng et al., 2015b; Section 6.4).

5.2 Agulhas Leakage

5.2.1 General features

The Agulhas Current, the western boundary current of the southern Indian Ocean gyre, (Fig. 10), flows southward along the South African coastline. At the tip of Africa, the current retroflects with most of the flow heading eastwards, on the northern edge of the ACC, and recirculates back into the Indian Ocean. Around 20-30% of the Agulhas Current enters the Atlantic Ocean as Agulhas leakage in the form of Agulhas rings and cyclones (van Sebille, 2010a). Agulhas leakage estimates are sensitive to the definition used to calculate the leakage, ranging roughly between 10 and 20 Sv (van Sebille et al., 2010b; Beron-Vera et al., 2013; Cheng et al., 2016; Holton et al., 2017). Bars et al. (2014) proposed an algorithm to measure Agulhas leakage anomalies using absolute dynamic topography data from satellites.

The division of flow between Agulhas Leakage and Agulhas retroflection can be influenced by the upstream Agulhas Current. In a Lagrangian particle tracking experiment, van Sebille et al. (2009) found that a weaker Agulhas Current,

1315   detaching farther downstream and generating anti-cyclonic vorticity, potentially leads to more Agulhas leakage and larger

1316   Indian-Atlantic inter-ocean exchange. However, eddy-resolving model results suggest that as model resolution increases,

1317   the sensitivity of the leakage to Agulhas Current transport anomalies is reduced (Loveday et al., 2014). In addition, the ITF

1318   potentially influences the Agulhas leakage (Le Bars et al., 2013), as model outputs suggest that the Indian Ocean contributes

1319   12.6 Sv, half of which is from the ITF, to the Agulhas leakage (Durgadoo et al., 2017).

5.2.2 Variability, dynamics and influence on climate

1321   The magnitude of the Agulhas leakage is controlled by wind forcing including the trade winds and the Southern Hemisphere

1322   Westerlies (e.g., Durgadoo et al., 2013). The poleward shift in the Southern Hemisphere westerlies associated with

1323   anthropogenic forcing induced a clear increase in the Agulhas leakage during 1995-2004 as shown in numerical simulations

1324   (Biastoch et al., 2009; Biastoch and Böning, 2013). Increased wind stress curl in the South Indian Ocean associated with the

1325   southward shift of westerlies led to significant warming in the Agulhas Current system since the 1980's (Rouault et al.,

1326   2009); however further work showed that this is due to an increase in eddies leading to a broadening of the current as

1327   opposed to intensification (Beal and Elipot, 2016). Given the non-linear nature of Agulhas leakage and the lack and

1328   difficulties of observing it, combined with ocean model biases in the region, quantifying Agulhas leakage is very challenging

1329   (Holton et al., 2017). At seasonal time scales, the Agulhas leakage variability is controlled by eddies, however recent studies

1330   have shown that eddies might not contribute as significantly to leakage as was thought and the non-eddy leakage transport

1331   is likely to be constrained by large-scale forcing at longer time scales (e.g., Cheng et al., 2018). A recent study shows that

1332   the subsurface signal from the ENSO cycle influences the Agulhas leakage through Rossby waves with a time lag of 2 years

1333   (Paris et al., 2018).

1334   The Agulhas leakage carries warm and saline water from the Indo-Pacific Ocean into the Atlantic Ocean. The Agulhas

1335   leakage has been suggested to influence the Atlantic Meridional Overturning Circulation strength (AMOC; Beal et al.

1336   2011;Weijer and van Sebille, 2014, Biastoch et al. 2015) and modify the AMOC convective stability (e.g., Haarsma et al.,

1337   2011; Caley et al., 2012; Castellanos et al., 2017). It is suggested that the increases in the Agulhas leakage due to

1338   anthropogenic warming during the past decades would act to strengthen the Atlantic overturning circulation (e.g., Beal et

1339   al., 2011).

1340   The Agulhas leakage is an important source of decadal variability in the AMOC through Rossby waves (Biastoch et al.,

1341   2008; 2015). Source waters from the Agulhas Current take more than 4 years and mostly one to four decades to end in the

1342   North Atlantic Ocean (van Sebille et al., 2011; Rühs et al., 2013). The increased Agulhas leakage during 1995-2004 has

1343   contributed to the salinification of the South Atlantic thermocline waters (Biastoch et al., 2009). Hindcast experiments

1344   suggest that the Agulhas leakage increases by about 45% during 1960s-2000s and leads to the observed warming trend in

1345   the upper tropical Atlantic Ocean (Lübbecke et al., 2015).

5.3 Supergyre connection to the South Pacific

The extreme strong westerly wind stress in the Southern Hemisphere gives rise to a wide and energetic subtropical supergyre
(Figure 16) that connects three ocean basins, the Southern Hemisphere supergyre (e.g., Ridgway and Dunn, 2007; Speich et
al., 2007; Cessi, 2019). The supergyre is the subtropical gyre of the southern hemisphere. As such, its flow is primarily
determined by the westward integration of wind stress curl from the eastern boundaries as determined by Sverdrup dynamics.
The latitudinal position of the Subtropical Front associated with the supergyre is found to be controlled by strong bottom
pressure torque due to the interaction between the ACC and the ocean floor topography (De Boer et al., 2013). Not much is
known about the decadal and multidecadal variability of the supergyre. According to one analysis on SODA (Duan et al.,
2013), the water masses in the supergyre became cooler and fresher and shifted southward by about 2.5º due to changes in
the basin-scale wind forcing during 1958–2007.
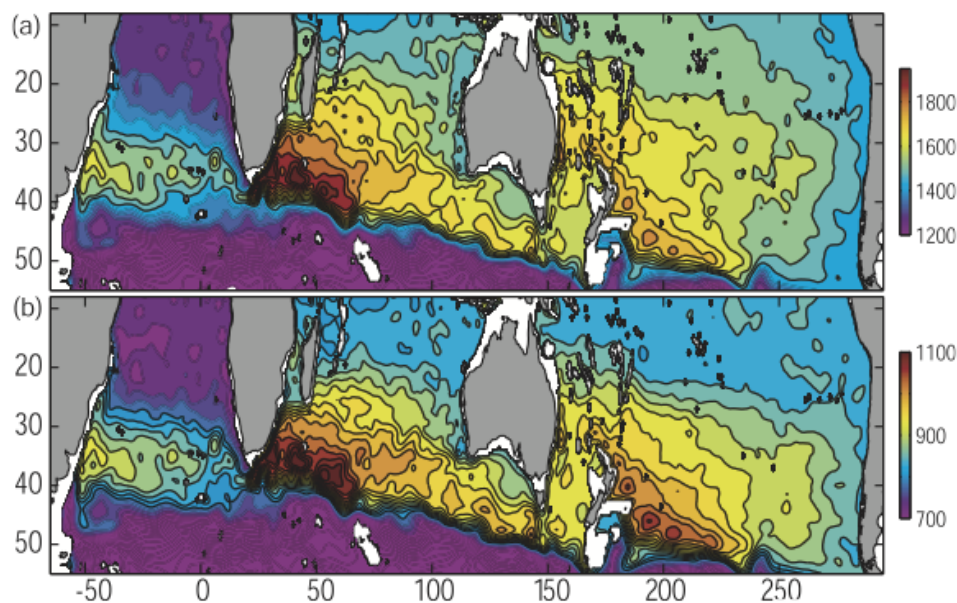
**Figure 16: The interbasin supergyre system for the Pacific and Indian Oceans as shown by the depth-integrated
steric height (a) $P_{0/2000}$, and (b) $P_{400/2000}$, derived from the CARS climatological temperature and salinity fields. The
contour interval in (a) is 50 m^2 and in (b) is 25 m^2. Taken from Ridgway and Dunn 2007.**

The regional ocean circulation system including the ITF and Leeuwin Current are thought to be dynamically connected to
the supergyre, which connects the Indian and Pacific Oceans by the Tasman Gateway and the Indonesian seas (Lambert et
al., 2016). Lagrangian experiments indicate the existence of a "superconvergent", which is a surface convergent pathway
connecting the subtropical South Indian and South Pacific Ocean, and confirmed that current variability in the Southern
Hemisphere supergyre is essential to sustaining the superconvergent (Maes et al., 2018).

1365   A recent study using altimeter observations shows a clear strengthening of the Southern Hemisphere supergyre in all three

1366   oceans since 1993 as indicated in the large trends of sea surface height and their contrast. Argo observations and ECCO

1367   assimilations suggest that the strengthening extends to deeper than 2000 m (Qu et al., 2019). Qu et al. (2019) found that the

1368   spin-up of the Southern Hemisphere supergyre is attributed to the poleward shift and strengthening of westerly winds that

1369   are linked to an increasingly positive southern annular mode.

1370   Although the near-surface circulation is eastward across the SIO, there are subsurface westward flows beneath (Schott and

1371   McCreary 2001, Domingues et al. 2007, Furue et al. 2017), and the depth-integrated circulation reveals the westward return

1372   flow of the equatorward side of the anti-clockwise subtropical gyre. The southern Indian Ocean hosts a "supergyre" (Speich

1373   et al. 2007, Ridgway and Dunn 2007). In Figure 16, the southern side of the Indian Ocean subtropical gyre extends eastward

1374   south of Australia to connect with the western Pacific subtropical gyre. The return flow is accomplished via a pathway that

1375   includes the East Australian Current, the South Pacific's western boundary flow; the Tasman Leakage, a westward flow

1376   south of Tasmania that carries Pacific Ocean water back to the Indian Ocean (distinct from the Flinders Current that hugs

1377   the continental slope, Duran et al 2020; Section 4.2.4); and northwestward flow in the eastern Indian Ocean to close the

1378   circulation.

5.4 Roles of salinity in inter-ocean exchange

1379

1380   Oceanic salinity is one of the basic variables that determines the oceanic stratification, sea level change and climate change

1381   (e.g., Llovel and Lee, 2015; Kido and Tozuka, 2017; Sprintall et al., 2019). However, the role of salinity in ocean circulation

1382   has been largely underestimated until the recent decade when the comprehensive suite of *in situ* observations of subsurface

1383   and surface salinity from Argo and satellite salinity missions became available. These new observations revolutionize our

1384   understanding of the influence of salinity on ocean circulation and dynamics (Vinogradova et al. 2019, and references

1385   therein).

1386

1387   Four major processes control the salinity in the Indian Ocean: net air-sea fluxes (evaporation minus precipitation), freshwater

1388   inflow from large rivers in the Bay of Bengal, inflow of relatively fresh waters from the Pacific Ocean through the Indonesian

1389   Throughflow straits, and inflow of saltier waters from the Red Sea and the Persian/Arabian Gulf. These different drivers

1390   combine to give the Indian Ocean salinity its unique flavour: a strong east-west gradient in the North Indian Ocean (salty in

1391   the Arabian Sea and fresh in the Bay of Bengal) and strong north-south gradients in the South Indian Ocean (fresh in the

1392   tropics, and salty in the subtropics) (Fig. 4).

1393

1394   As the new observations are revealing, salinity is a crucial variable to understand Indian Ocean dynamics. For instance,

1395   salinity has strong ties with the Indian Ocean Dipole (e.g., Du and Zhang, 2015; Durand et al., 2013; Grunseich et al., 2011;

1396   Kido and Tozuka, 2017; Nyadjro and Subrahmanyam, 2014; Zhang et al. 2016), the EGC (Menezes et al., 2013), LC

1397 transport, Ningaloo Niño and marine heatwaves off western Australia (e.g., Feng et al., 2015a), and the El Niño/La Niña

1398 climate mode (e.g., Hu and Sprintall, 2016, Zhang et al., 2016). Salinity plays an essential role in the dynamics of the

1399 seasonal Wyrtki Jets in the equatorial zone (e.g., Masson et al., 2003), extra-equatorial Rossby waves (Heffner et al., 2008;

1400 Menezes et al., 2014b; Vargas-Hernandez et al., 2015; Banks et al., 2016), Madden-Julian and Intraseasonal Oscillations

1401 (e.g., Grunseinch et al., 2013; Guan et al., 2014; Subrahmanyam et al., 2018), barrier-layer dynamics (e.g., Drushka et al.,

1402 2014; Felton et al., 2014), and the North Indian Ocean (e.g., D'Addezio et al., 2015, Fournier et al., 2017; Mahadevan et

1403 al., 2016; Nyadjro et al., 2011, 2012, 2013; Wilson and Riser, 2016; Spiro Jaeger and Mahadevan, 2018), and salinity

1404 controls the sea level change in the southeastern Indian Ocean (Llovel and Lee, 2015).

1405

1406 Salinity variability within the Indonesian Seas has been shown to control the transport of the ITF. Andersson and Stigebrandt

1407 (2005) proposed that a downstream buoyancy pool in the outflowing ITF region acts to regulate the ITF transport. Gordon

1408 et al. (2003, 2012) pointed out that low salinity surface water from the South China Sea is drawn into the Java Sea. Combined

1409 with the monsoonal precipitation over the Maritime Continent and seasonal monsoon winds, this freshwater plug contributes

1410 to the seasonal fluctuation of the Makassar Strait Throughflow transport and inhibits the inflow of tropical Pacific surface

1411 water from the Mindanao Current (e.g., Gordon et al., 2012; Lee et al., 2019). Recently, Hu and Sprintall (2016) found that

1412 about 36% of the interannua---l ITF transport is attributable to the salinity effect associated with freshwater input anomalies

1413 due to the ENSO cycle. A significant strengthening of the ITF transport in the 2000s has given rise to a subsequent warming

1414 and freshening of the eastern Indian Ocean (e.g., Hu and Sprintall, 2017a, 2017b, Section 6.1). Recently, Jyoti et al. (2019)

1415 further examined the salinity effect in the ITF transport following Hu and Sprintall (2016) and found that the unprecedented

1416 sea-level rise in the southern Indian Ocean since the beginning of the 21st Century is attributed to the accelerated heat and

1417 freshwater intrusion by the ITF.

1418

1419 **6 Modes of Interannual Climate Variability in the Indian Ocean**

1420 **6.1 ENSO teleconnection and the Indian Ocean Basin mode**

1421 ENSO influences the Indian Ocean circulation through the Pacific-to-Indian Ocean oceanic waveguide and the atmospheric

1422 teleconnection. Through the atmospheric bridge, El Niño conditions in the Pacific induce an anticyclonic wind anomaly

1423 pattern in the southeast Indian Ocean (Xie et al., 2002), whereas La Niña induces a cyclonic wind anomaly pattern (Feng et

1424 al., 2013). The ENSO teleconnection also drives SST variability over the western Indian Ocean during ENSO development.

1425 The tropical Indian Ocean experiences prolonged warming (cooling) that peaks in the following boreal spring and persists

1426 into boreal summer, after the decay of El Niño (La Niña) events, the so-called Indian Ocean Basin (IOB) mode (Yang et al.,

1427 2007). The westward propagating Rossby waves induced by ENSO may also help sustain the warming (cooling) of the

1428   tropical Indian Ocean (Xie et al., 2002), fueled by regional air-sea coupling (Du et al., 2009). The IOB warming has a

1429   capacitor effect for El Niño to influence boreal summer climate in the northwest Pacific (Xie et al., 2009). The relationship

1430   between ENSO and IOB evolves on a decadal time scale, and the persistent IOB warming after El Niño has been evident

1431   since the 1970s (Xie et al., 2010). Based on the CMIP5 multi-model experiments, the IOB warming tends to persist longer

1432   after the El Niño events under global warming scenarios (Zheng et al., 2013).

1433   The ITF transport is stronger after a La Niña and weaker after an El Niño (Meyers, 1996; England and Huang, 2005). The

1434   ITF variability lags ENSO by 8-9-months, found in ocean model results (England and Huang, 2005) and derived from the

1435   geostrophic transport across an Australia-Indonesia XBT section (Liu et al., 2015). The variability of the ITF transport drives

1436   sea level and upper ocean heat content anomalies in the southeast Indian Ocean. Through the waveguide, ENSO has a direct

1437   influence on the strength of the Leeuwin Current (Section 4.2.4), with a stronger poleward volume and heat transport during

1438   a La Niña event (Feng et al., 2008). A stronger Leeuwin Current during La Niña events leads to greater baroclinic instability

1439   of the current and enhanced generation of eddies that leads to interannual variability of the eddy kinetic energy in the

1440   southeast Indian Ocean (Feng et al., 2005; Zheng et al., 2018). The increase of the ITF transport and enhancement of rainfall

1441   in the Indonesian Seas during strong La Niña events can drive up to 0.2-0.3 psu freshening anomalies in the upper southeast

1442   Indian Ocean (Phillips et al., 2005; Feng et al., 2015a; Hu and Sprintall, 2017a), which may have a compound effect in

1443   accelerating the Leeuwin Current (Feng et al., 2015a). Both ENSO and the IOD (see Section 6.2) influence the ITF and thus

1444   the exchange of heat from the Pacific into the Indian Ocean, but in concurrent IOD and ENSO events it appears that the

1445   influence from the IOD dominates (Sprintall and Revelard, 2014).

1446   Due to the opposing effects of the winds and dissipation, ENSO induced sea level and upper ocean heat content anomalies

1447   in the southeast Indian Ocean do not propagate far into the western Indian Ocean; instead, wind anomalies generate sea level

1448   and heat content anomalies of opposite signs in the western Indian Ocean through Rossby wave propagations (Masumoto

1449   and Meyers, 1998; Xie et al., 2002; Zhuang et al., 2013; Ma et al., 2019). Thus, the joint forcing of the oceanic waveguide

1450   and atmospheric teleconnection results in variations of meridional overturning circulation and heat transport in the Indian

1451   Ocean on a multi-year time scale, in phase with the ITF variability (Ma et al., 2019).

1452   **6.2 The Indian Ocean Dipole**

1453   There is increasing evidence that positive IOD events are more frequent and intense during the 20th century (e.g., Abram et

1454   al., 2008; Cai et al., 2013; Abram et al., 2020a,b; and references therein). A rare occurrence of three consecutive positive

1455   IOD events took place in 2006-2008 (Cai et al., 2009b). The skewness towards more positive and fewer negative IOD events

1456   (Cai et al., 2009a) is due potentially to an anthropogenically-driven shoaling thermocline in the eastern Indian Ocean (Cai

1457   et al., 2008). The three consecutive positive IOD events rarely occurred in Coupled Model Intercomparison phase 5 (CMIP5)

1458   models and the more recent frequent occurrence was consistent with regional Indo-Pacific Walker circulation trends (Cai et

1459   al., 2009c,d). An anthropogenic contribution was proposed since positive IOD events became more frequent over the period

1460   1950–1999 in the CMIP5 models. Projected mean-state changes in the Indian Ocean with stronger easterly winds and a

1461   shoaling thermocline in the southeast Indian Ocean during austral spring favour positive IOD development, with a reduction

1462   in skewness between positive and negative IOD events likely (Cai et al., 2013; Figure 17), and a three-fold increase in

1463   frequency of extreme positive IOD events by 2100 compared to the previous century (Cai et al., 2014a). Based on a

1464   millennial IOD reconstruction from corals, extreme positive IOD events, as were observed in 1997 and 2019, were

1465   historically rare (Abram et al., 2020b). In the reconstruction, only ten extreme positive IOD events occurred and yet four

1466   events occurred in the last 60 years (Abram et al., 2020b). The increase in event frequency and intensity highlights the need

1467   to improve preparedness in regions affected by IOD events and minimize future climate risks.
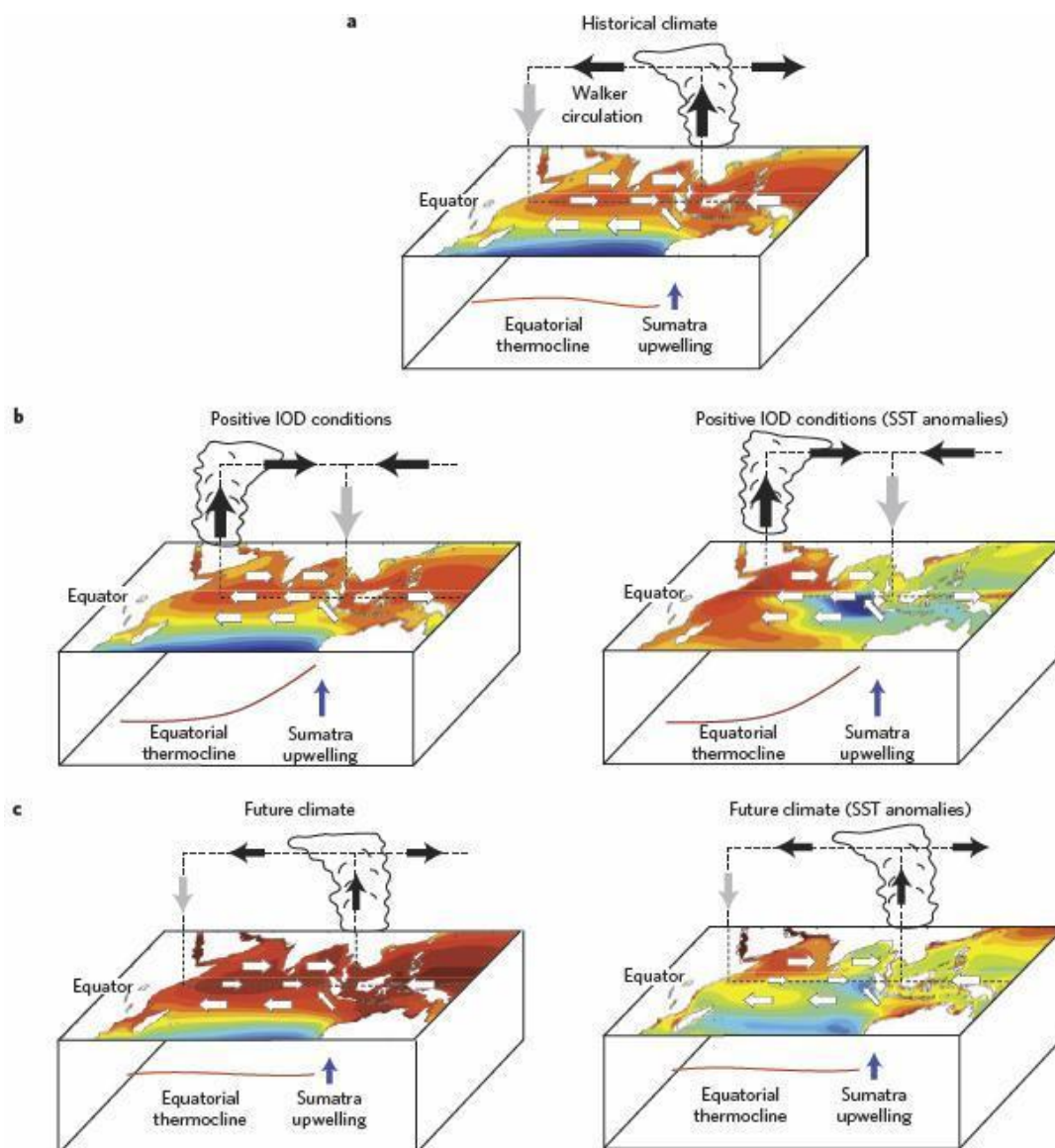
1468

Figure 17: Historical austral spring mean climate and positive IOD conditions for the twentieth century, and future austral spring mean climate. a, Historical mean climate, indicating SSTs, surface winds, the associated atmospheric Walker circulation, the mean position of convection and the thermocline. In the western Indian Ocean, the descending branch is broad and not well-defined, as indicated by a grey arrow. b, Typical conditions during a positive IOD event. c, Projected future mean climate based on a CMIP5 multi-model ensemble average. Diagrams with total SST fields are shown on the left; diagrams with SST anomalies referenced to the 1961–1999 mean for b, and

1475 **referenced to the basin mean for c, are shown on the right. Reprinted from Cai et al. (2013) with permission from**

1476 **Springer Nature.**

1477 While model simulations and paleo proxy records suggest changes in the frequency and magnitude of IOD events in a

1478 warming climate, there is less observational evidence from other sources. Given the short observational record in the Indian

1479 Ocean, the role of decadal to multi-decadal variability across the broader Indo-Pacific region has recently emerged as a

1480 compounding factor: the number and frequency of IOD events have been observed to vary on decadal timescales. Decadal

1481 variations in SST featuring an IOD-like out-of-phase pattern between the western and eastern tropical Indian Ocean have

1482 been linked to the PDO (Krishnamurthy and Krishnamurthy, 2016) or IPO (Dong et al., 2016). A combination of processes

1483 transmits the signal from the Pacific to the Indian Ocean through both the atmospheric and oceanic bridges, leading to

1484 variations in the subsurface temperature structure in the Indian Ocean (Zhou et al., 2017; Jin et al., 2018a). Decadal

1485 modulations of the background state of the eastern Indian Ocean thermocline depth can thus pre-condition the Indian Ocean

1486 to more or less IOD events (Annamalai et al., 2005). Consequently, positive IOD events were unusually common in the

1487 1960s and 1990s with a relatively shallow eastern Indian Ocean thermocline, while the deeper thermocline in the 1970s and

1488 1980s was associated with frequent negative IOD and rare positive IOD events (Ummenhofer et al., 2017). The Indian

1489 Ocean stands out as a region with high skill in decadal predictions (Guemas et al., 2013) and improved understanding of

1490 decadal modulation of IOD events can aid in decadal prediction efforts for the Indian Ocean region.

1491 The relationship between ENSO and the IOD has been subject to ongoing debate. Recent research has shown that around

1492 two-thirds of IOD variability arises as a remote response to ENSO (Stuecker et al., 2017; Yang et al., 2015), with the

1493 remaining variability being independent of ENSO. Stuecker et al. (2017) argue that the ENSO-driven IOD can be seen as a

1494 combination of remotely driven wind and heat flux anomalies modulated by seasonally-varying Bjerknes feedback in the

1495 Indian Ocean. Further, they suggest that the ENSO-independent IOD events arise out of white noise atmospheric forcing

1496 coupled to these feedbacks (Stuecker et al., 2017). Variability internal to the Indian Ocean basin and unrelated to ENSO,

1497 arising from ocean-atmosphere feedback processes, does however modulate the evolution of IOD events and can lead to

1498 early termination of IOD events; as a result, including internal variability improves the predictability of the IOD (Yang et

1499 al., 2015). The relationship between ENSO and the IOD is not only one-way: IOD events have also been shown to influence

1500 the development of ENSO in the following year (Izumo et al., 2010; Wang et al., 2019; Cai et al., 2019; and references

1501 therein).

1502 Different types of IOD events have been described, each with distinct evolution and regional impacts (Du et al., 2013; Endo

1503 and Tozuka, 2016). Du et al. (2013) distinguished three types of IOD events according to the timing of their peak amplitude

1504 and overall duration: 'unseasonable' events that develop and mature mostly within June-August (JJA), 'normal' events that

1505 develop and mature mostly within September-November (SON), and 'prolonged' events that develop in JJA and mature in

1506 SON, with the latter two described as the canonical IOD events (Du et al., 2013). The unseasonable IOD events have only

been observed since the mid-1970s and have been suggested to be a response to the rapidly warming Indian Ocean SST and a weakened Walker circulation during austral winter (Du et al., 2013). The seasonal evolution and type of ENSO also seems to play a role in determining the IOD evolution and type, with atmospheric influences transmitted through variations in the Walker Circulation and oceanic ones through anomalous oceanic Rossby waves affecting timing and evolution of IOD events, especially during their developing phase (Guo et al., 2015; Zhang et al. 2015; Fan et al., 2017). However, Sun et al. (2015) suggested more IOD events independent of ENSO since the 1980s, along with higher correlations between the IOD and Indian summer monsoon activity, likely due to mean-state change in the tropical Indian Ocean due to weaker equatorial westerlies. The relationship between ENSO and the IOD has weakened in recent decades, linked to changes in the ENSO-induced rainfall anomalies over the Maritime Continent (Han et al., 2017).

Recent advances in understanding variability and change in IOD characteristics have implications for the relationships between SST and regional rainfall patterns in Indian Ocean rim countries. For example, different types of IOD events exhibit distinct regional impacts, with only the canonical events associated with enhanced rainfall over East Africa due to the low-level moisture convergence over the region (Endo and Tozuka, 2016). The effect of Indian Ocean SST on East African rainfall is most pronounced during the short rains (September-November), though Williams and Funk (2011) argued that warming Indian Ocean SST in recent decades were also associated with reduced long rains for the March-June season in Ethiopia and Kenya. Changes in the tropical atmospheric circulation across the Indo-Pacific on multi-decadal timescales (Vecchi and Soden, 2007; L'Heureux et al., 2013) have further implications for the relationship between Indian Ocean SST and regional rainfall: When the Pacific Walker cell weakened and the Indian Ocean one strengthened post-1961, the East African short rains became more variable and wetter (Nicholson, 2015). Similarly, Manatsa and Behera (2013) described an epochal strengthening in the relationship between the IOD and East African rainfall post-1961, with 73% of short rain variability in East Africa explained by the IOD, up from 50% in previous decades. After 1997, this increased further to 82%, explaining spatially coherent events across the region and frequent rainfall extremes (Manatsa and Behera, 2013). Recent observed and projected changes in frequency and intensity of IOD events highlight the increasing need for preparedness in vulnerable regions affected by these events.

IOD events are associated with distinct changes in primary productivity, as measured by chlorophyll. During positive IOD events, increased chlorophyll indicative of phytoplankton blooms is apparent in the normally oligotrophic eastern Indian Ocean in fall (Wiggert et al., 2009; Currie et al., 2013). Positive chlorophyll anomalies occur in the southeastern Bay of Bengal in boreal winter, while negative anomalies are observed over much of the Arabian Sea and southern tip of India. In a case study of the 2006 positive IOD event, Iskandar et al. (2010) using an eddy-resolving biophysical model found the offshore chlorophyll signal in the southeastern Indian Ocean to be associated with regions of high eddy kinetic energy implying that cyclonic eddies injected nutrient-rich water into the upper layer enabling the bloom. Currie et al. (2013) emphasize the importance of assessing the relative contributions of IOD events and remote impacts from ENSO on primary productivity in the Indian Ocean through their respective influence on upper-ocean properties for improved understanding

1540   and ultimately predictions of productivity, ecosystems, and fisheries within the basin. Little attention has been paid so far

1541   to resultant effects of these blooms on biogeochemical cycling (Wiggert et al., 2009).

6.3 The subtropical Indian Ocean Dipole

1543   The subtropical Indian Ocean Dipole (SIOD) is a climate mode in the southern Indian Ocean, which tends to arise and peak

1544   in the austral summer (Behera and Yamagata, 2001). During the SIOD's positive phase, the climate mode has positive SST

1545   anomalies in the southwestern Indian Ocean and negative SST anomalies in the northeastern region (Behera and Yamagata,

1546   2001; Suzuki et al., 2004; Hermes and Reason, 2005). During the positive phase, enhanced precipitation occurs over

1547   southern Africa (Behera and Yamagata 2001; Reason 2001, 2002). Recent studies have shown that the SIOD affects the

1548   Indian summer monsoon rainfall (Terray et al., 2003), rainfall over southwestern Australia (England et al., 2006), and

1549   tropical cyclone trajectories in the southern Indian Ocean (Ash and Matyas, 2012).

1550   Initially, SST anomalies associated with the SIOD were considered to be generated directly by latent heat flux anomalies

1551   (Behera and Yamagata, 2001). However, recent studies (Morioka et al. 2010, 2012) based on a mixed layer heat budget

1552   analysis revealed the importance of mixed layer depth anomalies generated by latent heat flux anomalies. Wind anomalies

1553   associated with the anomalous Mascarene High suppress latent heat loss and shoal the mixed layer in the southwestern part,

1554   while latent heat release is enhanced and the mixed layer deepens anomalously in the northeastern part (Morioka et al. 2010,

1555   2012). With these changes in the upper ocean heat capacity, warming of the surface mixed layer by the climatological

1556   shortwave radiation is enhanced in the southwestern part and becomes less effective in the northeastern part. As a result, the

1557   dipole SST anomalies appear in the southern Indian Ocean.

1558   Because the above mechanism operates more effectively as the thickness of the mixed layer becomes thinner, the return

1559   period of the SIOD is becoming shorter associated with the shoaling trend of the mixed layer (Yamagami and Tozuka,

1560   2015). Whether this mechanism is associated with decadal-to-interdecadal variations and/or global warming awaits further

1561   study. Many coupled models are relatively successful in simulating the SIOD with some biases in the location and structure

1562   of the SST anomaly (Kataoka et al., 2012). However, no study has examined if the SIOD is modulated by climate modes of

1563   variability with decadal-to-interdecadal timescales or changes with global ocean warming.

6.4 Ningaloo Niño and marine heatwaves in the Indian Ocean

1565   The Ningaloo Niño (Niña) phenomenon is an interannual climate mode associated with anomalously warm (cold) water in

1566   the eastern Indian Ocean (Feng et al., 2013; see Figure 18). This mode is seasonally phase-locked, with a peak during austral

1567   summer (Kataoka et al., 2014). The mode exerts significant impacts on rainfall over Australia (Kataoka et al., 2014) and

1568   affects marine ecosystems and fisheries (e.g. Pearce et al. 2011). The phenomenon can alter biological productivity, with

1569 negative chlorophyll anomalies during Ningaloo Niño (Narayanasetti et al., 2016). Ningaloo Niños can develop in response

1570 to remote ENSO forcing from the western Pacific transmitted as a coastally trapped wave (Kataoka et al., 2014). During the

1571 La Niña events, high sea level anomalies propagate poleward along the west coast of Australia, intensifying the Leeuwin

1572 Current and causing poleward advection of heat and anomalously warm waters (e.g. Benthuysen et al., 2014; Section 4.2.4).

1573 Poleward transport of tropical, low salinity waters can further enhance the total geostrophic transport (Feng et al., 2015a).
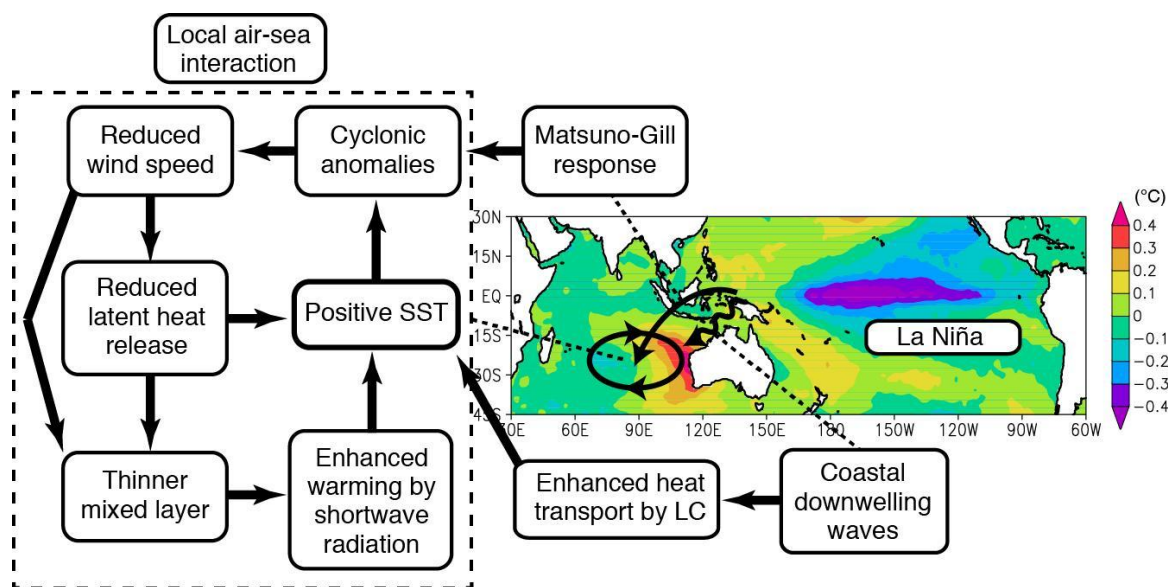
1574

1575 **Figure 18: Schematic diagram illustrating generation mechanisms (i.e. local air-sea interaction, atmospheric**

1576 **teleconnection, and oceanic wave propagation) of the Ningaloo Niño. SST anomalies are regressed against the**

1577 **Ningaloo Niño Index to illustrate typical SST anomalies associated with the phenomenon.**

1578 Atmospheric teleconnection can further enhance the development of Ningaloo Niño. A reduction in southerly winds over

1579 the shelf, which would strengthen the Leeuwin Current, can arise through a Gill-type response with low sea level pressure

1580 anomalies in the southeast Indian Ocean owing to the Niño3.4 SST anomalies (Feng et al., 2013; Tozuka et al., 2014).

1581 Ningaloo Niños can arise from local air-sea interactions off western Australia, through the wind-evaporation-SST feedback

1582 during its initial stage (Marshall et al., 2015) and coastal SST-wind-Leeuwin Current (Bjerknes) feedback (Kataoka et al.

1583 2014). In the coastal feedback mechanism, positive SST anomalies lead to northerly alongshore wind anomalies and coastal

1584 downwelling anomalies, causing enhancement of the positive SST anomalies (Kataoka et al., 2014). During the Ningaloo

1585 Nino's development phase, estimates of air-sea heat flux contributions have been found to be dependent on products and

1586 their resolution and bulk flux algorithms (Feng and Shinoda, 2019). Since the late 1990s, Ningaloo Niño events have

1587 occurred more frequently (Feng et al., 2015b). This decadal increase is corroborated by coral proxy records of Leeuwin

1588   Current strength, with the most extreme SST anomalies associated with Ningaloo Niños occurring since 1980 (Zinke et al.,

1589   2014).

1590   More generally, marine heatwaves refer to prolonged, extremely warm water events. Over the past decade, most studies on

1591   marine heatwaves in the Indian Ocean have focused on the eastern sector of the Indian Ocean. Major events in the Indian

1592   Ocean have been associated with phases of ENSO. Along the west coast of Australia, marine heatwaves have occurred

1593   predominantly at subtropical reefs during La Niña events due to increased heat transport (Zhang et al., 2017). The term

1594   "marine heatwave" was first coined owing to a +5°C warm water event in 2011 off Western Australia during a strong La

1595   Niña (Pearce et al., 2011). The 2011 event was associated with the strongest recorded Leeuwin Current transport anomaly,

1596   bringing warm tropical waters south, and was partly due to air-sea heat fluxes (Feng et al., 2013; Benthuysen et al., 2014).

1597   Across Australia's northwestern shelf, marine heatwaves have been found to occur at tropical coral reefs from El Niño due

1598   to solar radiation and a weakened monsoon (Zhang et al., 2017). During the strong El Niño of 2015-2016, the southeast

1599   tropical Indian Ocean experienced the warmest and longest marine heatwave on record, with weakened monsoon activity

1600   and anomalously high air-sea heat flux into the ocean (Benthuysen et al., 2018). The anomalously warm water conditions

1601   persisted into winter, during one of the strongest negative IOD events (Benthuysen et al., 2018). The 2016 marine heatwave

1602   was associated with coral bleaching spanning Australia's inshore Kimberley region to remote coral reef atolls (Gilmour et

1603   al., 2019). More broadly across the Indian Ocean during 2016, marine heatwaves have been studied in terms of their

1604   ecological impacts, such as coral bleaching in the western Indian Ocean (e.g. Gudka et al., 2018), the Maldives (e.g. Ibrahim

1605   et al., 2017) and consequences for fishes in the Chagos Archipelago (Taylor et al., 2019).

1606   Trends in marine heatwave metrics indicate widespread regions across the Indian Ocean where events have increased in

1607   frequency, based on SST from 1982-2016, especially in the central and southwestern sectors (Oliver et al., 2018). Over the

1608   same time period, the duration and intensity of marine heatwaves have increased (Oliver et al. 2018). Primary climate modes

1609   of variability correlated with an increased occurrence of marine heatwaves include the following: (1) the positive phase of

1610   the Dipole Mode Index for the northwestern sector, the tropical sector, and south to the Seychelles Islands, (2) the positive

1611   phase of the Niño3.4 index for the south-central sector, and (3) the negative phase of the El Niño Modoki index, which

1612   measures the strength of the Central Pacific ENSO, for the eastern Indian Ocean (Holbrook et al., 2019). While the marine

1613   heatwaves in the eastern Indian Ocean have been well documented, there have been fewer studies into the physical

1614   mechanisms causing marine heatwaves across the basin and other regions and less confidence, for example in the Bay of

1615   Bengal, in the local processes causing reported events on a range of time scales (Holbrook et al. 2019). There are indications

1616   that increased extremes in El Niño (Cai et al., 2014b) and La Niña events (Cai et al., 2015) due to mean ocean warming

1617   trends increase the likelihood of marine heatwave occurrence in the southeast Indian Ocean (Zhang et al., 2017).

1618

7. Multiscale upper ocean processes in the Bay of Bengal

Reflective of its name, the Bay of Bengal is in many ways analogous to a large-scale estuary with seasonally reversing winds and boundary currents that facilitate the transport, stirring, and mixing of water masses. To the north, the Ganga-Brahmaputra-Meghna watershed delivers on average 1300 km^3 in annual runoff of freshwater with a seasonal peak in discharge from July to September (Sengupta et al., 2006). During the southwest monsoon (boreal summer), the Summer Monsoon Current (Fig. 10) flows eastward advecting high salinity waters from the Arabian Sea into the southern Bay of Bengal, balancing the Bay's net outflow of freshwater. Instabilities and eddies result in mesoscale stirring of these different water types and create a strongly filamented and complex near-surface thermohaline structure. Lateral and vertical gradients in stratification are further modified by submesoscale processes, instabilities, and mixing. The resultant shallow stratification allows for rapid coupling with the atmosphere. Collectively, these conditions present a natural laboratory to study multi-scale mixing processes and their link to air-sea interaction. This section discusses new understanding of physical processes in the Bay from the large-scale to sub-mesoscale and finally at the smallest mixing scales.

Recent focus on the Bay of Bengal's upper ocean structure has been prompted by the need to understand atmosphere and ocean coupling with the aim of ultimately informing monsoon forecasting efforts at the intraseasonal timescale and shorter. Several bi-lateral international collaborations (Lucas et al., 2014; Wijesekera et al., 2016; Mahadevan et al., 2016; Vinaychandran et al., 2018; Gordon et al., 2019, 2020) have collectively supported multiple field campaigns, beginning in 2013 and concluding in 2019, using a combination of shipboard, moored, and autonomous platforms. These atmospheric and oceanic measurements have provided new insights into the BoB's structure and the processes that regulate that structure, particularly at fine lateral scales (<5 km).

Results from these combined efforts span from large-scales, e.g., the quantification of coastal transport along the Sri Lankan coast (Lee et al., 2016) and the mesoscale stirring of freshwater (Sree Lekha et al., 2018), to intermediate scales, e.g., high-resolution (order 100 m) frontal surveys that hint at the roles of submesoscale (Ramachandran et al., 2018) and non-hydrostatic processes in setting stratification (Sarkar et al., 2016), to small-scales with direct measurements of microstructure yielding new insights into the BoB's mixing regimes (Jinadasa et al., 2016; Thakur et al., 2019; Cherian et al. 2020).

7.1 The Bay's Forcing and Upper Ocean Structure

At the largest scales, the Bay is forced by air-sea fluxes of buoyancy and momentum, which are strongly modulated by the monsoon and vice versa. Precipitation and multiple river systems, including the Ganga-Brahmaputra-Meghna system, contribute to freshwater input that creates a barrier layer in the surface Bay of Bengal, which is strongest in the northern Bay weakening toward the south. The Bay's stratification, in particular its barrier layer, is unique in how it impacts the evolution of seasonal SST, in turn setting the lower boundary condition for the development of the monsoon (Li et al., 2017).

1649   For this reason, recent emphasis has been placed on understanding of processes determining the Bay's upper ocean salinity

1650   and temperature structure.

1651   The monsoon cycle of surface forcing plays a first-order role in control of the Bay's upper ocean temperature structure.

1652   Direct flux measurements are a critical component in our ability to accurately capture/represent and predict the magnitude

1653   and variability of monsoon air-sea coupling. Recent studies have shown that of the air-sea heat flux terms, shortwave

1654   radiation and latent heat flux are the largest drivers of variability to the total heat tendency. These variables are also those

1655   which reanalysis products struggle most to accurately represent, showing biases up to 75 W/m^2 (Sanchez-Franks et al.,

1656   2018). High-quality air-sea surface flux measurements over the BoB historically have been limited to the few sites

1657   maintained by the RAMA array (McPhaden et al., 2009). However, regional measurement efforts have expanded and

1658   baseline surface measurements are now collected and sustained through India's National Institute of Ocean Technology's

1659   met-ocean buoy program (Venkatesan et al., 2018), as well as the recent transition of an 18°N air-sea flux buoy from Woods

1660   Hole Oceanographic Institution to Indian National Centre for Ocean Information Services (Weller et al., 2016).

1661   Precipitation and riverine discharge along the Bay's margins respectively contribute roughly 60% and 40% of the 0.14 Sv

1662   net freshwater delivered to the Bay (Sengupta et al. 2006; Wilson and Riser, 2016). Precipitation peaks in early summer

1663   (June) with a value near 0.4 m month^{-1}, while discharge peaks slightly later in summer (August) with a value near 0.3 m

1664   month^{-1}. Evaporative loss (included in the net 0.14 Sv) is relatively steady throughout the year at 0.1 m month^{-1} (Wilson

1665   and, Riser 2016). Estimates of river discharge from gauged sources are known to have uncertainties (underestimates) related

1666   to unmonitored tributaries and streams. For large deltas, altimeter-based elevations offer a means of extrapolating gauge

1667   data over space and time. Papa et al. (2010, 2012) applied such an approach to the Ganga-Brahmaputra River system for

1668   the period 1998-2011. This time series allows for assessment of interannual variability over time ranges not spanned by

1669   gauged efforts. Papa et al. (2012) note a 12,500 m^3/s standard deviation in interannual variability in the Ganga-Brahmaputra

1670   discharge. Importantly, such data sets are also easily accessible by the general public, facilitating progress and understanding

1671   by the scientific community.

1672   The Bay's upper ocean temperature and salinity structure is an integrated representation of the above summarized

1673   sources/sinks of heat and freshwater, combined with the physical processes that redistribute these quantities. The

1674   thermohaline structure of the Bay is remarkable in several regards—for shallow mixed layer depths (< 5 m, Sengupta and

1675   Ravichandran, 1998), for inversions of temperature (Shroyer et al., 2016, 2019; Thadathil et al. 2016), for large-scale

1676   coherent layering that spans 100 kms (Shroyer et al., 2019), an active mesoscale field and the strong influence of river

1677   discharge over the interior basin. The Bay's salinity stratification is a critical, if not dominant, contributor to the upper

1678   ocean density stratification. It supports the formation of barrier layers that are frequently observed to be warmer than the

1679   mixed layer thereby providing a substantial subsurface heat reservoir with the potential to modify air-sea interaction

1680   (Girishkumar et al., 2011; Shroyer et al., 2016). For example, in conditions supportive of formation of a diurnal warm layer

1681   (low winds, strong insolation), subsurface turbulent fluxes can act to modulate the diurnal SST cycle by transporting
1682   (typically) warm barrier layer waters into the mixed layer at night while still cooling the base of the diurnal warm layer
1683   (DWL) during the day (Shroyer et al., 2016). A similar phenomenon, albeit on a much different scale, results with passage
1684   of cyclones, which often show a salty wake even in the absence of a cool wake which is common for cyclones elsewhere
1685   (for e.g. Chaudhuri et al. 2019, Qiu et al. 2019). Below, we review recent progress on understanding of processes that
1686   determine the Bay's upper ocean thermohaline structure.

1687   **7.2 Lateral Processes**

1688   **7.2.1 Stirring from the Margins**

1689   The Bay of Bengal has an active mesoscale eddy field that stirs diverse source waters into the interior of the Bay of Bengal.
1690   The origins of these source waters are the Arabian Sea waters to the west, the Ganga-Brahmaputra-Meghna at the northern
1691   tip, Andaman Sea waters to the east, and Equatorial waters to the south. This stirring effectively contributes to a quasi-
1692   stationary balance of the fresher waters from the north and the high salinity waters from the west and south over time. Lateral
1693   advection is a fundamental contributor to the formation of the barrier layer (George et al., 2019) and the freshwater budget
1694   of the Bay (e.g. Sree Lekha et al., 2018). In the northern Bay, the dispersal of water from the periphery into the interior
1695   depends critically on mesoscale stirring and the time varying Ekman transport, as indicated from mooring (Sree Lekha et
1696   al., 2018) and ship-based surveys (Shroyer et al., 2019), and constrained by modelling results (Sree Lekha et al., 2018).
1697   Here, the advection of freshwater by the mesoscale stirring also plays an important role in determining SST over the northern
1698   BoB (Buckley et al. 2020), as these waters are typically associated with relatively shallow mixed layers. In the southern
1699   Bay, measurements have suggested the competing influences of mixing and advection of salty Arabian Sea water in the
1700   erosion and reformation of the barrier layer during the southwest monsoon (George et al., 2019; Vinayachandran et al.,
1701   2018). In particular, George et al. (2019) show that maintenance of the barrier layer and the associated maximum depth of
1702   mixing was critically dependent on horizontal advection through its impact on stratification. Surface freshwater input also
1703   has an impact on barrier layer evolution; several freshening events were captured at various stages of their seasonal evolution
1704   in the southern Bay of Bengal in recent observations (Vinayachandran et al., 2018). These events play a significant role in
1705   the formation of a thick barrier layer, showing that during the southwest monsoon the shoaling of the mixed layer in the
1706   southern BoB has a similar magnitude and behaviour to that in the northern BoB (Vinaychandran et al., 2018).

1707   **7.2.2 Inter-basin exchange**

1708   Inter-basin exchange is critical to the Bay's salinity budget; since the Bay receives net freshwater input, this freshwater must
1709   be balanced by salty water imported from either the Arabian Sea or the western equatorial Indian Ocean (Jensen et al., 2001;
1710   Sanchez-Franks et al., 2019), and turbulent transport of salt into the fresh water layer is necessary to maintain the BoB's

1711   long-term salinity balance. Observations show that intrusion of high salinity water from the Arabian Sea enters the BoB
1712   between 80°-90°E during the southwest monsoon, (e.g. Murty et al, 1992; Vinayachandran et al., 2013) and has been found
1713   in several models (e.g. Vinayachandran et al., 1999; Han and McCreary, 2001 and Jensen, 2001). More recent observational
1714   and modeling studies show that both lateral and vertical transfer of heat and salt occur at multiple space-time scales. Seasonal
1715   currents play an important role in transporting heat and salt in and out of the BoB, but the role of mesoscale eddies on lateral
1716   transports is not well known.

1717   Using unique year-long mixing measurements detailed in Section 7.3, Cherian et al. (2020) tentatively estimated a turbulent
1718   salt flux of 1.5e-6 psu m/s out of Arabian Sea water averaged between 85°E and 88.5°E at 8°N through the 34.75 psu
1719   isohaline between August and January. Over those 6 months, this flux would increase the salinity of a 75m layer of water
1720   by 0.3 psu, though much of this would be cancelled out by surface fluxes. The magnitude and timing of this salt flux roughly
1721   match that necessary to restore the Bay's near-surface salinity after the large freshwater input in August as estimated by a
1722   few modelling studies (Akhil et al., 2014; Benshila et al., 2014; Wilson and Riser, 2016). This is the first direct measurement
1723   of turbulence that supports the hypothesis of intrusion of high salinity water from the Arabian Sea during the southwest
1724   monsoon (Vinayachandran et al., 2013).

1725   **7.2.2.1 Andaman Sea Exchange**

1726   The Irrawady river drains into the Andaman Sea, a marginal sea at the eastern edge of the Bay. Export from the Andaman
1727   is then another source of freshwater for the Bay, particularly at intermediate densities (22-25 kg m^{-3}). A striking example of
1728   the interaction between strong surface forcing and an anticyclonic eddy can be found in the fortuitous crossing of an
1729   intrathermocline eddy (ITE) in 2013. The water mass characteristics clearly identify ITE waters from the Andaman Sea;
1730   and, analysis of ancillary Argo data suggest a similar water type often penetrates westward into the Bay extending from the
1731   three passages connecting the two basins (Gordon et al., 2017). While at the time of transit the observed ITE had a very
1732   weak surface expression, a week prior to encountering the ITE a clear sea surface high (>10 cm) is evident in AVISO SSHA.
1733   Tropical cyclone Lehar passed near the location of this sea surface high in the interim, and the working conjecture is that
1734   the winds associated with Lehar were sufficient to modify a typical mode-1 anticyclone into the observed ITE.

1735   **7.2.2.2 Arabian Sea Exchange**

1736   Near-surface exchange from the Arabian Sea into the Bay of Bengal is influenced by the Sri Lanka Dome (SLD), an
1737   upwelling thermal dome that recurs seasonally within the SMC in the wind shadow of Sri Lanka (Vinayachandran and
1738   Yamagata 1998, de Vos et al. 2014, Burns et al. 2017). The SLD has long been recognized as a prominent circulation feature
1739   in the southwestern bay during the summer monsoon; and it has been noted as a region of enhanced productivity
1740   (Vinayachandran et al., 2004, de Vos et al. 2014), cool SST (Burns et al. 2017), and consequently depressed convection
1741   (Figure 15). The SLD displays pronounced interannual variability (Cullen and Shroyer 2019). In some years the SLD has a

1742   strong surface manifestation (amplitude of the low ~30 cm) that persists well beyond the southwest monsoon; in other years
1743   the SLD has a weak expression that is intermittent and short-lived (~1-2 months). The SLD is not fixed in location despite
1744   its strong association with the wind stress curl. Its position varies from year-to-year as well as over the course of one season.
1745   Variations in its location and strength may influence the properties of waters entrained and upwelled within the SLD.

1746   At intermediate depths (<~200 m), the signature of the neighboring Arabian Sea is notable across much of the basin (Gordon
1747   et al., 2016). During summer, Arabian Sea High Salinity Water (ASHSW; density near 22-24 kg m^{-3}) is carried/advected
1748   into the Bay of Bengal as a 'high salinity core' via the Southwest Monsoon Current (SMC, Webber et al., 2018; Sanchez-
1749   Franks et al., 2019) and then spread north along the bay's central spine (Hormann et al., 2019). During this journey, salt is
1750   mixed upward into the near-surface fresh layer (Cherian et al 2020; see Section 7.3 Vertical Mixing). Nearly two-year long
1751   moored current observations in the southern BoB captured SMC and Northeast Monsoon Current, seasonally varying large
1752   eddies including a cyclonic eddy, the SLD, and an anticyclonic eddy southeast of the SLD (Wijesekera et al. 2016c). These
1753   observations revealed that the average transport over nearly a two year period into the BoB was about 2 Sv (1 Sv = 10^6 m^3
1754   s^{-1}) but likely exceeded 15 Sv during summer of 2014, which is consistent with the transport associated the SMC (e.g.,
1755   Schott et al. 2009; Weber et al. 2018). The observations further indicate that the water exchange away from coastal
1756   boundaries, in the interior of the BoB, may be largely influenced by the location and strength of the two eddies that modify
1757   the path of the SMC. The strength and location of the SMC itself is dependent on a combination of local and remote forcing
1758   (Webber et al., 2018).

1759   As discussed above several hypotheses have been suggested for cyclonic eddy (SLD) and anticyclonic eddy formation in
1760   the southern BoB. It has been suggested that the cyclonic wind stress-curl over southwestern BoB generates the SLD
1761   (McCreary at al., 1996; Vinayachandran and Yamagata 1998; Schott et al., 2001; Cullen and Shroyer 2019). Based on
1762   numerical simulations, de Vos et al., (2014) argued that the separation of SMC from the (southern) boundary of Sri Lanka
1763   may lead to SLD, where a cyclonic vorticity is generated by lateral frictional effects. A mechanism for the anticyclonic eddy
1764   formation has been proposed by Vinayachandran and Yamagata (1998), where the interaction of the SMC with Rossby
1765   waves arriving from the eastern boundary leads to the anticyclonic eddy. Pirro et al (2020a) proposed a new hypothesis
1766   wherein the anticyclonic eddy is generated by topographically trapped Rossby wave response of the SMC to perturbations
1767   by the Sri Lankan coast. They reported that observations of the size, location and origins of the SLD were broadly consistent
1768   with their hypothesis, based on a laboratory experiment designed to mimic natural flow in the BoB by creating an eastward
1769   jet (SMC) on a simulated β plane.

1770   High-resolution sampling of the interior BoB has provided a more detailed look at the lateral extent of typical 'patches' of
1771   Arabian Sea water, which tend to remain well-defined over scales of 10-50 km, suggesting the importance of eddy activity
1772   in exchange (Shroyer et al., 2019). While many studies have traced origins of ASHSW from the eastern Arabian Sea,
1773   entering the Bay of Bengal directly via the southwest monsoon current (e.g., Jensen et al, 2016); a recent study suggests an

1774 equatorial pathway may also be relevant (Sanchez-Franks et al., 2019; see Equatorial Connections). Highly salty and highly

1775 oxygenated waters from the Persian Gulf and the Red Sea have also been noted in the southern regions of the Bay of Bengal

1776 (Jain et al., 2017). These waters are injected into the Bay of Bengal via current systems (equatorial and the southwest

1777 monsoon current) with important repercussions for the oxygen concentrations of the Bay of Bengal oxygen minimum zone

1778 (Sheehan et al., 2020).

1779 Velocity and hydrographic profiles from a shipboard survey in December 2013 combined with drifter observations, satellite

1780 altimetry, global ocean nowcast/forecast products, and coupled model simulations were used to examine the circulation in

1781 the southern Bay of Bengal during Northeast monsoon (Wijesekera et al. 2015). The observations captured the southward

1782 flowing East India Coastal Current (EICC, e.g., Shetye et al. 1994) off southeast India and east of Sri Lanka. The EICC was

1783 approximately 100 km wide, with speeds exceeding 1 m s^{-1} in the upper 75 m. East of the EICC, a subsurface-intensified

1784 300-km-wide, northward current was observed, with maximum speeds as high as 1 m s^{-1} between 50 m and 75 m. The EICC

1785 transported low-salinity water out of the bay and the subsurface northward flow carried high-salinity water into the bay

1786 during typical northeast monsoon conditions (Wijesekera et al. 2015; Jensen et al. 2016).

1787 **7.2.3 Equatorial Connections**

1788 The Equatorial undercurrent (EUC) in the Indian ocean is seasonally variable. The summer–fall EUC tends to occur in the

1789 western basin in most years but exhibits evident interannual variability in the eastern basin (Chen et al. 2015), with different

1790 processes dominating its generation in the western and eastern basins. In the eastern basin reflected Rossby waves from the

1791 eastern boundary play a crucial role in the EUC, whereas directly forced Kelvin and Rossby waves control the EUC in the

1792 western basin.

1793 Equatorial Kelvin waves, commonly interpreted as Wyrtki (1973) jets, propagate eastward along the equator during

1794 April/May and September/October. Upon reflection from the IO eastern boundaries, energy of Wyrtki jets is reflected back

1795 in part as long Rossby waves that disperse slowly during the following two months and reach the central-eastern BoB during

1796 July-August (Han et al., 1999, 2001; Han, 2005; Nagura and McPhaden, 2010a). The remaining energy is partitioned into

1797 two coastally-trapped Kelvin waves traveling poleward (Moore, 1968), which excite long Rossby waves propagating

1798 westward. Therefore it is suggested that planetary waves driven by remote forcing from the interior IO contribute

1799 significantly to the formation, strength and intensity of BOB circulation (Vinayachandran et al. 1998; Nagura and

1800 McPhaden, 2010b; Chen, 2015). A subset of these planetary waves are the mainstay of intraseasonal oscillations (ISOs), a

1801 sub-seasonal phenomenon of periods less than 120 days. The genesis of oceanic ISOs has been attributed to multiple

1802 mechanisms: external forcing (e.g., atmospheric ISOs and Ekman pumping, e.g. Duncan and Han 2012) and internal

1803 processes (upper ocean processes and instabilities e.g. Zhang et al. 2018).

1804

1805   Observations in the IO have captured a range of variabilities in the 30 – 120 days frequency band (e.g., Girishkumar et al.,

1806   2013), and past research has identified roughly three distinct ISO bands in the context of thermocline: 30-60 days, 60-90

1807   days, and 120 days (Han et al., 2001; Girishkumar et al., 2013). Pirro et al. (2020b) discussed interaction between 30-60 day

1808   ISOs and the SMC in the southern BoB using long-term moored observations. They estimated that the background mean

1809   flow acceleration resulting from the meridional divergence of wave momentum flux in the thermocline was about 10^{-8} m s^{-2}.

1810   As a result, within a wave period, ISOs can enhance the eastward flow in the thermocline by about 25%. The negative

1811   shear production computed for the same period consistent with this finding suggesting that the mean flow gained kinetic

1812   energy at the expense of the ISO band. The meridional heat-flux divergence was -10^{-7} °C s^{-1} and has a tendency for cooling

1813   the thermocline by about 0.5°C when ISOs are active (Pirro et al., 2020b).

1814   High salinity waters from the western Arabian Sea and the western Equatorial Indian Ocean can route to the Bay of Bengal

1815   via the Somali Current and the Indian Ocean EUC (Sanchez-Franks et al., 2019). Changes in strength of the Bay of Bengal

1816   high salinity core are linked to the convergence of the East Africa Coastal Current and the wintertime southward-flowing

1817   Somali Current, with anomalously strong equatorial Undercurrent (Fig. 19). Because of the seasonal reversal of currents,

1818   two junctions form naturally, one in the western equatorial Indian Ocean (Somali Current) and another south of India

1819   (monsoon currents), which effectively act as 'railroad switches' rerouting water masses to different basins in the Indian

1820   Ocean depending on the season (Fig. 19, Sanchez-Franks et al., 2019).
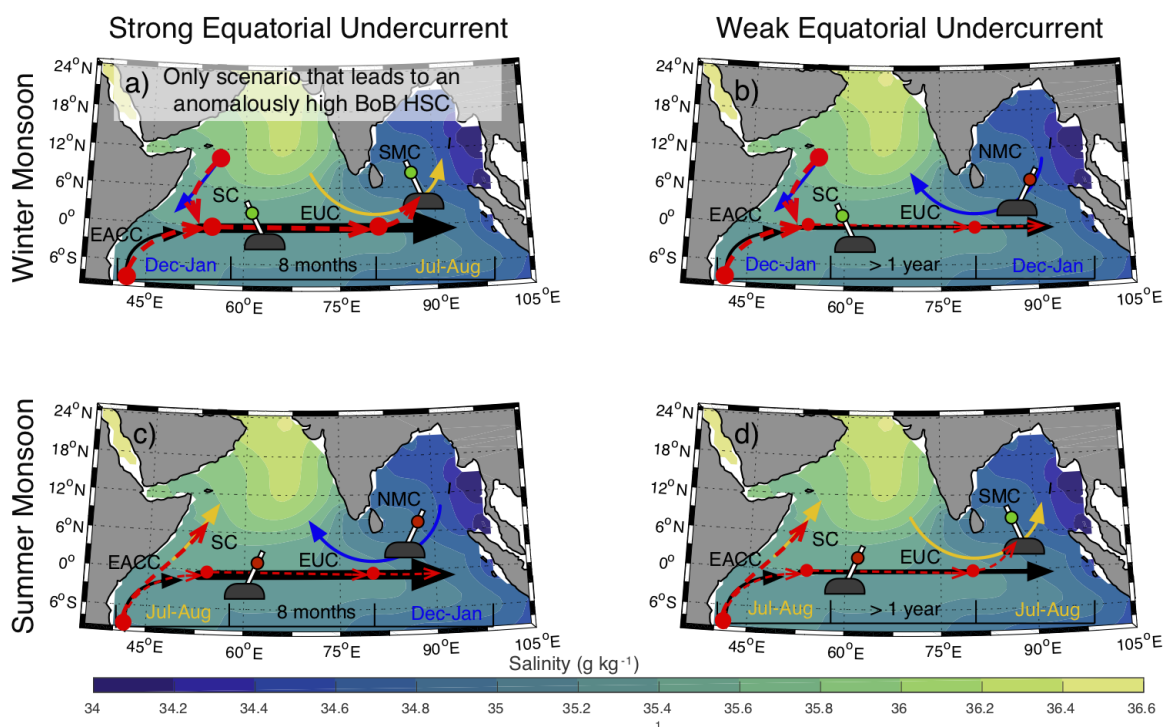
1821

Figure 19: Seasonal circulation pathways in the northern Indian Ocean, or Railroad Switch schematic, on subsurface (90 m) salinity climatology (psu; shaded) from the Argo optimally interpolated product for the four Equatorial Undercurrent scenarios: (a, b) winter monsoon and strong (weak) Equatorial Undercurrent and (c, d) summer monsoon and strong (weak) Equatorial Undercurrent. Red dashed arrows indicate high-salinity advection. BoB = Bay of Bengal; HSC = high-salinity core; SMC = Southwest Monsoon Current; SC = Somali Current; EUC = Equatorial Undercurrent; EACC = East African Coastal Current. From Sanchez-Franks et al. (2019).

7.3 Vertical Mixing

Strong stratification in the Bay of Bengal plays a critical role in setting the upper ocean turbulence, notably leading to relatively weak mixing compared to other regions (e.g. Gregg et al., 2006). However, large-scale inferences suggest that mixing must play a key role in at least two regards. First, the net surface flux during the southwest monsoon on average is warming but yet the SST cools (Shenoi et al, 2002). Second, the large scale salt balance must be closed through upward mixing of high-salinity water carried into the Bay via the Summer Monsoon Current (Vinayachandran et al., 2013).

Recent year-long direct measurements of mixing in the Bay have helped link the seasonal cycle in mixing to the seasonal cycle of winds, currents and freshwater. These year-long measurements were recorded by mixing meters called χpods. χpods consist of two temperature microstructure sensors and a suite of ancillary sensors necessary to infer the rate of dissipation of temperature variance at 1Hz frequency for up to a year (Moum & Nash, 2009). χpods have been deployed on moorings in three different regions of the Bay (Figure 20): the air-sea buoy at 18°N, top 65m (Thakur et al., 2019), RAMA moorings along 90°E (mixing measurements at 15m, 30m and 45m; Warner et al. 2016), and the EBoB array in the south-central Bay (mixing measurements spanning between 30m and 100m at sites in the region 85°E-88°E, 5°N-8°N, Cherian et al., 2020). Across the basin, turbulence within and near the base of the mixed layer shows strong seasonality that parallels the monsoon cycle in winds (Thakur et al., 2019, Warner et al., 2016). In the thermocline of the south-central Bay (EBoB array), mixing is correlated with packets of downward propagating near-inertial waves implicating wind forcing. As depicted in Figure 20, both near-surface and thermocline mixing are relatively high during the NE and SW monsoons (Dec-Feb, May-Sep) and relatively low during the transition (Mar, Apr). Cyclones during the post-monsoon months of October and November can drive a hundredfold increase in near-surface mixing both locally and throughout the Bay (Warner et al. 2016). Mixing profiles collected by a fast thermistor on a CTD rosette during a basin-wide survey before and after the passage of cyclone Madi (6-12 Dec, 2013) show a basin-wide increase in diffusivity linked to near-inertial waves forced by the cyclone (Wijesekera et al., 2016b).
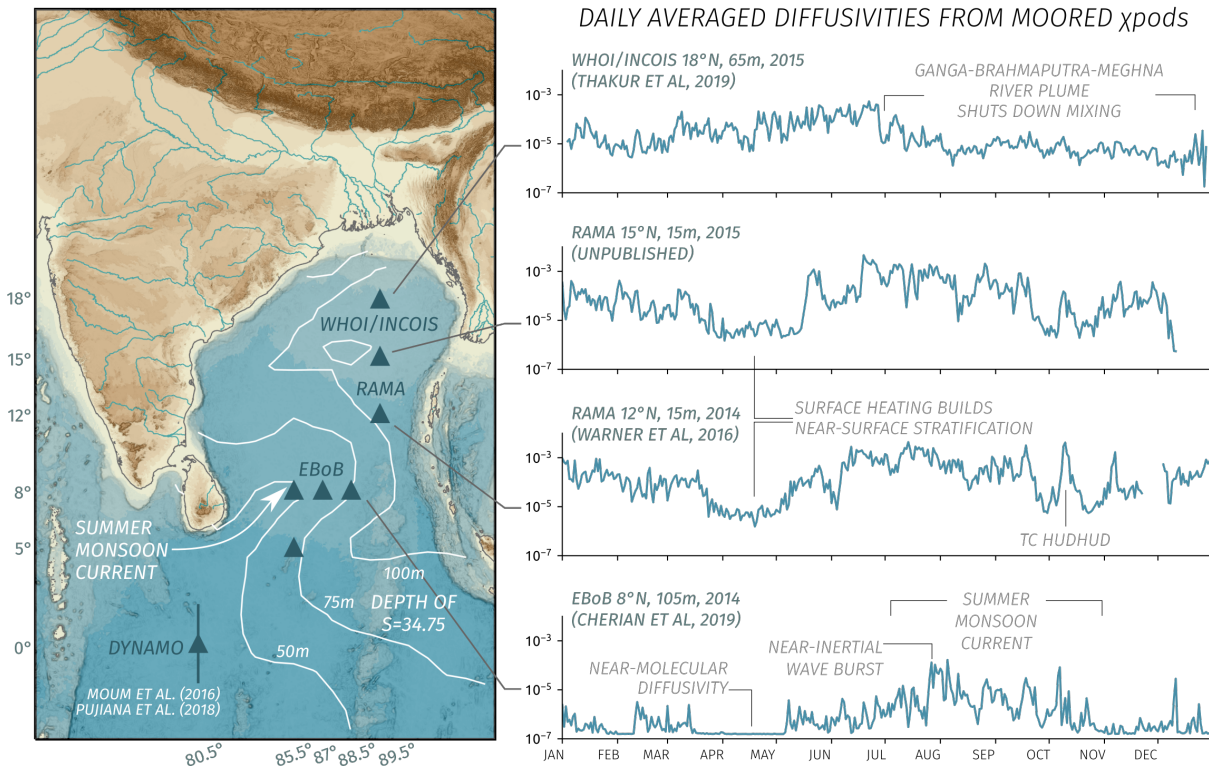
Figure 20: Annual cycle of daily averaged temperature diffusivities derived from χpod measurements. The data are from two different years, 2014 and 2015, depending on location. Note the similar wind-forced seasonal cycle at 12°N, 15m and 15°N, 15m and the dramatically different seasonal cycle at 8°N, 105m (reflecting near-inertial wave activity) and at 18°N, 65m reflecting freshwater influence.

The influence of freshwater is a critical caveat to the above generalizations: the arrival in August of the Ganga-Brahmaputra-Meghna freshwater plume at 18°N has been observed to suppress turbulence (diffusivity $K_T < 10^{-5}$ m² s⁻¹) for multiple months (Aug-Nov) at depths of approximately 50-65 m (Figure 20). This buoyant lens limited the vertical extent of the influence of Tropical Cyclone Komen as compared to a previous (weaker) storm (Chaudhuri et al 2019, Thakur et al 2019). Similar observations of extremely weak turbulence below strong, salinity-stratified surface layers have been reported throughout the Bay using data from a variety of platforms: ship-based microstructure (Jinadasa et al, 2016) profiling floats with a temperature microstructure sensor (Shroyer et al, 2016) and glider-based microstructure measurements (St. Laurent and Merrifield, 2017). Lucas et al (2016) find that near-inertial shear was elevated at the base of the mixed layer but not elevated at the base of the barrier layer — direct evidence that salinity stratification can insulate deeper depths from the effects of near-surface forcing (downward propagating near-inertial waves in this case). Li et al. (2017) use a combination of observations and modelling results to demonstrate that barrier layers in the Bay of Bengal influence the amplitude of

1866 intraseasonal oscillations in SST and precipitation. However, a recent coarse resolution coupled modelling study suggests

1867 that freshwater has little influence on SST or rainfall, since the SST tendency caused by a reduction in mixing is offset by

1868 changes in surface heat fluxes (Krishnamohan et al., 2019)

1869 Surface freshwater advection can create subsurface reservoirs of heat and salt that can be accessed when the winds are strong

1870 enough, such as during cyclones that regularly form in the Bay during October and November. In one dramatic example

1871 Qiu et al (2019) report up to 5 psu increases in SSS and only a smaller 0.5°C decrease in SST following the passage of

1872 Cyclone Phailin (2013). In this case, mooring records indicate that mixing was limited to the isothermal layer (Chaudhuri

1873 et al. 2019). Subsurface warm layers (i.e. temperature inversions stabilized by strong salinity stratification) are also observed,

1874 representing a reservoir of heat that can be accessed if a storm excites enough turbulence, as appears to have happened

1875 during the passage of Cyclone Hudhud (Warner et al, 2016). The influence of stratification in limiting the extent of vertical

1876 mixing and creating subsurface warm layers mean that cyclone-induced cooling is generally either weak or negligible in the

1877 Bay, unlike in other ocean basins (Sengupta et al, 2008).

1878 Long periods of near-molecular diffusivities (weeks to a month) were also inferred at multiple χpods along 8°N between 50

1879 m and 100 m during transition months of March and April. Here freshwater insulation does not appear to be the major factor.

1880 Instead the period of weak turbulence may be linked to low levels of near-inertial energy (a consequence of weak wind

1881 forcing in March and April) and the absence of strong mean oceanic flows during these transition months (Cherian et al

1882 2020). Relatively weak diffusivities are also present in the LADCP fine structure estimate of depth-integrated (thermocline

1883 to bottom) turbulent kinetic energy dissipation ε (Kunze et al, 2006) and the Argo fine structure-based 250-500 m diffusivity

1884 estimates of Whalen et al. (2012). The extended presence of such weak turbulence suggests that the Bay's internal wave

1885 field is weaker than might be expected from the Garrett-Munk internal wave spectrum at least during some months of the

1886 year. Another (related) question is the issue of representation of such weak background mixing in climate models and

1887 whether that matters to known biases in such models.

1888 Published efforts so far have been directed towards understanding the modulation of turbulence by larger-scale variations

1889 in the wind, currents and freshwater. Questions remain as to the impact of small-scale mixing on the large-scale long-term

1890 T-S structure in the Bay as well as the influence of subsurface mixing and the ensuing modification of SST on coupled

1891 ocean-atmosphere phenomena such as the MJO and the MISO (Section 3.2)

1892 **7.4 Where vertical and lateral processes meet: The Role of Submesoscale**

1893 Freshwater inflow from the Ganga-Brahmaputra-Meghna (GBM) and the Irrawady river in the Bay of Bengal is stirred by

1894 the mesoscale eddies into sharp frontal gradients (in salinity and in density) at O(1-10km) scales with shallow vertical extent.

1895 These fronts are acted upon by winds seasonally, setting up complex sub-mesoscale structures with salinity differences O(1

1896   psu) over 1-10 km, developing bore-like features with O(0.5 psu) difference over a few meters horizontally (Nash et al 2016;
1897   Figure 21). Wavenumber spectra of temperature at O(1-10km) scale show a −2 slope in many regions of the Bay (Mackinnon
1898   et al 2016), a signature of frontogenesis in the Bay at these scales. The BoB is thus replete with fronts which evidently slump
1899   at sub-mesoscales due to both symmetric and baroclinic instabilities (Ramachandran et al. 2018), and show higher
1900   stratification near fronts (Sree Lekha 2019) .
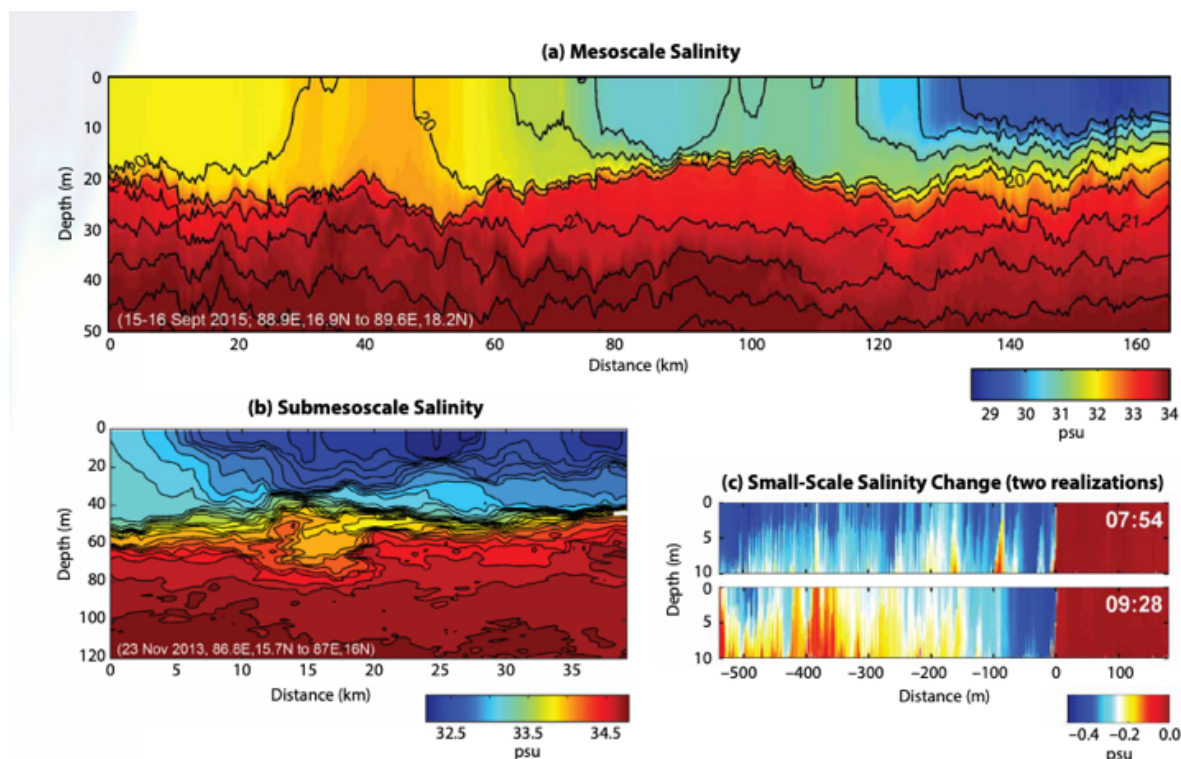
1901

1902   **Figure 21: Observed salinity gradients at mesoscale, sub-mesoscales and small horizontal scales from in the Bay of**
1903   **Bengal (Nash et al. 2016).**

1904   The fronts and filaments at O(1-10km), which are dominated by salinity gradients and weakly compensated, have strong
1905   implications for setting up the density stratification in the top 50-100m in the BoB (Section 4.4.1). The stratification in this
1906   depth range often has multi-layered structure with stratification varying at O(1-10km) scales (Lucas et al 2016), showing
1907   evidence that the stratification in the Bay cannot be explained simply in terms of vertical processes, and horizontal
1908   submesoscale processes are intimately coupled with the vertical processes at these scales. Ramachandran et al. (2018) show
1909   that a mesoscale strained region with strong fronts (O(1kg/m^3 over 40km)) and weak down front wind shows multiple
1910   dynamical signatures of sub-mesoscale instabilities. Ageostrophic secondary circulations arising near the fronts and the
1911   accompanied sheared advection plays an important role in setting the stratification (Pham and Sarkar 2019). Both

1912   observations and process modeling show O(1-10km) patches of low potential vorticity consisting of subducted warm water

1913   patches due to combination of baroclinic and forced symmetric instabilities, creating barrier layers whose thickness varies

1914   laterally at sub-mesoscales (Ramachandran and Tandon, 2020 JGR-in review).

1915   During winter, the temperature gradients in the horizontal compensate for the salinity gradients to reduce the density

1916   gradient, and the sub-mesoscale processes in BoB lead to a unique situation. Jaeger & Mahadevan (2018) show that surface

1917   cooling fluxes combined with submesoscale instabilities of the haline fronts during wintertime leads to shallower mixed

1918   layers on the less saline (cooler) side. Therefore, cold SSTs in wintertime in the Bay mark surface trapped waters (Fig. 22),

1919   whereas in other regions of the world ocean, cold filaments mark upwelling of nutrient-rich waters. Further, since the shallow

1920   fresher mixed layers lead to larger drops in temperature, this develops the correlation between SST and SSS at O(1-10km)

1921   scales.
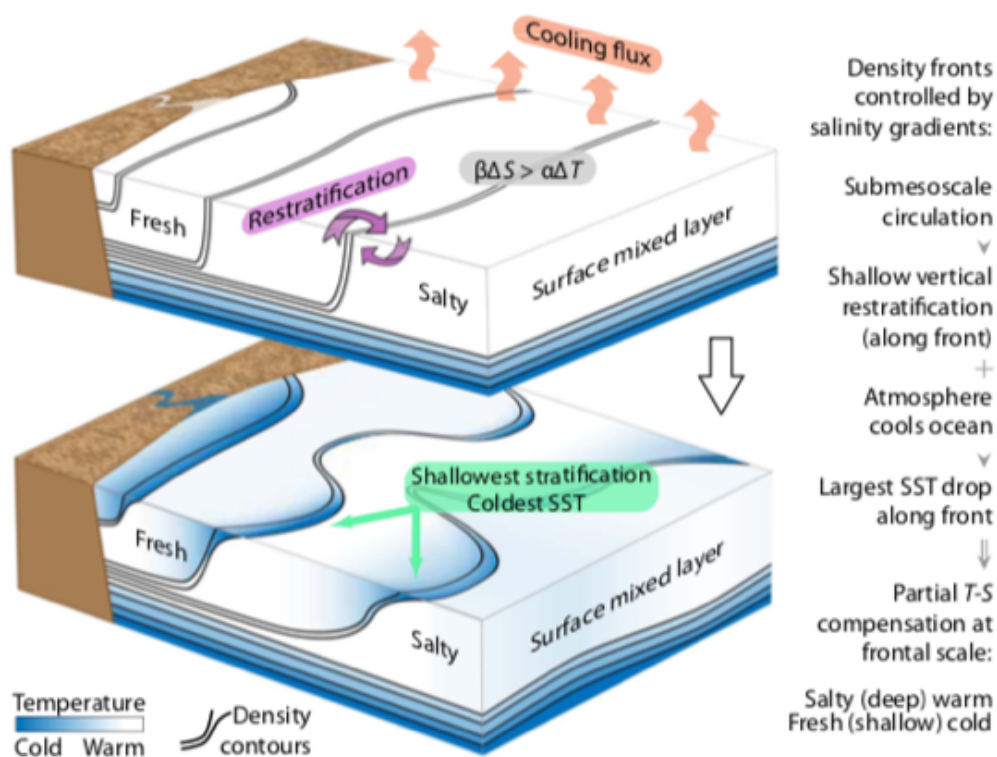
1922

1923   **Figure 22: Interaction of submesoscale salinity gradients with atmospheric cooling leads to shallow cold regions**

1924   **(From Spiro Jaeger and Mahadevan, Science Advances 2018)**

7.5 Putting the Pieces Together

1925

7.5.1 Coupled ocean-atmosphere phenomena

1926

Due to the presence of a barrier layer over much of the Bay of Bengal, entrainment and upwelling of waters from the
thermocline are inhibited, and the evolution of SST is largely driven by net air-sea heat flux variability (Duncan and Han,
2009). However, the dependency of SST on surface fluxes is controlled by subsurface processes such as formation of barrier
layers, entrainment warming and cooling of the mixed layer, penetrative solar radiation and zonal advection (Thangaprakash
et al., 2016). Advection is important in influencing the SST as lateral variations in the mixed layer depth alone can result in
variations in air-sea fluxes of roughly 20 Wm^{-2} over distances of kilometers (Adams et al., 2019). This magnitude is similar
to uncertainty in air-sea flux products (Weller et al. 2016) thus implying that variations in sub-mesoscales are important for
heat balance in the northern BoB. The coupling of the ocean-atmosphere over BoB at large scales implicates the air-sea
interaction and the mixed layer heat budget in BoB (Rahaman et al. 2019), although at oceanic mesoscale and finer scales
in the horizontal and at sub-seasonal timescales this coupling is a topic of active research.

7.5.2 Implications for biogeochemistry in the Bay

1937

Eddies in the central BoB arise not by the baroclinic instability of boundary currents but rather due to planetary wave
dynamics off the equator that triggers coastal Kelvin waves around the Bay. The Kelvin waves then trigger south-westward
propagating Rossby waves, which result in large mesoscale structures in the Bay (Cheng et al. 2018). The Andaman and
Nicobar Islands are also shown to be very important for the generation of these eddies; without these islands the number of
eddies would have reduced to almost half in the western bay of Bengal (Mukherjee et al., 2019).These eddies provide much
of the horizontal stretching and stirring of the tracers, including those relevant to the ecosystems

Eddies have tremendous potential to influence ocean biogeochemistry by providing "new" nutrients to the ocean's euphotic
layer (Stramma et al., 2013). However, we do not fully understand the spatial distribution of nutrients within the eddy
surface area – e.g., there is a debate whether nutrients upwell at the core and downwell at the edge of the eddy, or vice versa.
Further, such discrepancy also continues in the type of eddies – i.e., whether upwelling occurs in cyclonic and downwelling
occurs in anticyclonic eddies and vice versa (Mahadevan, 2014; Mahadevan et al., 2012; Martin and Richards, 2001). But
there is a consensus that eddies do impact biogeochemistry (McGillicuddy et al., 2007).

There have been only a handful of studies on the role of eddies in biological productivity in this region (Kumar et al., 2007;
Singh et al., 2015). Kumar et al. (2007) observed an increase in surface nutrients in the Bay through eddies during both fall-
2002 and spring-2003 followed by higher biomass. Despite being highly eutrophic, biological activity did not increase
following cyclonic eddies during the summer-2003 in the northern Bay (Muraleedharan et al., 2007). But primary production
switched from 'regenerated' to 'new' production during summer-2003. In a ^{15}N based new production estimate to assess the

1955   role of cyclonic eddies in enhancing primary production, Singh et al. (2015) carried out measurements of ^{13}C based primary

1956   production at four stations in the Bay of Bengal (around a cyclonic eddy close to 17.8°N, 87.5°E) during winter 2007. The

1957   measurements sampled one cyclonic eddy during the campaign. The highest surface productivity (2.71 μM C d^{-1}) and

1958   chlorophyll a (0.18 μg L^{-1}) were observed within the eddy due to intrusion of nutrients from subsurface waters. Given new

1959   nitrogen input via vertical mixing, river discharge or aerosol deposition, the additional primary production due to this new

1960   nutrient input and its contribution to the total production increased from 40% to 70%. Eddies could be a reason for the

1961   otherwise unexplained high new production rates in the Bay of Bengal (Singh and Ramesh, 2015). Eddies also seem to have

1962   a potential for transferring a high fraction of fixed carbon to the deep.

1963   **8. Summary and open questions**

1964   This paper illustrates that IIOE-2 and related efforts have driven a suite of new studies in the Indian ocean. An increase in

1965   high quality observations (both increased spatial resolution and the acquisition of longer time series) has led to a substantial

1966   increase in our understanding of processes and interactions. These in-situ observations, in combination with remote sensing,

1967   detailed syntheses and modeling have increased our knowledge of the surface circulation and its complex implications for

1968   biological production, along with an increased understanding of air-sea interaction in the Indian ocean.

1969   There are, however, a number of outstanding questions that require prioritised efforts. Compared to the Atlantic and Pacific,

1970   where the important boundary currents are now being monitored with a suite of gliders with repeated and sustained sections,

1971   the boundary currents and their variability in the Indian Ocean remain poorly constrained. Given the anomalous warming

1972   of the Indian Ocean, the frequency of heatwaves, and the population supported by the Indian Ocean and Monsoons, the air-

1973   sea fluxes and the coupled atmosphere-ocean exchange in this ocean remain poorly understood at many scales.

1974   Understanding of the intermediate, deep and abyssal layer circulation and the vertical overturning cells that connect these

1975   layers in the Indian Ocean is lacking.

1976   There are still large uncertainties in air-sea fluxes. Even in the regional basin of the Bay of Bengal where there have been

1977   focused international efforts, the river discharge and rain need to be better represented in the models, along with the

1978   processes that set the shallow salinity stratification. These have important feedbacks on the SST which impacts atmospheric

1979   convection with a global reach. At longer time scales, the salinity feedbacks to climate at interannual to decadal timescales

1980   need to be investigated in further detail. The decadal variability of the Indian Ocean Dipole and its link to the Pacific decadal

1981   variability also needs to be better understood.

1982   On the influence of small scale mixing, increased measurements of ocean mixing both along the equator and new long term

1983   measurements in the Bay of Bengal, have shown intensively enhanced mixing during the passage of eddies and during

1984 cyclones. However, there are still significant uncertainties in subsurface ocean mixing in setting the large scale balance in
1985 the Indian ocean.

1986 There are still many gaps in current understanding of Indian Ocean biogeochemical cycles. Although the characterization
1987 of the temporal and spatial variability in chlorophyll concentration and primary production has greatly improved as a result
1988 of recent in situ measurements and satellite remote sensing, there are still many areas where there is little or no information
1989 about how this relates to changes in planktonic food web structure and particulate organic matter export to the deep ocean.
1990 Although nutrient limitation patterns were not discussed in this review, it should be pointed out that the importance of
1991 nitrogen verses iron and silica limitation in the Arabian Sea and elsewhere in the Indian Ocean is still a subject of debate -
1992 more nutrient and trace metal measurements are needed along with nutrient limitation bioassays throughout the Indian
1993 Ocean.

1994 The number of nitrogen fixation rate measurements in the Indian Ocean has also increased significantly over the last decade,
1995 but the importance of this process as a source of new nitrogen to the surface ocean has been quantified in only a few regions
1996 (e.g., off northwest Australia) and its contribution to bloom formation (e.g., the Madagascar Bloom) is still uncertain. From
1997 a spatial standpoint, the quantification of biogeochemical variability in the northern Indian Ocean (Arabian Sea and Bay of
1998 Bengal) has benefited, in particular, from numerous shipboard measurements, moorings and biogeochemical Argo float
1999 deployments in the last decade. Many questions still remain, for example, related to the influence of freshwater inputs on
2000 biogeochemical cycles in the Bay of Bengal. Remarkably, the biogeochemical and ecological impacts of the Indonesian
2001 Throughflow have been examined in only a handful of studies. Similarly, there are very few studies that focus on the
2002 biogeochemical and ecological impacts of the Seychelles-Chagos Thermocline Ridge (SCTR). The ITF and the SCTR are
2003 unique features of the Indian Ocean, yet the understanding of their biogeochemical and ecological impacts is rudimentary
2004 at best. Finally, the quantification of biogeochemical variability in the Leeuwin and Agulhas Currents and adjacent waters
2005 has also benefited from recent measurements, though it is important to point out that the biogeochemical impacts of boundary
2006 currents in the Indian Ocean are still poorly understood compared to the Atlantic and Pacific.

2007 Modeling and observational efforts have both pointed to the increased role of air-sea coupling at higher frequencies to
2008 improve the predictions of sub-seasonal Monsoon forecasts. Observations and models indicate that MISOs may be slowing
2009 down because of the warming in the Indian Ocean (e.g. Sabeerali et al. 2013), which needs to be understood better for
2010 providing reliable monsoon predictions and projections in this climate vulnerable region.

2011 **Code Availability**

2012 No original data analyses were undertaken as part of this review paper.

Data Availability

No original data analyses were undertaken as part of this review paper. All data presented in this manuscript have been previously published and are available from sources identified in the original manuscripts.

Author Contributions

HEP and AT designed the review, wrote the introductory and concluding parts and sections in their areas of expertise. HP and AT reviewed the contributions of the authors and made editorial adjustments. RF wrote sections in his area of expertise and contributed editorial advice. RH wrote the sections on biogeochemical variability in Section 4. All co-authors contributed to the writing of sections relevant to their areas of expertise. All authors contributed to refining the manuscript for submission.

Competing interests

The authors declare that they have no conflict of interest.

Acknowledgements

The authors acknowledge the sustained efforts of researchers and funding agencies in observing and modelling the oceanic and atmospheric processes that control climate variability in the Indian Ocean region. These contributions during the International Indian Ocean Expeditions (I and II) and in the intervening years are fundamental to improving our knowledge of these systems and increasing our skill at forecasting variability and extreme events. We thank the IIOE-2 leadership team (https://iioe-2.incois.gov.in/) for their unwavering efforts to share new discoveries and promote understanding of the importance of the Indian Ocean to the climate system and Earth's inhabitants. HEP acknowledges support from the Australian Government's National Environmental Science Programme.

References

Abram, N. J., Gagan, M. K., Cole, J. E., Hantoro, W. S., and Mudelsee, M.: Recent intensification of tropical climate variability in the Indian Ocean. Nature Geoscience, 1, 849–853, https://doi.org/10.1038/ngeo357, 2008.

Abram, N. J., Hargreaves, J. A., Wright, N. M., Thirumalai, K., Ummenhofer, C. C., and England, M. H.: Palaeoclimate perspectives on the Indian Ocean Dipole. Quat. Sci. Rev., 237, 106302, https://doi.org/10.1016/j.quascirev.2020.106302, 2020a.

Abram, N. J., Wright, N. M., Ellis, B., Dixon, B. C., Wurtzel, J. B., England, M. H., Ummenhofer, C. C., Philibosian, B., Cahyarini, S. Y., Yu, T.-L., Shen, C.-C., Cheng, H., Edwards, R. L., and Heslop, D.: Coupling of Indo-Pacific climate variability over the last millennium, Nature, 579, 385-392, https://doi.org/10.1038/s41586-020-2084-4, 2020b.

Akhil, V. P., Durand, F., Lengaigne, M., Vialard, J., Keerthi, M. G., Gopalakrishna, V. V., Deltel, C., Papa, F. and De Boyer Montégut, C.: A modeling study of the processes of surface salinity seasonal cycle in the Bay of Bengal, J. Geophys. Res. Ocean., doi:10.1002/2013JC009632, 2014.

Alory, G., Wijffels, S., and Meyers, G.: Observed temperature trends in the Indian Ocean over 1960–1999 and associated mechanisms. Geophys. Res. Lett., 34, L02606, https://doi.org/10.1029/2006GL028044, 2007.

Anderson, D. L. T., and Gill, A. E.: Spin-up of a stratified ocean, with applications to upwelling, Deep Sea Res., 22(9), 583–596, https://doi.org/10.1016/0011-7471(75)90046-7, 1975.

Andrews, J.C.: Eddy structure and the West Australian current, Deep Sea Research, 24(12), 1133–1148, https://doi.org/10.1016/0146-6291(77)90517-3, 1977.

Annamalai, H., Potemra, J., Murtugudde, R., and McCreary, J. P.: Effect of preconditioning on the extreme climate events in the tropical Indian Ocean, J. Climate, 18, 3450–3469, https://doi.org/10.1175/JCLI3494.1, 2005.

Anutaliya, A., Send, U., Mcclean, J., Sprintall, J., Rainville, L., M. Lee, C., Jinadasa, S., Wallcraft, A, J., Metzger, E.: An undercurrent off the east coast of Sri Lanka. Ocean Sci. Discuss. 13, 1–15, 2017.

Ash, K. D., and Matyas, C. J.: The influences of ENSO and the Subtropical Indian Ocean Dipole on tropical cyclone trajectories in the South Indian Ocean, Int. J. Climatol., 32, 41–56, https://doi.org/10.1002/joc.2249, 2012.

Ayers, J. M., Strutton, P. G., Coles, V. J., Hood, R. R. and Matear, R. J.: Indonesian throughflow nutrient fluxes and their potential impact on Indian Ocean productivity, Geophys. Res. Lett., doi:10.1002/2014GL060593, 2014.

Bahmanpour, M. H., Pattiaratchi, C., Wijeratne, E. M. S., Steinberg, C., and D'Adamo, N.: Multi-year observation of Holloway Current along the shelf edge of North Western Australia, J. Coast. Res., 517–521, https://doi.org/10.2112/SI75-104.1, 2016.

Banse, K. and English, D. C.: Geographical differences in seasonality of CZCS-derived phytoplankton pigment in the Arabian Sea for 1978-1986, Deep. Res. Part II Top. Stud. Oceanogr., doi:10.1016/S0967-0645(99)00157-5, 2000.

Banse, K. and McClain, C.: Winter blooms of phytoplankton in the Arabian Sea as observed by the Coastal Zone Color Scanner, Mar. Ecol. Prog. Ser., doi:10.3354/meps034201, 1986.

Barlow, R., Lamont, T., Kyewalyanga, M., Sessions, H. and Morris, T.: Phytoplankton production and physiological adaptation on the southeastern shelf of the Agulhas ecosystem, Cont. Shelf Res., doi:10.1016/j.csr.2010.05.007, 2010.

Barlow, R., Lamont, T., Morris, T., Sessions, H. and van den Berg, M.: Adaptation of phytoplankton communities to mesoscale eddies in the Mozambique Channel, Deep. Res. Part II Top. Stud. Oceanogr., doi:10.1016/j.dsr2.2013.10.020, 2014.

Beal, L. M. and Bryden, H. L.: The velocity and vorticity structure of the Agulhas Current at 32°S, J. Geophys. Res. Ocean., doi:10.1029/1998jc900056, 1999.

Beal, L. M., De Ruijter, W. P. M., Biastoch, A., Zahn, R., Cronin, M., Hermes, J., Lutjeharms, J., Quartly, G., Tozuka, T., Baker-Yeboah, S., Bornman, T., Cipollini, P., Dijkstra, H., Hall, I., Park, W., Peeters, F., Penven, P., Ridderinkhof, H. and Zinke, J.: On the role of the Agulhas system in ocean circulation and climate, Nature, doi:10.1038/nature09983, 2011.

Beal, L. M. and Donohue, K. A.: The Great Whirl: Observations of its seasonal development and interannual variability, J. Geophys. Res. Ocean., doi:10.1029/2012JC008198, 2013.

Beal, L. and Elipot, S.: Broadening not strengthening of the Agulhas Current since the early 1990s. *Nature,* 540, 570–573, https://doi.org/10.1038/nature19853, 2016.

Beal, L. M., Vialard, J., Roxy, M. K., Li, J., Andres, M., Annamalai, H., Feng, M., Han, W., Hood, R., Lee, T., Lengaigne, M., Lumpkin, R., Masumoto, Y., McPhaden, M. J., Ravichandran, M., Shinoda, T., Sloyan, B. M., Strutton, P. G., Subramanian, A. C., Tozuka, T., Ummenhofer, C. C., Unnikrishnan, A. S., Wiggert, J., Yu, L., Cheng, L., Desbruyères, D. G., & Parvathi, V.: A Road Map to IndOOS-2: Better Observations of the Rapidly Warming Indian

2084   Ocean, Bulletin of the American Meteorological Society, 101(11), E1891-E1913,
2085   https://journals.ametsoc.org/view/journals/bams/101/11/bamsD190209.xml, 2020.
2086 Behera, S.K., and Yamagata, T.: Subtropical SST dipole events in the southern Indian Ocean, Geophys. Res. Lett., 28,
2087   327–330, https://doi.org/2000GL011451, 2001.
2088 Bellon, G., Sobel, A. H., and Vialard, J.: Ocean-atmosphere coupling in the monsoon intraseasonal oscillation: A simple
2089   model study, J. Clim., 21(20), 5254–5270, http://doi.org/10.1175/2008JCLI2305.1, 2008.
2090 Benthuysen, J., Feng, M., and Zhong, L.: Spatial patterns of warming off Western Australia during the 2011 Ningaloo
2091   Niño: quantifying impacts of remote and local forcing, Continental Shelf Res., 91, 232–246,
2092   https://doi.org/10.1016/j.csr.2014.09.014, 2014a.
2093 Benthuysen, J., Furue, R., McCreary, J. P., Bindoff, N. L., and Phillips, H. E.: Dynamics of the Leeuwin Current: Part 2.
2094   Impacts of mixing, friction, and advection on a buoyancy-driven eastern boundary current over a shelf, Dyn. Atmos.
2095   Oceans, 65, 39–63, https://doi.org/10.1016/j.dynatmoce.2013.10.004, 2014b.
2096 Benthuysen, J. A., Oliver, E.C.J. , Feng, M., and Marshall, A. G.: Extreme marine warming across tropical Australia
2097   during austral summer 2015–2016, J. Geophys. Res.: Oceans, 123, 1301-1326, https://doi.org/10.1002/2017JC013326,
2098   2018.
2099 Bergman, J. W., Hendon, H. H., and Weickmann, K. M.: Intraseasonal air-sea interactions at the onset of El Nino, J.
2100   Climate, 14, 1702–1719, 2001.
2101 Beron-Vera, F. J., Wang, Y., Olascoaga, M. J., Goni, G. J. and Haller, G.: Objective detection of oceanic eddies and the
2102   agulhas leakage, J. Phys. Oceanogr., doi:10.1175/JPO-D-12-0171.1, 2013.
2103 Biastoch, A., Böning, C. W. and Lutjeharms, J. R. E.: Agulhas leakage dynamics affects decadal variability in Atlantic
2104   overturning circulation, Nature, doi:10.1038/nature07426, 2008.
2105 Biastoch, A., Böning, C. W., Schwarzkopf, F. U. and Lutjeharms, J. R. E.: Increase in Agulhas leakage due to poleward
2106   shift of Southern Hemisphere westerlies, Nature, doi:10.1038/nature08519, 2009.
2107 Biastoch, A. and Böning, C. W.: Anthropogenic impact on Agulhas leakage, Geophys. Res. Lett., doi:10.1002/grl.50243,
2108   2013.
2109 Biastoch, A., Durgadoo, J. V., Morrison, A. K., Van Sebille, E., Weijer, W. and Griffies, S. M.: Atlantic multi-decadal
2110   oscillation covaries with Agulhas leakage, Nat. Commun., doi:10.1038/ncomms10082, 2015.
2111 Boyd, A. J. and Shillington, F. A.: Physical forcing and circulation patterns on the Agulhas Bank, S. Afr. J. Sci., 90(3)
2112   114-122, 1994.
2113 Brock, J. C. and McClain, C. R.: Interannual variability in phytoplankton blooms observed in the northwestern Arabian
2114   Sea during the southwest monsoon, J. Geophys. Res., doi:10.1029/91JC02225, 1992.
2115 Brown, S. L., Landry, M. R., Barber, R. T., Campbell, L., Garrison, D. L. and Gowing, M. M.: Picophytoplankton
2116   dynamics and production in the Arabian Sea during the 1995 Southwest Monsoon, Deep. Res. Part II Top. Stud.
2117   Oceanogr., doi:10.1016/S0967-0645(99)00042-9, 1999.
2118 Bryden, H. and Beal, L.: Role of the Agulhas Current in Indian Ocean circulation and associated heat and freshwater
2119   fluxes. Deep-Sea Research I, 48(8), 1821-1845, 2001.
2120 Burchall, J. : An evaluation of primary productivity studies in the continental shelf region of the Agulhas Current near
2121   Durban (1961-1966), Investigational Report, Oceanographic Research Institute, 20: 16 pp, 1968.
2122 Cai, W., Sullivan, A., and Cowan, T.: Shoaling of the off-equatorial south Indian Ocean thermocline: Is it driven by
2123   anthropogenic forcing? Geophys. Res. Lett., 35, https://doi.org/10.1029/2008GL034174, 2008.
2124 Cai, W., Cowan, T., and Sullivan, A.: Recent unprecedented skewness towards positive Indian Ocean Dipole
2125   occurrences and their impact on Australian rainfall. Geophys. Res. Lett., 36, https://doi.org/10.1029/2009GL037604,
2126   2009a.
2127 Cai, W., Pan, A., Roemmich, D., Cowan, T., and Guo, X.: Argo profiles a rare occurrence of three consecutive positive
2128   Indian Ocean Dipole events, 2006–2008, Geophys. Res. Lett., 36, https://doi.org/10.1029/2008GL037038, 2009b.

Cai, W., Sullivan, A., and Cowan, T.: Climate change contributes to more frequent consecutive positive Indian Ocean Dipole events. Geophys. Res. Lett., 36 (L23704), https://doi.org/10.1029/2009GL040163, 2009c.

Cai, W., Sullivan, A., and Cowan, T.: How rare are the 2006–2008 positive Indian Ocean Dipole events? An IPCC AR4 climate model perspective, Geophys. Res. Lett., 36 (L08702), https://doi.org/10.1029/2009GL037982, 2009d.

Cai, W., Zheng, X.-T. , Weller, E., Collins, M., Cowan, T., Lengaigne, M., Yu, W., and Yamagata, T.: Projected response of the Indian Ocean Dipole to greenhouse warming, Nat. Geosci., 6, 999-1007, https://doi.org/10.1038/ngeo2009, 2013.

Cai, W., Santoso, A., Wang, G., Weller, E., Wu, L., Ashok, K., Masumoto, Y., and Yamagata, T.: Increased frequency of extreme Indian Ocean Dipole events due to greenhouse warming, Nature, 510, 254-258, https://doi.org/10.1038/nature13327, 2014a.

Cai, W. , Borlace, S., Lengaigne, M., van Rensch, P., Collins, M., Vecchi, G., Timmermann, A., Santoso, A., McPhaden, M. J., Wu, L,. and England, M. H.: Increasing frequency of extreme El Niño events due to greenhouse warming, Nat. Clim. Change, 4, 2, 111–116, https://doi.org/10.1038/nclimate2100, 2014b.

Cai, W. Wang, G., Santoso, A., McPhaden, M. J., Wu, L., Jin, F. F., Timmermann, A., Collins, M., Vecchi, G., Lengaigne, M., and England, M. H.: Increased frequency of extreme La Niña events under greenhouse warming, Nat. Clim. Change, 5, 2, 132–137, https://doi.org/10.1038/nclimate2492, 2015.

Cai, W. et al.: Pantropical climate interactions. Science, 363, doi:10.1126/science.aav4236, 2019.

Caley, T., Giraudeau, J., Malaizé, B., Rossignol, L. and Pierre, C.: Agulhas leakage as a key process in the modes of Quaternary climate changes, Proc. Natl. Acad. Sci. U. S. A., doi:10.1073/pnas.1115545109, 2012.

Caputi, N., de Lestang, S., Feng, M., and Pearce, A. F.: Seasonal variation in the long-term warming trend in water temperature off the Western Australian coast. Mar. Freshw. Res., 60, 129-139, 2009.

Carter, R. A. and Schleyer, M. H.: Plankton distributions in Natal coastal waters., E. H. Schumann (ed.), Coastal Ocean Studies off Natal, South Africa (Springer-Verlag: New York), 2012.

Castellanos, P., Campos, E. J. D., Piera, J., Sato, O. T. and Silva Dias, M. A. F.: Impacts of Agulhas leakage on the tropical Atlantic western boundary systems, J. Clim., doi:10.1175/JCLI-D-15-0878.1, 2017.

Cessi, P.: The Global Overturning Circulation, Annual Review of Marine Science, 11(1), 249-270, https://doi.org/10.1146/annurev-marine-010318-095241, 2019.

Chatterjee, A., Shankar, D., McCreary, J. P., Vinayachandran, P. N. and Mukherjee, A.: Dynamics of Andaman Sea circulation and its role in connecting the equatorial Indian Ocean to the Bay of Bengal, J. Geophys. Res. Ocean., doi:10.1002/2016JC012300, 2017.

Chaudhuri, D., Sengupta, D., D'Asaro, E., Venkatesan, R. and Ravichandran, M.: Response of the salinity-stratified bay of Bengal to Cyclone Phailin, J. Phys. Oceanogr., doi:10.1175/JPO-D-18-0051.1, 2019.

Chen, G., Han, W., Li, Y., Wang, D. and McPhaden, M. J.: Seasonal-to-interannual time-scale dynamics of the equatorial undercurrent in the Indian Ocean, J. Phys. Oceanogr., doi:10.1175/JPO-D-14-0225.1, 2015.

Cheng, Y., Putrasahan, D., Beal, L. and Kirtman, B.: Quantifying Agulhas leakage in a high-resolution climate model, J. Clim., doi:10.1175/JCLI-D-15-0568.1, 2016.

Cheng, Y., Beal, L.M., Kirtman, B.P., and Putrasahan, D.: Interannual Agulhas Leakage Variability and Its Regional Climate Imprints, J. Climate, 31(24), 10105–10121, 2018.

Cheng, X., McCreary, J. P., Qiu, B., Qi, Y., Du, Y. and Chen, X.: Dynamics of Eddy Generation in the Central Bay of Bengal, J. Geophys. Res. Ocean., doi:10.1029/2018JC014100, 2018.

Chi, N.-H., Lien, R.-C., D'Asaro, E. A., and Ma, B. B.: The surface mixed layer heat budget from mooring observations in the central Indian Ocean during Madden-Julian Oscillation events, J. Geophys. Res. Ocean., 119(7), 4638–4652, https://doi.org/10.1002/2014JC010192, 2014.

Chowdary, J. S., Bandgar, A. B., Gnanaseelan, C., and Luo, J. J.: Role of tropical Indian Ocean air-sea interactions in modulating Indian summer monsoon in a coupled model, Atmos. Sci. Lett., 16(2), 170–176, doi:10.1002/asl2.561, 2015.

Ocean Science

Discussions

2174 Church, J.A., Cresswell, G.R., and Godfrey J.S.: The Leeuwin Current, in: Poleward Flows Along Eastern Ocean
2175 Boundaries, Coastal and Estuarine Studies (formerly Lecture Notes on Coastal and Estuarine Studies), vol 34, edited by:
2176 Neshyba, S.J., Mooers, C.N.K., Smith, R.L., and Barber, R.T., Springer, New York, 230–254,
2177 https://doi.org/10.1007/978-1-4613-8963-7_16, 1989.

2178 Cirano, M. and Middleton, J.F.: Aspects of the mean wintertime circulation along Australia's southern shelves:
2179 Numerical studies. J. Phys. Oceanogr., 34, 668–684, https://doi.org/10.1175/2509.1, 2004.

2180 Coles, V. J., Wilson, C. and Hood, R. R.: Remote sensing of new production fuelled by nitrogen fixation, Geophys. Res.
2181 Lett., doi:10.1029/2003gl019018, 2004.

2182 Cullen, K. E. and Shroyer, E. L.: Seasonality and interannual variability of the Sri Lanka dome, Deep. Res. Part II Top.
2183 Stud. Oceanogr., doi:10.1016/j.dsr2.2019.104642, 2019.

2184 Currie, J. C., Lengaigne, M., Vialard, J., Kaplan, D. M., Aumont, O., Naqvi, S. W. A., and Maury, O.: Indian Ocean
2185 Dipole and El Niño/Southern Oscillation impacts on regional chlorophyll anomalies in the Indian Ocean.
2186 Biogeosciences, 10, 6677-6698, 2013.

2187 D'Adamo, N., Fandry, C., Buchan, S., Domingues, C.: Northern sources of the Leeuwin Current and the "Holloway
2188 Current" on the North West Shelf, J. Roy. Soc. Western Australia, 92(2), 53–66, http://nora.nerc.ac.uk/id/eprint/526029,
2189 2009.

2190 de Vos, A., Pattiaratchi, C. B. and Wijeratne, E. M. S.: Surface circulation and upwelling patterns around Sri Lanka,
2191 Biogeosciences, doi:10.5194/bg-11-5909-2014, 2014.

2192 Demarcq, H., Barlow, R. G. and Shillington, F. A.: Climatology and variability of sea surface temperature and surface
2193 chlorophyll in the benguela and agulhas ecosystems as observed by satellite imagery, African J. Mar. Sci.,
2194 doi:10.2989/18142320309504022, 2003.

2195 DeMott, C. A., Klingaman, N. P., and Woolnough, S. J.: Atmosphere-ocean coupled processes in the Madden-Julian
2196 oscillation, Rev. Geophys., 53, 1099–1154, http://doi.org/10.1002/2014RG000478, 2015.

2197 Desbruyères, D. G., McDonagh, E. L., King, B. A., and Thierry, V.: Global and Full-Depth Ocean Temperature Trends
2198 during the Early Twenty-First Century from Argo and Repeat Hydrography, J. Climate, https://doi.org/10.1175/JCLI-D-
2199 16-0396.1, 2017.

2200 Deshpande, A., Gnanaseelan, C., Chowdary, J., and Rahul, S.: Interannual spring Wyrtki jet variability and its regional
2201 impacts, Dyn. Atmos. Oceans, 78, 26–37, 2017.

2202 Dilmahamod, Ahmad Fehmi: Links between the Seychelles-Chagos thermocline ridge and large scale climate modes
2203 and primary productivity and the annual cycle of chlorophyll-a, PhD thesis, University of Cape Town, 2014.

2204 Dilmahamod, A. F., Aguiar-González, B., Penven, P., Reason, C. J. C., De Ruijter, W. P. M., Malan, N., & Hermes, J.
2205 C.: SIDDIES corridor: A major east-west pathway of long-lived surface and subsurface eddies crossing the subtropical
2206 south indian ocean. Journal of Geophysical Research: Oceans, 123, 5406– 5425. https://doi.org/10.1029/2018JC013828,
2207 2018.

2208 Dilmahamod, A. F., Penven, P., Aguiar-González, B., Reason, C. J. C., & Hermes, J. C.: A new definition of the South-
2209 East Madagascar Bloom and analysis of its variability. Journal of Geophysical Research: Oceans, 124, 1717–1735.
2210 https://doi.org/10.1029/2018JC014582, 2019.

2211 Divakaran, P., and Brassington, G.B.: Arterial ocean circulation of the southeast Indian Ocean, Geophys. Res. Lett., 38,
2212 L01802, https://doi.org/10.1029/2010GL045574, 2011.

2213 Domingues, C. M., Wijffels, S. E., Maltrud, M. E., Church, J. A. and Tomczak, M.: Role of eddies in cooling the
2214 Leeuwin Current, Geophys. Res. Lett., doi:10.1029/2005GL025216, 2006.

2215 Domingues, C. M., Maltrud, M. E., Wijffels, S. E., Church, J. A., Tomczak, M.: Simulated Lagrangian pathways
2216 between the Leeuwin Current System and the upper-ocean circulation of the southeast Indian Ocean, Deep Sea Res. II,
2217 54, 797–817, http://doi.org/10.1016/j.dsr2.2006.10.003, 2007.

2218 Dong, L., Zhou, T., Dai, A., Song, F., Wu, B., and Chen, X.: The footprint of the inter-decadal Pacific oscillation in
2219 Indian Ocean sea surface temperatures, Sci. Rep., 6, 21251, https://doi.org/10.1038/srep21251, 2016.

Donohue, K. A. and Toole, J. M.: A near-synoptic survey of the Southwest Indian Ocean, Deep. Res. Part II Top. Stud. Oceanogr., doi:10.1016/S0967-0645(03)00039-0, 2003.

Drushka, K., Sprintall, J., Gille, S. T. and Brodjonegoro, I.: Vertical structure of Kelvin waves in the Indonesian throughflow exit passages, J. Phys. Oceanogr., doi:10.1175/2010JPO4380.1, 2010.

Drushka, K., Sprintall, J., Gille, S. T. and Wijffels, S.: In situ observations of Madden-Julian oscillation mixed layer dynamics in the Indian and western Pacific Oceans, J. Clim., 25(7), 2306–2328, doi:10.1175/JCLI-D-11-00203.1, 2012.

Du, Y., Xie, S.-P., Huang, G., and Hu, K.: Role of air–sea interaction in the long persistence of El Niño–induced north Indian Ocean warming, J. Clim., 22, 2023-2038, https://doi.org/10.1175/2008JCLI2590.1, 2009.

Du, Y., Cai, W., and Wu, Y.: A new type of the Indian Ocean dipole since the mid-1970s, J. Climate, 26, 959-972, https://doi.org/10.1175/JCLI-D-12-00047.1, 2013.

Du, Y., Y. Zhang, M. Feng, T. Wang, N. Zhang, and S. Wijffels, S.: Decadal trends of the upper ocean salinity in the tropical Indo-Pacific since mid-1990s, Scientific Reports, 5, 16050, 2015.

Dufois, F., Hardman-Mountford, N. J., Greenwood, J., Richardson, A. J., Feng, M., Herbette, S. and Matear, R.: Impact of eddies on surface chlorophyll in the South Indian Ocean, J. Geophys. Res. Ocean.,119, 8061-77, doi:10.1002/2014JC010164, 2014.

Duncan, B. and Han, W.: Influence of atmospheric intraseasonal oscillations on seasonal and interannual variability in the upper Indian Ocean, J. Geophys. Res. Ocean.,117,1-24 doi:10.1029/2012JC008190, 2012.

Duran, E. R.: An investigation of the Leeuwin Undercurrent source waters and pathways. Honours thesis, University of Tasmania, 2015.

Duran, E.R., Phillips, H.E., Furue, R., Spence, P., and Bindoff, N.L.: Southern Australia Current System based on a gridded hydrography and a high-resolution model, Prog. Oceanogr., 181, 102254, https://doi.org/10.1016/j.pocean.2019.102254, 2020.

Durgadoo, J. V., Loveday, B. R., Reason, C. J. C., Penven, P. and Biastoch, A.: Agulhas leakage predominantly responds to the southern hemisphere westerlies, J. Phys. Oceanogr., 43, 2113-2131, doi:10.1175/JPO-D-13-047.1, 2013.

Durgadoo, J. V., Rühs, S., Biastoch, A. and Böning, C. W. B.: Indian Ocean sources of Agulhas leakage, J. Geophys. Res. Ocean., doi:10.1002/2016JC012676, 2017.

Elipot, S., & Beal, L. M.: Characteristics, energetics, and origins of agulhas current meanders and their limited influence on ring shedding. *Journal of Physical Oceanography*, *45*(9), 2294-2314. https://doi.org/10.1175/JPO-D-14-0254.1, 2015.

Endo, S., and Tozuka, T.: Two flavors of the Indian Ocean dipole, Climate Dyn., 46, 3371-3385, https://doi.org/10.1007/s00382-015-2773-0, 2016.

England, M. H., and Huang, F.: On the interannual variability on the Indonesian Throughflow and its linkage with ENSO, J. Climate, 18(9), 1435-1444, https://doi.org/10.1175/JCLI3322.1, 2005.

England, M. H., Ummenhofer, C. C. and Santoso, A.: Interannual rainfall extremes over southwest Western Australia linked to Indian Ocean climate variability, J. Clim., doi:10.1175/JCLI3700.1, 2006.

Fan, L., Liu, Q., Wang, C., and Guo, F.: Indian Ocean dipole modes associated with different types of ENSO development, J. Climate, 30, 2233–2249, https://doi.org/10.1175/JCLI-D-16-0426.1, 2017.

Fang, F., and Morrow, R.: Evolution, movement and decay of warm-core Leeuwin Current eddies, Deep Sea Res. II, 50(12–13), 2245–2261, https://doi.org/10.1016/S0967-0645(03)00055-9, 2003.

Fang, G., Susanto, R. D., Wirasantosa, S., Qiao, F., Supangat, A., Fan, B., Wei, Z., Sulistiyo, B. and Li, S.: Volume, heat, and freshwater transports from the South China Sea to Indonesian seas in the boreal winter of 2007-2008, J. Geophys. Res. Ocean., doi:10.1029/2010JC006225, 2010.

Feng, M., and Wijffels, S.:Intraseasonal variability in the South Equatorial Current of the East Indian Ocean. *Journal of Physical Oceanography*, 32, 265-277, 2002.

Feng, M., Meyers, G., Pearce, A., and Wijffels, S.: Annual and interannual variations of the Leeuwin Current at 32°S, J. Geophys. Res., 108(C11), 3355, https://doi.org/10.1029/2002JC001763, 2003.

Feng, M., Wijffels, S., Godfrey, S., and Meyers, G.: Do eddies play a role in the momentum balance of the Leeuwin Current? J. Phys. Oceanogr., 35, 964–975, https://doi.org/10.1175/JPO2730.1, 2005.

Feng, M., Majewski, L.J., Fandry, C.B., Waite, A.M., Characteristics of two counter-rotating eddies in the Leeuwin Current system off the Western Australian coast, Deep Sea Research II, 54(8–10), 961–980, https://doi.org/10.1016/j.dsr2.2006.11.022, 2007.

Feng, M., Biastoch, A., Böning, C., Caputi, N., and Meyers, G.: Seasonal and interannual variations of upper ocean heat balance off the west coast of Australia, J. Geophys. Res., 113, C12025, http://doi.org/10.1029/2008JC004908, 2008.

Feng, M., Böning, C.W., Biastoch, A., Behrens, E., Weller, E., Masumoto, Y.: The reversal of the multi-decadal trends of the equatorial Pacific easterly winds, and the Indonesian Throughflow and Leeuwin Current transports. Geophys. Res.Lett. 38, L11604, 2011.

Feng, M., McPhaden, M.J., Xie, S.P., and Hafner, J.: La Niña forces unprecedented Leeuwin Current warming in 2011, Sci. Rep., 3, 1277, https://doi.org/10.1038/srep01277, 2013.

Feng, M., Benthuysen, J., Zhang, N., and Slawinski, D.:Freshening anomalies in the Indonesian throughflow and impacts on the Leeuwin Current during 2010–2011, Geophys. Res. Lett., 42, 8555–8562, https://doi.org/10.1002/2015GL065848, 2015a.

Feng, M., Hendon, H. H., Xie, S.-P., Marshall, A. G., Schiller, A., Kosaka, Y., Caputi, N., and Pearce, A.: Decadal increase in Ningaloo Niño since the late 1990s, Geophys. Res. Lett., 42, 1, 104-112, https://doi.org/10.1002/2014GL062509, 2015b.

Feng, M., Zhang, X., Oke, P., Monselesan, D., Chamberlain, M., Matear, R., and Schiller, A.: Invigorating ocean boundary current systems around Australia during 1979–2014: As simulated in a near-global eddy-resolving ocean model. J. Geophys. Res. Oceans, 121(5), 3395–3408, https://doi.org/10.1002/2016JC011842, 2016.

Feng, M., Zhang, N., Liu, Q. and Wijffels, S.: The Indonesian throughflow, its variability and centennial change, Geosci. Lett., doi:10.1186/s40562-018-0102-2, 2018.

Feng, X., and Shinoda, T.: Air-sea heat flux variability in the southeast Indian Ocean and its relation with Ningaloo Niño. Front. Mar. Sci., 6, 266, https://doi.org/10.3389/fmars.2019.00266, 2019.

Fieux, M., Schott, F. and Swallow, J. C.: Deep boundary currents in the western Indian Ocean revisited, Deep Sea Res. Part A, Oceanogr. Res. Pap., doi:10.1016/0198-0149(86)90124-X, 1986.

Fine, R. A., Smethie W. M., Bullister, J. L., Rhein M., Min, D. H., Warner, M. J., Poisson, A., Weiss, R. F.: Decadal ventilation and mixing of Indian Ocean waters. Deep-Sea Res I, 55, 20–37, https://doi.org/10.1016/j.dsr.2007.10.002, 2008.

Foltz, G. R., Vialard, J., Kumar, B. P. and Mcphaden, M. J.: Seasonal mixed layer heat balance of the southwestern tropical Indian Ocean, J. Clim., doi:10.1175/2009JCLI3268.1, 2010.

Francis, P.A., Jithin, A. K., Effy, J. B., Chatterjee, A., Chakraborty, K. et al.: High-resolution operational ocean forecast and reanalysis system for the Indian Ocean. Bulletin of the American Met. Soc., 101(8), E1340-E1356, https://journals.ametsoc.org/view/journals/bams/101/8/bamsD190083.xml, 2020.

Furnas, M.: Intra-seasonal and inter-annual variations in phytoplankton biomass, primary production and bacterial production at North West Cape, Western Australia: Links to the 1997-1998 El Niño event, Cont. Shelf Res., doi:10.1016/j.csr.2007.01.002, 2007.

Furue, R., McCreary, J. P., Benthuysen, J., Phillips, H. E., and Bindoff, N. L.: Dynamics of the Leeuwin Current: Part 1. Coastal flows in an inviscid, variable-density, layer model, Dyn. Atmos. Oceans, 63, 24–59, https://doi.org/10.1016/j.dynatmoce.2013.03.003, 2013.

Furue, R., Guerreiro, K., Phillips, H. E., McCreary, J. P., and Bindoff, N. L.: On the Leeuwin Current System and its linkage to zonal flows in the South Indian Ocean as inferred from a gridded hydrography, J. Phys. Oceanogr., 47, 583–602, https://doi.org/10.1175/JPO-D-16-0170.1, 2017.

Furue, R.: The three-dimensional structure of the Leeuwin Current System in density coordinates in an eddy-resolving OGCM, Ocean Modelling, 138, 36–50, https://doi.org/10.1016/j.ocemod.2019.03.001, 2019.

Ganachaud, A., Wunsch, C., Marotzke, J. and Toole, J.: Meridional overturning and large-scale circulation of the Indian Ocean, J. Geophys. Res. Ocean., doi:10.1029/2000jc900122, 2000.

Gandhi, N., Singh, A., Prakash, S., Ramesh, R., Raman, M., Sheshshayee, M. and Shetye, S.: First direct measurements of N_2 fixation during a *Trichodesmium* bloom in the eastern Arabian Sea, Global Biogeochemical Cycles, 25(4), 2011.

Garrison, D. L., Gowing, M. M., Hughes, M. P., Campbell, L., Caron, D. A., Dennett, M. R., Shalapyonok, A., Olson, R. J., Landry, M. R., Brown, S. L., Liu, H. Bin, Azam, F., Steward, G. F., Ducklow, H. W. and Smith, D. C.: Microbial food web structure in the Arabian Sea: A US JGOFS study, Deep. Res. Part II Top. Stud. Oceanogr., doi:10.1016/S0967-0645(99)00148-4, 2000.

Gaube, P., Chelton, D. B., Strutton, P. G. and Behrenfeld, M. J.: Satellite observations of chlorophyll, phytoplankton biomass, and Ekman pumping in nonlinear mesoscale eddies, J. Geophys. Res. Ocean., doi:10.1002/2013JC009027, 2013.

George, J. V., Nuncio, M., Chacko, R., Anilkumar, N., Noronha, S. B., Patil, S. M., Pavithran, S., Alappattu, D. P., Krishnan, K. P. and Achuthankutty, C. T.: Role of physical processes in chlorophyll distribution in the western tropical Indian Ocean, J. Mar. Syst., doi:10.1016/j.jmarsys.2012.12.001, 2013.

George, J. V., Vinayachandran, P. N., Vijith, V., Thusaraa, V., Nayaka, A. A, Pargaonkara, S. K., Amol, P., Vijaykumar, K., and Matthews, A. J.: Mechanisms of barrier layer formation and erosion from in situ observations in the Bay of Bengal, J. Phys. Oceanogr., 49, 1183–1200, https://doi.org/10.1175/JPO-D-18-0204.1, 2019.

Gilmour, J. P., Cook, K. L., Ryan, N. M., Puotinen, M. L., Green, R. H., Shedrawi, G., Hobbs, J.-P. A., Thmson, D.P., Babcock, R.C., Buckee, J., Foster, T., Richards, Z. T., Wilson, S. K., Barnes, P. B., Coutts, T. B., Radford, B. T., Piggott, C. H., Depczynski, M., Evans, S. N., Schoepf, V., Evans, R. D., Halford, A. H., Nutt, C. D., Bancroft, K. P., Heyward, A. J., Oades, D.: The state of Western Australia's coral reefs, Coral Reefs, 38, 4, 651-667, https://doi.org/10.1007/s00338-019-01795-8, 2019.

Girishkumar, M. S., Joseph, J., Thangaprakash, V. P., Pottapinjara, V. and McPhaden, M. J.: Mixed Layer Temperature Budget for the Northward Propagating Summer Monsoon Intraseasonal Oscillation (MISO) in the Central Bay of Bengal, J. Geophys. Res. Ocean., 122(11), 8841–8854, doi:10.1002/2017JC013073, 2017.

Gnanaseelan, C., Deshpande, A. and McPhaden, M. J.: Impact of Indian Ocean Dipole and El Nio/Southern Oscillation wind-forcing on the Wyrtki jets, J. Geophys. Res. Ocean., doi:10.1029/2012JC007918, 2012.

Godfrey, J. S., and Ridgway, K. R.: The large-scale environment of the poleward-flowing Leeuwin Current, Western Australia: longshore steric height gradients, wind stresses and geostrophic flow, J. Phys. Oceanogr., 15(5), 481–495, https://doi.org/10.1175/1520-0485(1985)015<0481:TLSEOT>2.0.CO;2, 1985.

Godfrey, J. S., and Weaver, A.: Why are there such strong steric height gradients off Western Australia? In: Proceedings of the Western Pacific International Meeting and Workshop on TOGA COARE, May 24–30, 1989, Noumea, New Caledonia, 215–222, http://hdl.handle.net/102.100.100/262338, 1989.

Godfrey, J.S., and Weaver, A.J.: Is the Leeuwin Current driven by Pacific heating and winds? Prog. Oceanogr., 27(3–4), 225–272, https://doi.org/10.1016/0079-6611(91)90026-I, 1991.

Goericke, R., Olson, R. J. and Shalapyonok, A.: A novel niche for Prochlorococcus sp. in low-light suboxic environments in the Arabian Sea and the Eastern Tropical North Pacific, Deep. Res. Part I Oceanogr. Res. Pap., doi:10.1016/S0967-0637(99)00108-9, 2000.

Goes, J. I., Tian, H., Gomes, H. do R., Anderson, O. R., Al-Hashmi, K., deRada, S., Luo, H., Al-Kharusi, L., Al-Azri, A. and Martinson, D. G.: Ecosystem state change in the Arabian Sea fuelled by the recent loss of snow over the Himalayan-Tibetan Plateau region, Sci. Rep., doi:10.1038/s41598-020-64360-2, 2020.

Gomes, H. D., Goes, J. I., Matondkar, S. G. P., Buskey, E. J., Basu, S., Parab, S. and Thoppil, P.: Massive outbreaks of Noctiluca scintillans blooms in the Arabian Sea due to spread of hypoxia, Nat. Commun., doi:10.1038/ncomms5862, 2014.

2356   Gordon, A. L., Susanto, R. D. and Vranes, K.: Cool Indonesian throughflow as a consequence of restricted surface layer
2357   flow, Nature, doi:10.1038/nature02038, 2003.

2358   Gordon, A. L., Susanto, R. D., Ffield, A., Huber, B. A., Pranowo, W. and Wirasantosa, S.: Makassar Strait throughflow,
2359   2004 to 2006, Geophys. Res. Lett., doi:10.1029/2008GL036372, 2008.

2360   Gordon, A. L., Sprintall, J., Van Aken, H. M., Susanto, R. D., Wijffels, S., Molcard, R., Ffield, A., Pranowo, W. and
2361   Wirasantosa, S.: The Indonesian throughflow during 2004-2006 as observed by the INSTANT program, Dyn. Atmos.
2362   Ocean., doi:10.1016/j.dynatmoce.2009.12.002, 2010.

2363   Gordon, A. L., Huber, B. A., Metzger, E. J., Susanto, R. D., Hurlburt, H. E. and Adi, T. R.: South China Sea
2364   throughflow impact on the Indonesian throughflow, Geophys. Res. Lett., doi:10.1029/2012GL052021, 2012.

2365   Gordon, A. L., Shroyer, E. L., Mahadevan, A., Sengupta, D. and Freilich, M.: Bay of Bengal: 2013 Northeast monsoon
2366   upper-ocean circulation, Oceanography, doi:10.5670/oceanog.2016.41, 2016.

2367   Gordon, A., Shroyer, E. & Murty, V: An Intrathermocline Eddy and a tropical cyclone in the Bay of Bengal. *Sci Rep* 7,
2368   46218, https://doi.org/10.1038/srep46218, 2017.

2369   Goschen, W. S., Schumann, E. H., Bernard, K. S., Bailey, S. E. and Deyzel, S. H. P.: Upwelling and ocean structures off
2370   Algoa Bay and the south-east coast of South Africa, African J. Mar. Sci., doi:10.2989/1814232X.2012.749810, 2012.

2371   Goswami, B. B., Mukhopadhyay, P., Khairoutdinov, M. and Goswami, B. N.: Simulation of Indian summer monsoon
2372   intraseasonal oscillations in a superparameterized coupled climate model: Need to improve the embedded cloud
2373   resolving model, Clim. Dyn., 41(5–6), 1497–1507, https://doi.org/10.1007/s00382-012-1563-1, 2013.

2374   Gudka, M., Obura, D., Mwaura, J., Porter, S. Yahya, S., and Mabwa, R.: Impact of the 3rd Global Coral Bleaching
2375   Event on the Western Indian Ocean in 2016, Global Coral Reef Monitoring Network (GCRMN)/Indian Ocean
2376   Commission, pp. 67, http://hdl.handle.net/20.500.11822/25700, 2018.

2377   Guemas, V., Corti, S., Garcia-Serrano, J., Doblas-Reyes, F. J., Balmaseda, M., and Magnusson, L.: The Indian Ocean:
2378   The region of highest skill worldwide in decadal climate prediction. J. Climate, 26, 726–739, 2013.

2379   Gundersen, J. S., Gardner, W. D., Richardson, M. J. and Walsh, I. D.: Effects of monsoons on the seasonal and spatial
2380   distributions of POC and chlorophyll in the Arabian Sea, Deep. Res. Part II Top. Stud. Oceanogr., doi:10.1016/S0967-
2381   0645(98)00065-4, 1998.

2382   Guo, F., Liu, Q., Sun, S., and Yang, J.: Three types of Indian Ocean dipoles. J. Climate, 28, 3073-3092, 2015.

2383   Haarsma, R. J., Campos, E. J. D., Drijfhout, S., Hazeleger, W. and Severijns, C.: Impacts of interruption of the Agulhas
2384   leakage on the tropical Atlantic in coupled ocean-atmosphere simulations, Clim. Dyn., doi:10.1007/s00382-009-0692-7,
2385   2011.

2386   Haine, T. W. N., Watson, A. J., Liddicoat, M. I. and Dickson, R. R.: The flow of Antarctic bottom water to the
2387   southwest Indian Ocean estimated using CFCs, J. Geophys. Res. Ocean., doi:10.1029/98JC02476, 1998.

2388   Halkides, D. J., Waliser, D. E., Lee, T., Menemenlis, D. and Guan, B.: Quantifying the processes controlling
2389   intraseasonal mixed-layer temperature variability in the tropical Indian Ocean, J. Geophys. Res. Ocean., 120(2), 692–
2390   715, doi:10.1002/2014JC010139, 2015.

2391   Han, W., McCreary, J. P., Anderson, D. L. T. and Mariano, A. J.: Dynamics of the eastern surface jets in the equatorial
2392   Indian Ocean, J. Phys. Oceanogr., doi:10.1175/1520-0485(1999)029<2191:DOTESJ>2.0.CO;2, 1999.

2393   Han, W., Webster, P., Lukas, R., Hacker, P. and Hu, A.: Impact of atmospheric intraseasonal variability in the Indian
2394   Ocean: Low-frequency rectification in equatorial surface current and transport, J. Phys. Oceanogr., doi:10.1175/1520-
2395   0485(2004)034<1350:IOAIVI>2.0.CO;2, 2004.

2396   Han, W., Yuan, D., Liu, W. T. and Halkides, D. J.: Intraseasonal variability of Indian Ocean sea surface temperature
2397   during boreal winter: Madden-Julian Oscillation versus submonthly forcing and processes, J. Geophys. Res. Ocean.,
2398   112(4), 1–20, doi:10.1029/2006JC003791, 2007.

2399   Han, W., Vialard, J., McPhaden, M. J., Lee, T., Masumoto, Y., Feng, M. and De Ruijter, W. P. M.: Indian ocean decadal
2400   variability: A review, Bull. Am. Meteorol. Soc., doi:10.1175/BAMS-D-13-00028.1, 2014.

Hanson, C. E., Waite, A. M., Thompson, P. A. and Pattiaratchi, C. B.: Phytoplankton community structure and nitrogen nutrition in Leeuwin Current and coastal waters off the Gascoyne region of Western Australia, Deep. Res. Part II Top. Stud. Oceanogr., doi:10.1016/j.dsr2.2006.10.002, 2007.

Hazra, A., Chaudhari, H. S., Saha, S. K., Pokhrel, S. and Goswami, B. N.: Progress Towards Achieving the Challenge of Indian Summer Monsoon Climate Simulation in a Coupled Ocean-Atmosphere Model, J. Adv. Model. Earth Syst., doi:10.1002/2017MS000966, 2017.

Hermes, J. C. and Reason, C. J. C.: Ocean model diagnosis of interannual coevolving SST variability in the South Indian and South Atlantic Oceans, J. Clim., doi:10.1175/JCLI3422.1, 2005.

Hermes, J. C., and C. J. C. Reason: Annual cycle of the South Indian Ocean (Seychelles-Chagos) thermocline ridge in a regional ocean model, Journal of Geophysical Research, 113: C04035, doi:10.1029/2007JC004363, 2008.

Hermes J. C., Masumoto Y., Beal L. M., Roxy M. K., Vialard J., Andres M., Annamalai H., Behera S., D'Adamo N., Doi T., Feng M., Han W., Hardman-Mountford N., Hendon H., Hood R., Kido S., Lee C., Lee T., Lengaigne M., Li J., Lumpkin R., Navaneeth K. N., Milligan B., McPhaden M. J., Ravichandran M., Shinoda T., Singh A., Sloyan B., Strutton P. G., Subramanian A. C., Thurston S., Tozuka T., Ummenhofer C. C., Unnikrishnan A. S., Venkatesan R., Wang D., Wiggert J., Yu L., Yu W.: A Sustained Ocean Observing System in the Indian Ocean for Climate Related Scientific Knowledge and Societal Needs. Frontiers in Marine Science, 6, 355, 1-21, doi/10.3389/fmars.2019.00355, 2019.

Hitchcock, G. L., L. Key, E. and Masters, J.: The fate of upwelled waters in the Great Whirl, August 1995, Deep. Res. Part II Top. Stud. Oceanogr., doi:10.1016/S0967-0645(99)00156-3, 2000.

Ho, C. R., Zheng, Q. and Kuo, N. J.: SeaWiFs observations of upwelling south of Madagascar: Long-term variability and interaction with East Madagascar Current, Deep. Res. Part II Top. Stud. Oceanogr., doi:10.1016/j.dsr2.2003.05.001, 2004.

Holbrook, N. J., Scannell, H.A., Sen Gupta, A., Benthuysen, J.A., Feng, M., Oliver, E.C.J., Alexander, L.V., Burrow, M.T., Donat, M.G., Hobday, A.J., Moore, P.J., Perkins-Kirkpatrick, S.E., Smale, D.A., Straub, S. C., and Wernberg, T.: A global assessment of marine heatwaves and their drivers, Nature Commun., 10, 2624, https://doi.org/10.1038/s41467-019-10206-z, 2019.

Holloway, P. E.: Leeuwin current observations on the Australian North West Shelf, May-June 1993, Deep. Res. Part I, doi:10.1016/0967-0637(95)00004-P, 1995.

Holloway, P. E. and Nye, H. C.: Leeuwin current and wind distributions on the southern part of the australian north west shelf between january 1982 and july 1983, Mar. Freshw. Res., doi:10.1071/MF9850123, 1985.

Holton, L., J. Deshayes, B. C. Backeberg, B. R. Loveday, J. C. Hermes, and C. J. C. Reason, Spatio-temporal characteristics of Agulhas leakage: a model inter-comparison study, Climate Dynamics, 48(7), 2107-2121, 2017.

Hood, R. R., Coles, V. J. and Capone, D. G.: Modeling the distribution of Trichodesmium and nitrogen fixation in the Atlantic Ocean, J. Geophys. Res. C Ocean., doi:10.1029/2002JC001753, 2004.

Hood, R. R., Beckley, L. E., and Wiggert, J. D.: Biogeochemical and ecological impacts of boundary currents in the Indian Ocean, Prog. Oceanogr., 156, pp. 290–325, 2017.

Hood, R.R., H.W. Bange, L. Beal, L.E. Beckley, P. Burkill, G.L. Cowie, N. D'Adamo, G. Ganssen, H. Hendon, J. Hermes, M. Honda, M. McPhaden, M. Roberts, S. Singh, E. Urban, and W. Yu. : Science Plan of the Second International Indian Ocean Expedition (IIOE-2): A Basin-Wide Research Program. Scientific Committee on Oceanic Research, Newark, Delaware, USA, 2015

Hood, R. R., V. J. Coles, J. Huggett, M. Landry, M. Levy, J. W. Moffett, and J. Wiggert. in preparation. 'Indian Ocean Biogeochemistry: Nutrients, Phytoplankton and Zooplankton Variability and Limitations.' in C. C. Ummenhofer and R. R. Hood (eds.), The Indian Ocean and its Role in the Global Climate System (Elsevier).

Howden, S. D., and Murtugudde, R.: Effects of river inputs into the Bay of Bengal, J. Geophys. Res. Ocean., 106(C9), 19825–19843, https://doi.org/10.1029/2000jc000656, 2001.

Hu, D., Wu, L., Cai, W., Gupta, A. Sen, Ganachaud, A., Qiu, B., Gordon, A. L., Lin, X., Chen, Z., Hu, S., Wang, G., Wang, Q., Sprintall, J., Qu, T., Kashino, Y., Wang, F. and Kessler, W. S.: Pacific western boundary currents and their roles in climate, Nature, doi:10.1038/nature14504, 2015.

Hu, S. and Sprintall, J.: Interannual variability of the Indonesian Throughflow: The salinity effect, J. Geophys. Res. Ocean., doi:10.1002/2015JC011495, 2016.

Hu, S., and Sprintall, J.: Observed Strengthening of Interbasin Exchange via the Indonesian Seas Due to Rainfall Intensification, Geophysical Research Letters, 44(3), 1448-1456, 2017a.

Hu, S., and Sprintall, J.: A stronger Indonesian Throughflow Related to Enhanced Regional Rainfall, CLIVAR Exchanges, 71, 21-25, 2017b.

Huhn, F., von Kameke, A., Pérez-Muñuzuri, V., Olascoaga, M. J., and Beron-Vera, F. J.: The impact of advective transport by the South Indian Ocean countercurrent on the Madagascar bloom, Geophys. Res. Lett., 39, L06602, https://doi.org/10.1029/2012GL051246, 2012.

Huussen, T. N., Naveira-Garabato, A. C., Bryden, H. L. and McDonagh, E. L.: Is the deep Indian Ocean MOC sustained by breaking internal waves?, J. Geophys. Res. Ocean., doi:10.1029/2012JC008236, 2012.

Ibrahim, N., Mohamed, M., Basheer, A., Ismail, H., Nistharan, F., Schmidt, A., Naeem, R., Abdulla, A., and Grimsditch, G.: Status of Coral Bleaching in the Maldives in 2016, Marine Research Centre, Malé, Maldives, 47 pp., https://portals.iucn.org/library/node/46803, 2017.

Iskandar, I., Masumoto, Y. and Mizuno, K.: Subsurface equatorial zonal current in the eastern Indian Ocean, J. Geophys. Res. Ocean., doi:10.1029/2008JC005188, 2009.

Iskandar, I., Sasaki, H., Sasai, Y., Masumoto, Y., and Mizuno, K.: A numerical investigation of eddy-induced chlorophyll bloom in the southeastern tropical Indian Ocean during Indian Ocean Dipole—2006. Ocean Dyn., 60, 731-742, 2010.

Iskandar, I. and McPhaden, M. J.: Dynamics of wind-forced intraseasonal zonal current variations in the equatorial Indian Ocean, J. Geophys. Res. Ocean., 116(6), 1–16, doi:10.1029/2010JC006864, 2011.

Izumo, T., Vialard, J., Lengaigne, M., de Boyer Montegut, C., Behera, S. K., Luo, J.-J., Cravatte, S., Masson, S. and Yamagata, T.: Influence of the state of the Indian Ocean Dipole on the following year's El Niño, Nat. Geosci., 3(3), 168–172, doi:10.1038/ngeo760, 2010.

Jackson, J. M., Rainville, L., Roberts, M. J., McQuaid, C. D. and Lutjeharms, J. R. E.: Mesoscale bio-physical interactions between the Agulhas Current and the Agulhas Bank, South Africa, Cont. Shelf Res., doi:10.1016/j.csr.2012.09.005, 2012.

Jain, V., Shankar, D., Vinayachandran, P. N., Kankonkar, A., Chatterjee, A., Amol, P., Almeida, A. M., Michael, G. S., Mukherjee, A., Chatterjee, M., Fernandes, R., Luis, R., Kamble, A., Hegde, A. K., Chatterjee, S., Das, U. and Neema, C. P.: Evidence for the existence of Persian Gulf Water and Red Sea Water in the Bay of Bengal, Clim. Dyn., doi:10.1007/s00382-016-3259-4, 2017.

Jayakumar, A., Vialard, J., Lengaigne, M., Gnanaseelan, C., McCreary, J. P. and Kumar, B. P.: Processes controlling the surface temperature signature of the Madden-Julian Oscillation in the thermocline ridge of the Indian Ocean, Clim. Dyn., 37(11–12), 2217–2234, doi:10.1007/s00382-010-0953-5, 2011.

Jayakumar, A., Turner, A. G., Johnson, S. J., Rajagopal, E. N., Mohandas, S. and Mitra, A. K.: Boreal summer sub-seasonal variability of the South Asian monsoon in the Met Office GloSea5 initialized coupled model, Clim. Dyn., 49(5–6), 2035–2059, doi:10.1007/s00382-016-3423-x, 2017.

Jensen, T. G.: Arabian Sea and Bay of Bengal exchange of salt and tracers in an ocean model, Geophys. Res. Lett., 28(20), 3967–3970, doi:10.1029/2001GL013422, 2001.

Jensen, T. G., Wijesekera, H. W., Nyadjro, E. S., Thoppil, P. G., Shriver, J., Sandeep, K. K. and Pant, V.: Modeling Salinity Exchanges Between the Equatorial Indian Ocean and the Bay of Bengal, Oceanography, 29(2), 92–101, doi:10.5670/oceanog.2016.42, 2016.

2491   Jia, F., Wu, L., and Qiu, B.: Seasonal modulation of eddy kinetic energy and its formation mechanism in the southeast
2492   Indian Ocean, J. Phys. Oceanogr., 41(4), 657– 665, https://doi.org/10.1175/2010JPO4436.1, 2011a.

2493   Jia, F., Wu, L., and Qiu, B.: Interannual modulation of eddy kinetic energy in the southeast Indian ocean by Southern
2494   Annular Mode, J. Geophys. Res., 116, C02029, https://doi.org/10.1029/2010JC006699, 2011b.

2495   Jin, D., Waliser, D. E., Jones, C. and Murtugudde, R.: Modulation of tropical ocean surface chlorophyll by the Madden-
2496   Julian Oscillation, Clim. Dyn., 40(1–2), 39–58, doi:10.1007/s00382-012-1321-4, 2013a.

2497   Jin, D., Murtugudde, R. G. and Waliser, D. E.: Intraseasonal atmospheric forcing effects on the mean state of ocean
2498   surface chlorophyll, J. Geophys. Res. Ocean., 118(1), 184–196, doi:10.1029/2012JC008256, 2013b.

2499   Jin, X., Kwon, Y.-O., Ummenhofer, C. C., Seo, H., Schwarzkopf, F. U., Biastoch, A., Böning, C. W.,andWright, J. S.:
2500   Influences of Pacific climate variability on decadal subsurface ocean heat content variations in the Indian Ocean. J.
2501   Climate, 31, 4157–4174, 2018a.

2502   Jin, X., Kwon, Y.-O., Ummenhofer, C. C., Seo, H., Kosaka, Y., and Wright, J. S.: Distinct mechanisms of decadal
2503   subsurface heat content variations in the eastern and western Indian Ocean modulated by tropical Pacific SST. J.
2504   Climate, 31, 7751-7769, 2018b.

2505   Jinadasa, S. U. P., Lozovatsky, I., Planella-Morató, J., Nash, J. D., MacKinnon, J. A., Lucas, A. J., Wijesekera, H. W.
2506   and Fernando, H. J. S.: Ocean turbulence and mixing around Sri Lanka and in adjacent waters of the northern Bay of
2507   Bengal, Oceanography, doi:10.5670/oceanog.2016.49, 2016.

2508   Johnson, G. C., Musgrave, D. L., Warren, B. A., Ffield, A. and Olson, D. B.: Flow of bottom and deep water in the
2509   Amirante Passage and Mascarene Basin, J. Geophys. Res., 103, 30973-30984. doi:10.1029/1998JC90002, 1998.

2510   Johnson, G. C., Purkey, S. G, Bullister, J. L.: Warming and freshening in the abyssal southeastern Indian Ocean. J. Clim.
2511   21, 5351-5363. doi: 10.1175/2008JCLI2384.1, 2008a.

2512   Johnson, G. C., Purkey, S. G, Toole, J. M.: Reduced Antarctic meridional overturning circulation reaches the North
2513   Atlantic Ocean, Geophys. Res. Lett., 35, L22601. doi:10.1029/2008GL035619, 2008b.

2514   José, Y. S., Aumont, O., Machu, E., Penven, P., Moloney, C. L. and Maury, O.: Influence of mesoscale eddies on
2515   biological production in the Mozambique Channel: Several contrasted examples from a coupled ocean-biogeochemistry
2516   model, Deep. Res. Part II Top. Stud. Oceanogr., doi:10.1016/j.dsr2.2013.10.018, 2014.

2517   Joseph, S., Wallcraft, A. J., Jensen, T. G., Ravichandran, M., Shenoi, S. S. C. and Nayak, S.: Weakening of spring
2518   Wyrtki jets in the Indian Ocean during 2006-2011, J. Geophys. Res. Ocean., doi:10.1029/2011JC007581, 2012.

2519   Jyothibabu, R., Madhu, N. V., Maheswaran, P. A., Jayalakshmy, K. V., Nair, K. K. C. and Achuthankutty, C. T.:
2520   Seasonal variation of microzooplankton (20-200 µm) and its possible implications on the vertical carbon flux in the
2521   western Bay of Bengal, Cont. Shelf Res., doi:10.1016/j.csr.2007.12.011, 2008.

2522   Jyoti, J., Swapna, P., Krishnan, R. and Naidu, C. V.: Pacific modulation of accelerated south Indian Ocean sea level rise
2523   during the early 21st Century, Clim. Dyn., doi:10.1007/s00382-019-04795-0, 2019.

2524   Kataoka, T., Tozuka, T., Masumoto, Y., and Yamagata, T.: The Indian Ocean subtropical dipole mode simulated in the
2525   CMIP3 models, Climate Dyn., 39, 1385–1399, https://doi.org/10.1007/s00382-011-1271-2, 2012.

2526   Kataoka, T., Tozuka, T., Behera, S., and Yamagata, T.: On the Ningaloo Niño/Niña, Climate Dyn., 43, 1463–1482,
2527   https://doi.org/10.1007/s00382-013-1961-z, 2014.

2528   Kato, S., Loeb, N. G., Rose, F. G., Doelling, D. R., Rutan, D. A., Caldwell, T. E., Yu, L. and Weller, R. A.: Surface
2529   irradiances consistent with CERES-derived top-of-atmosphere shortwave and longwave irradiances, J. Clim., 26(9),
2530   2719–2740, doi:10.1175/JCLI-D-12-00436.1, 2013.

2531   Keen, T. R., Kindle, J. C. and Young, D. K.: The interaction of southwest monsoon upwelling, advection and primary
2532   production in the northwest Arabian Sea, J. Mar. Syst., doi:10.1016/S0924-7963(97)00003-1, 1997.

2533   Keerthi, M. G., Lengaigne, M., Drushka, K., Vialard, J., Montegut, C. D. B., Pous, S., Levy, M. and Muraleedharan, P.
2534   M.: Intraseasonal variability of mixed layer depth in the tropical Indian Ocean, Clim. Dyn., 46(7–8), 2633–2655,
2535   doi:10.1007/s00382-015-2721-z, 2016.

Kido, S., and Tozuka, T.: Salinity Variability Associated with the Positive Indian Ocean Dipole and Its Impact on the Upper Ocean Temperature. Journal of Climate, 30(19), 7885-7907, 2017.

Kim, H. S., Flagg, C. N. and Howden, S. D.: Northern Arabian Sea variability from TOPEX/Poseidon altimetry data: An extension of the US JGOFS/ONR shipboard ADCP study, Deep. Res. Part II Top. Stud. Oceanogr., doi:10.1016/S0967-0645(00)00131-4, 2001.

Kobashi, F., and Kubokawa, A.: Review on North Pacific Subtropical Countercurrents and Subtropical Fronts: role of mode waters in ocean circulation and climate, J. Oceanogr., 68, 21–43, https://doi.org/10.1007/s10872-011-0083-7, 2012.

Koslow, J. A., Pesant, S., Feng, M., Pearce, A., Fearns, P., Moore, T., Matear, R. and Waite, A.: The effect of the Leeuwin Current on phytoplankton biomass and production off Southwestern Australia, J. Geophys. Res. Ocean., doi:10.1029/2007JC004102, 2008.

Krishnamohan, K. S., Vialard, J., Lengaigne, M., Masson, S., Samson, G., Pous, S., Neetu, S., Durand, F., Shenoi, S. S. C. and Madec, G.: Is there an effect of Bay of Bengal salinity on the northern Indian Ocean climatological rainfall?, Deep Sea Res. Part II Top. Stud. Oceanogr., doi:10.1016/j.dsr2.2019.04.003, 2019.

Krishnamurthy, L., and Krishnamurthy, V.: Decadal and interannual variability of the Indian Ocean SST. Climate Dyn., 46, 57–70, 2016.

Kubokawa, A.: Ventilated thermocline strongly affected by a deep mixed layer: A theory for subtropical countercurrent. J. Phys. Oceanogr., 29, 1314–1333, https://doi.org/10.1175/1520-0485(1999)029<1314:VTSABA>2.0.CO;2, 1999.

Kubokawa, A. and Inui, T.: Subtropical countercurrent in an idealized ocean GCM. J. Phys. Oceanogr., 29, 1303–1313, https://doi.org/10.1175/1520-0485(1999)029<1303:SCIAIO>2.0.CO;2, 1999.

Kumar, S.P., Madhupratap, M., Dileep Kumar, M., Gauns, M., Muraleedharan, P. M., Sarma, V. V. S. S. and De Souza, S. N.: Physical control of primary productivity on a seasonal scale in central and eastern Arabian Sea, Proc. Indian Acad. Sci. Earth Planet. Sci., doi:10.1007/bf02708331, 2000.

Kumar, S.P., Muraleedharan, P. M., Prasad, T. G., Gauns, M., Ramaiah, N., De Souza, S. N., Sardesai, S. and Madhupratap, M.: Why is the Bay of Bengal less productive during summer monsoon compared to the Arabian Sea?, Geophys. Res. Lett., doi:10.1029/2002GL016013, 2002.

Kumar, S. P., Nuncio, M., Narvekar, J., Kumar, A., Sardesai, S., De Souza, S. N., Gauns, M., Ramaiah, N. and Madhupratap, M.: Are eddies nature's trigger to enhance biological productivity in the Bay of Bengal?, Geophys. Res. Lett., doi:10.1029/2003GL019274, 2004.

Kumar, S.P., Nuncio, M., Ramaiah, N., Sardesai, S., Narvekar, J., Fernandes, V. and Paul, J. T.: Eddy-mediated biological productivity in the Bay of Bengal during fall and spring intermonsoons, Deep. Res. Part I Oceanogr. Res. Pap., doi:10.1016/j.dsr.2007.06.002, 2007.

Kumar, P., Singh, A., Ramesh, R. and Nallathambi, T.: N_2 Fixation in the Eastern Arabian Sea: Probable Role of Heterotrophic Diazotrophs, Frontiers: Marine Science, 4, 80, 2017.

Kundu, P. K. and McCreary, J. P.: On the dynamics of the throughflow from the Pacific into the Indian Ocean, J. Phys. Oceanogr., 16,2191–162198, https://doi.org/10.1175/1520-0485(1986)016<2191:OTDOTT>2.0.CO;2, 1986.

Lambert, E., Le Bars, W., and de Ruijter, W. P. M.: The connection of the Indonesian Throughflow, South Indian Ocean Countercurrent and the Leeuwin Current, Ocean Science, 12(3), 771–780, https://doi.org/10.5194/os-12-771-2016, 2016.

Lamont, T., Barlow, R. G., Morris, T. and van den Berg, M. A.: Characterisation of mesoscale features and phytoplankton variability in the Mozambique Channel, Deep. Res. Part II Top. Stud. Oceanogr., doi:10.1016/j.dsr2.2013.10.019, 2014.

Lamont, T. and Barlow, R. G.: Environmental influence on phytoplankton production during summer on the KwaZulu-Natal shelf of the Agulhas ecosystem, African J. Mar. Sci., doi:10.2989/1814232X.2015.1108228, 2015.

Latasa, M. and Bidigare, R. R.: A comparison of phytoplankton populations of the Arabian Sea during the Spring Intermonsoon and Southwest Monsoon of 1995 as described by HPLC-analyzed pigments, Deep. Res. Part II Top. Stud. Oceanogr., doi:10.1016/S0967-0645(98)00066-6, 1998.

2583   Laurindo, L. C., Mariano, A. J. and Lumpkin, R.: An improved near-surface velocity climatology for the global ocean
2584   from drifter observations, Deep. Res. Part I Oceanogr. Res. Pap., doi:10.1016/j.dsr.2017.04.009, 2017.

2585   Le Bars, D., Dijkstra, H. A. and De Ruijter, W. P. M.: Impact of the Indonesian Throughflow on Agulhas leakage,
2586   Ocean Sci., doi:10.5194/os-9-773-2013, 2013.

2587   Le Bars, D., Durgadoo, J. V., Dijkstra, H. A., Biastoch, A. and De Ruijter, W. P. M.: An observed 20-year time series of
2588   Agulhas leakage, Ocean Sci., doi:10.5194/os-10-601-2014, 2014.

2589   Lee, C. M., Jones, B. H., Brink, K. H. and Fischer, A. S.: The upper-ocean response to monsoonal forcing in the Arabian
2590   Sea: Seasonal and spatial variability, Deep. Res. Part II Top. Stud. Oceanogr., doi:10.1016/S0967-0645(99)00141-1,
2591   2000.

2592   Lee, C. M., Jinadasa, S. U. P., Anutaliya, A., Centurioni, L. R., Fernando, H. J. S., Hormann, V., Lankhorst, M.,
2593   Rainville, L., Send, U. and Wijesekera, H. W.: Collaborative observations of boundary currents, water mass variability,
2594   and monsoon response in the southern Bay of Bengal, Oceanography, doi:10.5670/oceanog.2016.43, 2016.Lee, J. Y.,
2595   Wang, B., Wheeler, M. C., Fu, X., Waliser, D. E. and Kang, I. S.: Real-time multivariate indices for the boreal summer
2596   intraseasonal oscillation over the Asian summer monsoon region, Clim. Dyn., 40(1–2), 493–509, doi:10.1007/s00382-
2597   012-1544-4, 2013.

2598   Lee, S. K., Park, W., Baringer, M. O., Gordon, A. L., Huber, B. and Liu, Y.: Pacific origin of the abrupt increase in
2599   Indian Ocean heat content during the warming hiatus, Nat. Geosci., doi:10.1038/NGEO2438, 2015.

2600   Lee, T.: Decadal weakening of the shallow overturning circulation in the South Indian Ocean, Geophys. Res. Lett.,
2601   doi:10.1029/2004GL020884, 2004.

2602   Lee, T., Fournier, S., Gordon, A. L. and Sprintall, J.: Maritime Continent water cycle regulates low-latitude chokepoint
2603   of global ocean circulation, Nat. Commun., doi:10.1038/s41467-019-10109-z, 2019.

2604

2605   Legeckis, R., and Cresswell, G.: Satellite observations of sea-surface temperature fronts off the coast of western and
2606   southern Australia, Deep Sea Res. I, 28, 297–306, https://doi.org/10.1016/0198-0149(81)90069-8, 1981.

2607   L'Heureux, M. L., Lee, S. Lyon, B.: Recent multidecadal strengthening of the Walker circulation across the tropical
2608   Pacific. Nat. Clim. Cha., 3, 571–576, 2013.

2609   Li, Y., Han, W., Ravichandran, M., Wang, W., Shinoda, T. and Lee, T.: Bay of Bengal salinity stratification and Indian
2610   summer monsoon intraseasonal oscillation: 1. Intraseasonal variability and causes, J. Geophys. Res. Ocean.,
2611   doi:10.1002/2017JC012691, 2017a.

2612   Li, Y., Han, W., Wang, W., Ravichandran, M., Lee, T. and Shinoda, T.: Bay of Bengal salinity stratification and Indian
2613   summer monsoon intraseasonal oscillation: 2. Impact on SST and convection, J. Geophys. Res. Ocean., 122(5), 4312–
2614   4328, doi:10.1002/2017JC012692, 2017b.

2615   Li, Y., Han, W., Wang, W., Zhang, L. and Ravichandran, M.: The Indian summer monsoon intraseasonal oscillations in
2616   CFSv2 forecasts: Biases and importance of improving air-sea interaction processes, J. Clim., 31(14), 5351–5370,
2617   doi:10.1175/JCLI-D-17-0623.1, 2018a.

2618   Li, Y., Han, W., Hu, A., Meehl, G. A. and Wang, F.: Multidecadal changes of the upper Indian ocean heat content
2619   during 1965-2016, J. Clim., doi:10.1175/JCLI-D-18-0116.1, 2018b.

2620   Lierheimer, L. J. and Banse, K.: Seasonal and interannual variability of phytoplankton pigment in the Laccadive
2621   (Lakshadweep) Sea as observed by the Coastal Zone Color Scanner, Proc. Indian Acad. Sci. Earth Planet. Sci.,
2622   doi:10.1007/BF02981144, 2002.

2623   Liu, Q.-Y., Feng, M., Wang, D., and Wijffels, S.: Interannual variability of the Indonesian Throughflow transport: A
2624   revisit based on 30 year expendable bathythermograph data, J. Geophys. Res.: Oceans, 120(12), 8270-8282,
2625   https://doi.org/10.1002/2015JC011351, 2015.

2626   Llovel, W. and Lee, T.: Importance and origin of halosteric contribution to sea level change in the southeast Indian
2627   Ocean during 2005-2013, Geophys. Res. Lett., doi:10.1002/2014GL062611, 2015.

Longhurst, A.: A major seasonal phytoplankton bloom in the Madagascar Basin, Deep. Res. Part I Oceanogr. Res. Pap., doi:10.1016/S0967-0637(01)00024-3, 2001.

Lotliker, A. A., Omand, M. M., Lucas, A. J., Laney, S. R., Mahadevan, A. and Ravichandran, M.: Penetrative radiative flux in the Bay of Bengal, Oceanography, doi:10.5670/oceanog.2016.53, 2016.

Lourey, M. J., Dunn, J. R. and Waring, J.: A mixed-layer nutrient climatology of Leeuwin Current and Western Australian shelf waters: Seasonal nutrient dynamics and biomass, J. Mar. Syst., doi:10.1016/j.jmarsys.2005.10.001, 2006.

Lourey, M. J., Thompson, P. A., McLaughlin, M. J., Bonham, P. and Feng, M.: Primary production and phytoplankton community structure during a winter shelf-scale phytoplankton bloom off Western Australia, Mar. Biol., doi:10.1007/s00227-012-2093-4, 2013.

Loveday, B. R., Durgadoo, J. V., Reason, C. J. C., Biastoch, A. and Penven, P.: Decoupling of the Agulhas leakage from the Agulhas Current, J. Phys. Oceanogr., doi:10.1175/JPO-D-13-093.1, 2014.

Lübbecke, J. F., Durgadoo, J. V. and Biastoch, A.: Contribution of increased agulhas leakage to tropical Atlantic warming, J. Clim., doi:10.1175/JCLI-D-15-0258.1, 2015.

Lucas, A., Nash, J., Pinkel, R., MacKinnon, J., Tandon, A., Mahadevan, A., Omand, M., Freilich, M., Sengupta, D., Ravichandran, M. and Le Boyer, A.: Adrift Upon a Salinity-Stratified Sea: A View of Upper-Ocean Processes in the Bay of Bengal During the Southwest Monsoon, Oceanography, doi:10.5670/oceanog.2016.46, 2016.

Luis, A. J. and Kawamura, H.: Air-sea interaction, coastal circulation and primary production in the eastern Arabian Sea: A review, J. Oceanogr., 60, 205-18, doi:10.1023/B:JOCE.0000038327.33559.34, 2004.

Lumpkin, R., , and Speer,K.: Global ocean meridional overturning. *J. Phys. Oceanogr.*, **37**, 2550–2562, doi:10.1175/JPO3130.1, 2007.

Lutjeharms, J. R. E.: The Agulhas Current, Springer: Berlin, Heidelbert, New York, 2006.

Lutjeharms, J. R. E., Meyer, A. A., Ansorge, I. J., Eagle, G. A. and Orren, M. J.: The nutrient characteristics of the Agulhas bank, South African J. Mar. Sci., doi:10.2989/025776196784158464, 1996.

Lutjeharms, J. R. E. and Machu, E.: An upwelling cell inshore of the East Madagascar Current, Deep. Res. Part I Oceanogr. Res. Pap., doi:10.1016/S0967-0637(00)00026-1, 2000.

Ma, J., Feng, M., Sloyan, B. M. and Lan, J.: Pacific influences on the meridional temperature transport of the Indian Ocean, J. Clim., doi:10.1175/JCLI-D-18-0349.1, 2019.

Macdonald, A. M., Mecking, S., Robbins, P. E., Toole, J. M., Johnson, G. C., Talley, L. D., Cook, M., Wijffels, S., E.: The WOCE-era 3-D Pacific Ocean Circulation and Heat Budget. *Progress in Oceanography*, 82, 4, 281-325, 2009.

Machu, E. and Garçon, V.: Phytoplankton seasonal distribution from sea WiFS data in the Agulhas current system, J. Mar. Res., doi:10.1357/002224001762674944, 2001.

MacKinnon, J. A., Johnston, T. M. S. and Pinkel, R.: Strong transport and mixing of deep water through the Southwest Indian Ridge, Nat. Geosci., doi:10.1038/ngeo340, 2008.

Madden, R. A. and Julian, P. R.: Description of Global-Scale Circulation Cells in the Tropics with a 40–50 Day Period, J. Atmos. Sci., doi:10.1175/1520-0469(1972)029<1109:dogscc>2.0.co;2, 1972.

Madden, R. A. and Julian, P. R.: Detection of a 40–50 Day Oscillation in the Zonal Wind in the Tropical Pacific, J. Atmos. Sci., 28(5), 702–708, doi:10.1175/1520-0469(1971)028<0702:DOADOI>2.0.CO;2, 1971.

Madhupratap, M., Gauns, M., Ramaiah, N., Prasanna Kumar, S., Muraleedharan, P. M., De Sousa, S. N., Sardessai, S. and Muraleedharan, U.: Biogeochemistry of the Bay of Bengal: Physical, chemical and primary productivity characteristics of the central and western Bay of Bengal during summer monsoon 2001, Deep. Res. Part II Top. Stud. Oceanogr., doi:10.1016/S0967-0645(02)00611-2, 2003.

Maes, C., Grima, N., Blanke, B., Martinez, E., Paviet-Salomon, T. and Huck, T.: A Surface "Superconvergence" Pathway Connecting the South Indian Ocean to the Subtropical South Pacific Gyre, Geophys. Res. Lett., doi:10.1002/2017GL076366, 2018.

2673   Mahadevan, A.: Eddy effects on biogeochemistry, Nature, doi:10.1038/nature13048, 2014.

2674   Mahadevan, A., D'Asaro, E., Lee, C. and Perry, M. J.: Eddy-driven stratification initiates North Atlantic spring
2675   phytoplankton blooms, Science (80-.)., doi:10.1126/science.1218740, 2012.

2676   Mahadevan, A., Paluszkiewicz, T., Ravichandran, M., Sengupta, D. and Tandon, A.: Introduction to the Special Issue on
2677   the Bay of Bengal: From Monsoons to Mixing, Oceanography, doi:10.5670/oceanog.2016.34, 2016a.

2678   Mahadevan, A., Spiro Jaeger, G., Freilich, M., Omand, M., Shroyer, E. and Sengupta, D.: Freshwater in the Bay of
2679   Bengal: Its Fate and Role in Air-Sea Heat Exchange, Oceanography, 29(2), 72–81, doi:10.5670/oceanog.2016.40,
2680   2016b.

2681   Manatsa, D. and Behera, S. K.: On the epochal strengthening in the relationship between rainfall of East Africa and
2682   IOD, J. Clim., 26, 5655-5673, doi:10.1175/JCLI-D-12-00568.1, 2013.

2683   Manghnani, V., Morrison, J. M., Hopkins, T. S. and Böhm, E.: Advection of upwelled waters in the form of plumes off
2684   Oman during the Southwest Monsoon, Deep. Res. Part II Top. Stud. Oceanogr., doi:10.1016/S0967-0645(98)00062-9,
2685   1998.

2686   Mantyla, A. W. and Reid, J. L.: On the origins of deep and bottom waters of the Indian Ocean, J. Geophys. Res.,
2687   doi:10.1029/94JC02564, 1995.

2688   Marra, J., Dickey, T. D., Ho, C., Kinkade, C. S., Sigurdson, D. E., Weller, R. A. and Barber, R. T.: Variability in
2689   primary production as observed from moored sensors in the central Arabian Sea in 1995, Deep. Res. Part II Top. Stud.
2690   Oceanogr., doi:10.1016/S0967-0645(98)00070-8, 1998.

2691   Marsac, F. and Blanc, J.: Oceanographic changes during the 1997-1998 El Niño in the Indian Ocean and their impact on
2692   the purse seine fishery, IOTC Proc. no. 2, 1999.

2693   Marin, M., and Feng, M.: Intra-annual variability of the North West Shelf of Australia and its impact on the Holloway
2694   Current: Excitement and propagation of coastally trapped waves, Cont. Shelf Res.,
2695   https://doi.org/10.1016/j.csr.2019.08.001, 2019.

2696   Marshall, A.G. and Hendon, H.H.: Impacts of the MJO in the Indian Ocean and on the Western Australian coast.
2697   Climate Dyn., 42(3–4), 579–595, https://doi.org/10.1007/s00382-012-1643-2, 2014.

2698   Marshall, A. G., Hendon, H. H., Feng, M., and Schiller, A.: Initiation and amplification of the Ningaloo Niño, Climate
2699   Dyn., 45, 2367–2385, https://doi.org/10.1007/s00382-015-2477-5, 2015.

2700   Martin, A. P. and Richards, K. J.: Mechanisms for vertical nutrient transport within a North Atlantic mesoscale eddy,
2701   Deep. Res. Part II Top. Stud. Oceanogr., doi:10.1016/S0967-0645(00)00096-5, 2001.

2702   Masumoto, Y. and Meyers, G.: Forced Rossby waves in the southern tropical Indian Ocean, J. Geophys. Res. Ocean.,
2703   doi:10.1029/98JC02546, 1998.

2704   Masumoto, Y., Hase, H., Kuroda, Y., Matsuura, H. and Takeuchi, K.: Intraseasonal variability in the upper layer
2705   currents observed in the eastern equatorial Indian Ocean, Geophys. Res. Lett., doi:10.1029/2004GL021896, 2005.

2706   Maximenko, N., Niiler, P., Centurioni, L., Rio, M.-H., Melnichenko, O., Chambers, D., Zlotnicki, V., Galperin, B.:
2707   Mean dynamic topography of the ocean derived from satellite and drifting buoy data using three different techniques, J.
2708   Atmos. Oceanic Technol. 26 (9), 1910–1919, https://doi.org/10.1175/2009JTECHO672.1, 2009.

2709   Mayer, M., Alonso Balmaseda, M. and Haimberger, L.: Unprecedented 2015/2016 Indo-Pacific Heat Transfer Speeds
2710   Up Tropical Pacific Heat Recharge, Geophys. Res. Lett., doi:10.1002/2018GL077106, 2018.

2711   Mccave, I. N., Kiefer, T., Thornalley, D. J. R. and Elderfield, H.: Deep flow in the Madagascar-Mascarene Basin over
2712   the last 150 000 years, Philos. Trans. R. Soc. A Math. Phys. Eng. Sci., doi:10.1098/rsta.2004.1480, 2005.

2713   McCreary, J.P.: Equatorial beams. J. Mar. Res., 42(2), 395–430, https://doi.org/10.1357/002224084788502792, 1984.

2714   McCreary, J. P., Fukamachi, Y., and Lu, P.: A nonlinear mechanism for maintaining coastally trapped eastern boundary
2715   currents, J. Geophys. Res., 97 (C4), 5677–5692, https://doi.org/10.1029/92JC00035, 1992.

2716   McCreary, J. P., Shetye, S. R., and Kundu, P. K.: Thermohaline forcing of eastern boundary currents: With application
2717   to the circulation off the west coast of Australia, J. Mar. Res., 44, 71–92, https://doi.org/10.1357/002224086788460184,
2718   1986.

2719   McCreary, J. P., Kohler, K. E., Hood, R. R., Smith, S., Kindle, J., Fischer, A. S. and Weller, R. A.: Influences of diurnal
2720   and intraseasonal forcing on mixed-layer and biological variability in the central Arabian Sea, J. Geophys. Res. Ocean.,
2721   doi:10.1029/2000jc900156, 2001.

2722   McGillicuddy, D. J., Anderson, L. A., Bates, N. R., Bibby, T., Buesseler, K. O., Carlson, C. A., Davis, C. S., Ewart, C.,
2723   Falkowski, P. G., Goldthwait, S. A., Hansell, D. A., Jenkins, W. J., Johnson, R., Kosnyrev, V. K., Ledwell, J. R., Li, Q.
2724   P., Siegel, D. A. and Steinberg, D. K.: Eddy/Wind interactions stimulate extraordinary mid-ocean plankton blooms,
2725   Science (80-.)., doi:10.1126/science.1136256, 2007.

2726   McPhaden, M. J., Meyers, G., Ando, K., Masumoto, Y., Murty, V. S. N., Ravichandran, M., Syamsudin, F., Vialard, J.,
2727   Yu, L., & Yu, W. : RAMA: The Research Moored Array for African–Asian–Australian Monsoon Analysis and
2728   Prediction*, Bulletin of the American Meteorological Society, 90(4), 459-480.
2729   https://journals.ametsoc.org/view/journals/bams/90/4/2008bams2608_1.xml, 2009.

2730   McPhaden, M. J. and Foltz, G. R.: Intraseasonal variations in the surface layer heat balance of the central equatorial
2731   Indian Ocean: The importance of zonal advection and vertical mixing, Geophys. Res. Lett., 40(11), 2737–2741,
2732   doi:10.1002/grl.50536, 2013.

2733   McPhaden, M. J., Wang, Y. and Ravichandran, M.: Volume transports of the Wyrtki jets and their relationship to the
2734   Indian Ocean dipole, J. Geophys. Res. Oceans, 120(8), 5302–5317, 2015.

2735   Menezes, V. V., Phillips, H.E., Schiller, A., Domingues, C.M., and Bindoff, N.L.: Salinity dominance on the Indian
2736   Ocean Eastern Gyral current, Geophys. Res. Lett., 40, 5716– 5721, https://doi.org/10.1002/2013GL057887, 2013.

2737   Menezes, V. V., Phillips, H. E., Schiller, A., Bindoff, N. L., Domingues, C. M., and Vianna, M. L.: South Indian
2738   Countercurrent and associated fronts, J. Geophys. Res. Oceans, 119, 6763– 6791,
2739   https://doi.org/10.1002/2014JC010076, 2014.

2740   Menezes, V. V.: The structure and dynamics of the eastward flows of the South Indian Ocean, PhD Thesis, University of
2741   Tasmania, 244pp, http://eprints.utas.edu.au/23392/, 2015.

2742   Menezes, V. V., Phillips, H. E., Vianna, M. L., and Bindoff, N. L.: Interannual variability of the South Indian
2743   Countercurrent, J. Geophys. Res. Oceans, 121, 3465– 3487, https://doi.org/10.1002/2015JC011417, 2016.

2744   Merle, J., Rotschi, H., and Voituriez, B.: Zonal circulation in the tropical western South Pacific at 170°E. Bull. Japan
2745   Soc. Fish. Oceanogr., Special Issue (Prof. Uda's Commemorative Papers), 91–98, 1969.

2746   Meuleners, M.J., Pattiaratchi, C.B., and Ivey, G.N.: Numerical modelling of the mean flow characteristics of the
2747   Leeuwin Current System, Deep Sea Res. II, 54(8–10), 837–858, https://doi.org/10.1016/j.dsr2.2007.02.003, 2007.

2748   Meuleners, M.J., Ivey, G.N., and Pattiaratchi, C.B.: A numerical study of the eddying characteristics of the Leeuwin
2749   Current System, Deep Sea Res. I, 55(3), 261–276, https://doi.org/10.1016/j.dsr.2007.12.004, 2008.

2750   Meyers, G.: Variation of Indonesian throughflow and the El Niño Southern Oscillation, J. Geophys. Res., 101, C5,
2751   12255-12263, https://doi.org/10.1029/95JC03729, 1996.

2752   Moore, T. S., Matear, R. J., Marra, J. and Clementson, L.: Phytoplankton variability off the Western Australian Coast:
2753   Mesoscale eddies and their role in cross-shelf exchange, Deep. Res. Part II Top. Stud. Oceanogr.,
2754   doi:10.1016/j.dsr2.2007.02.006, 2007.

2755   Morel, A. and Antoine, D.: Heating Rate within the Upper Ocean in Relation to its Bio–optical State, J. Phys.
2756   Oceanogr., 24(7), 1652–1665, doi:10.1175/1520-0485(1994)024<1652:HRWTUO>2.0.CO;2, 1994.

2757   Morioka, Y., Tozuka, T. and Yamagata, T.: Climate variability in the southern Indian Ocean as revealed by self-
2758   organizing maps, Clim. Dyn., doi:10.1007/s00382-010-0843-x, 2010.

2759   Morioka, Y., Tozuka, T., Masson, S., Terray, P., Luo, J. J. and Yamagata, T.: Subtropical dipole modes simulated in a
2760   coupled general circulation model, J. Clim., doi:10.1175/JCLI-D-11-00396.1, 2012.

Moum, J. N. and Nash, J. D.: Mixing Measurements on an Equatorial Ocean Mooring, J. Atmos. Ocean. Technol., doi:10.1175/2008jtecho617.1, 2009.

Moum, J. N., de Szoeke, S. P., Smyth, W. D., Edson, J. B., DeWitt, H. L., Moulin, A. J., Thompson, E. J., Zappa, C. J., Rutledge, S. A., Johnson, R. H. and Fairall, C. W.: Air–Sea Interactions from Westerly Wind Bursts During the November 2011 MJO in the Indian Ocean, Bull. Am. Meteorol. Soc., 95(8), 1185–1199, doi:10.1175/BAMS-D-12-00225.1, 2014.

Moum, J. N., Pujiana, K., Lien, R. C. and Smyth, W. D.: Ocean feedback to pulses of the Madden-Julian Oscillation in the equatorial Indian Ocean, Nat. Commun., 7(May), 1–7, doi:10.1038/ncomms13203, 2016.

Mukherjee, A., Shankar, D., Fernando, V. *et al.* Observed seasonal and intraseasonal variability of the East India Coastal Current on the continental slope. *J Earth Syst Sci* 123, 1197–1232 , https://doi.org/10.1007/s12040-014-0471-7, 2014.

Mulholland, M. R., Bernhardt, P. W., Ozmon, I., Procise, L. A., Garrett, M., O'Neil, J. M., Heil, C. A. and Bronk, D. A.: Contribution of diazotrophy to nitrogen inputs supporting Karenia brevis blooms in the Gulf of Mexico, Harmful Algae, doi:10.1016/j.hal.2014.04.004, 2014.

Muraleedharan, K. R., Jasmine, P., Achuthankutty, C. T., Revichandran, C., Dinesh Kumar, P. K., Anand, P. and Rejomon, G.: Influence of basin-scale and mesoscale physical processes on biological productivity in the Bay of Bengal during the summer monsoon, Prog. Oceanogr., doi:10.1016/j.pocean.2006.09.012, 2007.

Murtugudde, R. and Busalacchi, A. J.: Interannual variability of the dynamics and thermodynamics of the tropical Indian Ocean, J. Clim., doi:10.1175/1520-0442(1999)012<2300:ivotda>2.0.co;2, 1999.

Murtugudde, R., McCreary, J. P. and Busalacchi, A. J.: Oceanic processes associated with anomalous events in the Indian Ocean with relevance to 1997-1998, J. Geophys. Res. Ocean., 105(C2), 3295–3306, doi:10.1029/1999JC900294, 2000.

Murtugudde, R., Beauchamp, J., McClain, C. R., Lewis, M. and Busalacchi, A. J.: Effects of penetrative radiation of the upper tropical ocean circulation, J. Clim., 15(5), 470–486, doi:10.1175/1520-0442(2002)015<0470:EOPROT>2.0.CO;2, 2002.

Murty, V. S. N., Gupta, G. V. M., Sarma, V. V., Rao, B. P., Jyothi, D., Shastri, P. N. M. and Supraveena, Y.: Effect of vertical stability and circulation on the depth of the chlorophyll maximum in the Bay of Bengal during May-June, 1996, Deep. Res. Part I Oceanogr. Res. Pap., doi:10.1016/S0967-0637(99)00071-0, 2000.

Nagura, M. and McPhaden, M. J.: Wyrtki jet dynamics: Seasonal variability, J. Geophys. Res. Oceans, 115(C7), 1–17, 2010a.

Nagura, M. and McPhaden, M. J.: Dynamics of zonal current variations associated with the Indian Ocean dipole, J. Geophys. Res. Oceans, 115 (C11), 1–12, 2010b.

Nagura, M. and McPhaden, M. J.: Zonal Propagation of Near-Surface Zonal Currents in Relation to Surface Wind Forcing in the Equatorial Indian Ocean, J. Phys. Ocean., 46, 3623–3638, doi: 10.1175/JPO-D-16-0157.1, 2016.

Naqvi, S. W. A., Jayakumar, D. A., Narvekar, P. V., Naik, H., Sarma, V. V. S. S., D'Souza, W., Joseph, S. and George, M. D.: Increased marine production of N2O due to intensifying anoxia on the Indian continental shelf, Nature, doi:10.1038/35042551, 2000.

Narayanasetti, S., Swapna, P., Ashok, K., Jadhav, J., and Krishnan, R.:. Changes in biological productivity associated with Ningaloo Niño/Niña events in the southern subtropical Indian Ocean in recent decades, Scientific Reports, 6, 27467, https://doi.org/10.1038/srep27467, 2016.

Nethery, D., and Shankar, D.: Vertical propagation of baroclinic Kelvin waves along the west coast of India, J. Earth. Syst. Sci., 116, 331–339, https://doi.org/10.1007/s12040-007-0030-6, 2007.

Nicholson, S. E.: Long-term variability of the East African "short rains" and its links to large-scale factors. Internat. J. Climatol., doi:10.1002/joc.4259, 2015.

Nieves, V., Willis, J. K. and Patzert, W. C.: Recent hiatus caused by decadal shift in Indo-Pacific heating, Science (80-.)., doi:10.1126/science.aaa4521, 2015.

2806 Niiler, P. P., Maximenko, N. A., and McWilliams, J. C.: Dynamically balanced absolute sea level of the global ocean
2807 derived from near-surface velocity observations, Geophys. Res. Lett., 30, 2164, https://doi.org/10.1029/2003GL018628,
2808 2003.

2809 Nof, D. and Olson, D. B.: How do western abyssal currents cross the equator?, Deep. Res. Part I, doi:10.1016/0967-
2810 0637(93)90002-K, 1993.

2811 O'Donoghue, S. H., Drapeau, L., Dudley, S. F. J. and Peddemors, V. M.: The KwaZulu-Natal sardine run: Shoal
2812 distribution in relation to nearshore environmental conditions, 1997-2007, African J. Mar. Sci.,
2813 doi:10.2989/1814232x.2010.501587, 2010.

2814 Oke, P. R., Griffin, D. A., Rykova, T., and de Oliveira, H. B.: Ocean circulation in the Great Australian Bight in an
2815 eddy-resolving ocean reanalysis: The eddy field, seasonal and interannual variability, Deep Sea Res. II, 157–158, 11–26,
2816 https://doi.org/10.1016/j.dsr2.2018.09.012, 2018.

2817 Oliver, E. C. J., and Thompson, K. R.: Madden-Julian oscillation and sea level: Local and remote forcing, J. Geophys.
2818 Res. Ocean., 115(1), 1–15, https://doi.org/10.1029/2009JC005337, 2010.

2819 Oliver, E.C.J., Herzfeld, M., and Holbrook, N.J.: Modelling the shelf circulation offeastern Tasmania. Continent. Shelf
2820 Res., 130, 14–33, 2016.

2821 Oliver, E. C., Donat, M. G., Burrows, M. T., Moore, P. J., Smale, D. A., Alexander, L. V., Benthuysen, J. A., Feng, M.,
2822 Sen Gupta, A., Hobday, A. J., Holbrook, N. J., Perkins-Kirkpatrick, S. E., Scannell, H. A., Straub, S. C., and
2823 Wernberg, T.: Longer and more frequent marine heatwaves over the past century, Nature Commun., 9, 1324,
2824 https://doi.org/10.1038/s41467-018-03732-9, 2018.

2825 Palastanga, V., van Leeuwen, P. J., Schouten, M. W., and de Ruijter, W. P. M.: Flow structure and variability in the
2826 subtropical Indian Ocean: instability of the South Indian Ocean Countercurrent, J. Geophys. Res., 112, C01001,
2827 https://doi.org/10.1029/2005JC003395, 2007.

2828 Parab, S. G., Prabhu Matondkar, S. G., Gomes, H. do R. and Goes, J. I.: Monsoon driven changes in phytoplankton
2829 populations in the eastern Arabian Sea as revealed by microscopy and HPLC pigment analysis, Cont. Shelf Res.,
2830 doi:10.1016/j.csr.2006.08.004, 2006.

2831 Paris, M. L., Subrahmanyam, B., Trott, C. B. and Murty, V. S. N.: Influence of ENSO Events on the Agulhas Leakage
2832 Region, Remote Sens. Earth Syst. Sci., doi:10.1007/s41976-018-0007-z, 2018.

2833 Paterson, H. L., Feng, M., Waite, A. M., Gomis, D., Beckley, L. E., Holliday, D. and Thompson, P. A.: Physical and
2834 chemical signatures of a developing anticyclonic eddy in the Leeuwin Current, eastern Indian Ocean, J. Geophys. Res.
2835 Ocean., doi:10.1029/2007JC004707, 2008.

2836 Paterson, J. S., Nayar, S., Mitchell, J. G. and Seuront, L.: Population-specific shifts in viral and microbial abundance
2837 within a cryptic upwelling, J. Mar. Syst., doi:10.1016/j.jmarsys.2012.12.009, 2013.

2838 Pearce, A. F., and Griffiths, R.W.: The mesoscale structure of the Leeuwin Current: A comparison of laboratory model
2839 and satellite images, J. Geophys. Res., 96, 16730–16757, https://doi.org/10.1029/91JC01712, 1991.

2840 Pearce, A. and Feng, M.: Observations of warming on the Western Australian continental shelf. Marine Freshw. Res.,
2841 58, 914-920, 2007.

2842 Pearce, A., Lenanton, R., Jackson, G., Moore, J., Feng, M., and Gaughan, D.: The "marine heat wave" off Western
2843 Australia during the summer of 2010/11, Fisheries Research Report No. 222, Department of Fisheries, Western
2844 Australia, 40pp, http://fish.wa.gov.au/Documents/research_reports/frr222.pdf, 2011.

2845 Peatman, S. C. and Klingaman, N. P.: The Indian summer monsoon in MetUM-GOML2.0: Effects of air-sea coupling
2846 and resolution, Geosci. Model Dev., 11(11), 4693–4709, doi:10.5194/gmd-11-4693-2018, 2018.

2847 Philander, S. G. H., and Yoon, J.-H.: Eastern boundary currents and coastal upwelling, J. Phys. Oceanogr., 12(8), 862–
2848 879, https://doi.org/10.1175/1520-0485(1982)012<0862:EBCACU>2.0.CO;2, 1982.

2849 Phillips, H.E., Wijffels, S.E. and Feng, M.: Interannual variability in the freshwater content of the Indonesian-Australian
2850 Basin. *Geophysical Research Letters.* Vol. 32, L03603, doi:10.1029/2004GL021755, 2005.

Pirro, A., Fernando, H. J. S., Wijesekera, H. W., Jensen, T. G., Centurioni, L. R. and Jinadasa, S. U. P.: Eddies and currents in the Bay of Bengal during summer monsoons, Deep. Res. Part II Top. Stud. Oceanogr., doi:10.1016/j.dsr2.2019.104728, 2020a.

Pirro, A., Wijesekera, H. W., Jarosz, E. and Fernando, H. J. S.: Dynamics of intraseasonal oscillations in the Bay of Bengal during summer monsoons captured by mooring observations, Deep. Res. Part II Top. Stud. Oceanogr., doi:10.1016/j.dsr2.2019.104718, 2020b.

Poulton, A. J., Stinchcombe, M. C. and Quartly, G. D.: High numbers of Trichodesmium and diazotrophic diatoms in the southwest Indian Ocean, Geophys. Res. Lett., doi:10.1029/2009GL039719, 2009.

Prerna, S., Chatterjee, A., Mukherjee, A., Ravichandran, M. and Shenoi, S. S. C.: Wyrtki Jets: Role of intraseasonal forcing, J. Earth Syst. Sci., doi:10.1007/s12040-018-1042-0, 2019.

Probyn, T., Mitchellinnes, B., Brown, P., Hutchings, L. and Carter, R.: A review of primary production and related processes on the Agulhas Bank, S. Afr. J. Sci., 1994.

Pujiana, K., Gordon, A. L. and Sprintall, J.: Intraseasonal Kelvin wave in Makassar strait, J. Geophys. Res. Ocean., doi:10.1002/jgrc.20069, 2013.

Purkey, S. G., Johnson, G. C.: Warming of global abyssal and deep Southern Ocean waters between the 1990s and 2000s: Contributions to global heat and sea level rise budgets. J. Clim. 23, 6336-6351. doi: 10.1175/2010JCLI3682.1, 2010.

Purkey, S. G. and Johnson, G. C.: Global contraction of Antarctic Bottom Water between the 1980s and 2000s, J. Clim., doi:10.1175/JCLI-D-11-00612.1, 2012.

Qiu, B., and Chen, S.: Seasonal modulations in the eddy field of the South Pacific Ocean, J. Phys. Oceanogr., 34(7), 1515–1527, https://doi.org/10.1175/1520-0485(2004)034<1515:SMITEF>2.0.CO;2, 2004.

Qiu, Y., Li, L., and Yu, W.: Behavior of the Wyrtki jet observed with surface drifting buoys and satellite altimeter. Geophys. Res. Lett., 36, L18607, https://doi.org/10.1029/2009GL039120, 2009.

Qiu, Y., Han, W., Lin, X., West, J., Li, Y., Xing, W., Zhang, X., Arulananthan, K. and Guo, X.: Upper-ocean response to the super tropical cyclone Phailin (2013) over the freshwater region of the Bay of Bengal, J. Phys. Oceanogr., doi:10.1175/JPO-D-18-0228.1, 2019.

Qu, T., Fukumori, I. and Fine, R. A.: Spin-Up of the Southern Hemisphere Super Gyre, J. Geophys. Res. Ocean., doi:10.1029/2018JC014391, 2019.

Quartly, G. D. and Srokosz, M. A.: Eddies in the southern Mozambique Channel, Deep. Res. Part II Top. Stud. Oceanogr., doi:10.1016/j.dsr2.2003.03.001, 2004.

Rahaman, H., Bharath Raj, G.N. & Ravichandran, M. Coupled Ocean–Atmosphere Summer Intraseasonal Oscillation over the Bay of Bengal. Pure Appl. Geophys. 176, 5415–5429, https://doi.org/10.1007/s00024-019-02275-4, 2019.

Raj, R. P., Peter, B. N. and Pushpadas, D.: Oceanic and atmospheric influences on the variability of phytoplankton bloom in the Southwestern Indian Ocean, J. Mar. Syst., doi:10.1016/j.jmarsys.2010.05.009, 2010.

Ramanantsoa, J. D., Penven, P., Krug, M., Gula, J., & Rouault, M.: Uncovering a new current: The Southwest MAdagascar Coastal Current. Geophysical Research Letters, 45, 1930–1938. https://doi.org/10.1002/2017GL075900, 2018.

Rao, R. R., Molinari, R. L. and Festa, J. F.: Evolution of the climatological near-surface thermal structure of the tropical Indian Ocean. 1. Description of mean monthly mixed layer depth, and sea surface temperature, surface current, and surface meteorological fields, J. Geophys. Res., doi:10.1029/jc094ic08p10801, 1989.

Rathore, S., Bindoff, N. L., Phillips, H. E. and Feng, M.: Recent hemispheric asymmetry in global ocean warming induced by climate change and internal variability, Nat. Commun., doi:10.1038/s41467-020-15754-3, 2020.

Ravichandran, M., Girishkumar, M. S. and Riser, S.: Observed variability of chlorophyll-a using Argo profiling floats in the southeastern Arabian Sea, Deep. Res. Part I Oceanogr. Res. Pap., doi:10.1016/j.dsr.2012.03.003, 2012.

Reason, C. J. C.: Subtropical Indian Ocean SST dipole events and southern African rainfall, Geophys. Res. Lett., doi:10.1029/2000GL012735, 2001.

Reason, C.J.C.: Sensitivity of the southern African circulation to dipole sea-surface-temperature patterns in the south Indian Ocean. Int. J. Climatol. 22, 377–393. https://doi.org/10.1002/joc.744, 2002.

Reppin, J., Schott, F. A., Fischer, J. and Quadfasel, D.: Equatorial currents and transports in the upper central Indian Ocean: Annual cycle and interannual variability, J. Geophys. Res. Ocean., doi:10.1029/1999jc900093, 1999.

Resplandy, L., Vialard, J., Lévy, M., Aumont, O. and Dandonneau, Y.: Seasonal and intraseasonal biogeochemical variability in the thermocline ridge of the southern tropical Indian Ocean, J. Geophys. Res. Ocean., doi:10.1029/2008JC005246, 2009.

Ridgway, K. R., and Condie, S. A.: The 5500-km–long boundary flow off western and southern Australia, J. Geophys. Res., 109, C04017, https://doi.org/10.1029/2003JC001921, 2004.

Ridgway, K. R., Godfrey, J.: The source of the Leeuwin Current seasonality, J. Geophys. Res., 120(10), 6843–6864, https://doi.org/10.1002/2015JC011049, 2015.

Robbins, P. E. and Toole, J. M.: The dissolved silica budget as a constraint on the meridional overturning circulation of the Indian Ocean, Deep. Res. Part I Oceanogr. Res. Pap., doi:10.1016/S0967-0637(96)00126-4, 1997.

Roberts, M. J.: Chokka squid (Loligo vulgaris reynaudii) abundance linked to changes in South Africa's Agulhas Bank ecosystem during spawning and the early life cycle, ICES J. Mar. Sci., doi:10.1016/j.icesjms.2004.10.002, 2005.

Roberts, M. J., Ternon, J. F. and Morris, T.: Interaction of dipole eddies with the western continental slope of the Mozambique Channel, Deep. Res. Part II Top. Stud. Oceanogr., doi:10.1016/j.dsr2.2013.10.016, 2014.

Robinson, J., Guillotreau, P., Jiménez-Toribio, R., Lantz, F., Nadzon, L., Dorizo, J., Gerry, C. and Marsac, F.: Impacts of climate variability on the tuna economy of Seychelles, Clim. Res., doi:10.3354/cr00890, 2010.

Rochford, D. J.: Seasonal interchange of high and low salinity surface waters off south-west Australia, Technical Paper, Division of Fisheries and Oceanography, CSIRO, Australia, http://hdl.handle.net/102.100.100/321788?index=1, 1969.

Roemmich, D., W. J. Gould and J Gilson: 135 years of global ocean warming between the Challenger expedition and the Argo Programme. Nature Climate Change volume 2, 425–428, 2012.

Rosell-Fieschi, M., Rintoul, S. R., Gourrion, J., and Pelegrí, J. L.: Tasman Leakage of intermediate waters as inferred from Argo floats, Geophys. Res. Lett., 40, 5456– 5460, https://doi.org/10.1002/2013GL057797, 2013.

Roxy, M., Tanimoto, Y., Preethi, B., Terray, P. and Krishnan, R.: Intraseasonal SST-precipitation relationship and its spatial variability over the tropical summer monsoon region, Clim. Dyn., 41(1), 45–61, doi:10.1007/s00382-012-1547-1, 2013.Roxy, M. K., Ritika, K., Terray, P. and Masson, S.: The curious case of Indian Ocean warming, J. Clim., doi:10.1175/JCLI-D-14-00471.1, 2014.

Roxy, M. K., Modi, A., Murtugudde, R., Valsala, V., Panickal, S., Prasanna Kumar, S., Ravichandran, M., Vichi, M. and Lévy, M.: A reduction in marine primary productivity driven by rapid warming over the tropical Indian Ocean, Geophys. Res. Lett., doi:10.1002/2015GL066979, 2016.

Rouault, M., Penven, P. and Pohl, B.: Warming in the Agulhas Current system since the 1980's, Geophys. Res. Lett., doi:10.1029/2009GL037987, 2009.

Rydbeck, A. V. and Jensen, T. G.: Oceanic impetus for convective onset of the Madden-Julian oscillation in the western Indian ocean, J. Clim., 30(11), 4299–4316, doi:10.1175/JCLI-D-16-0595.1, 2017.

Rydbeck, A. V., Jensen, T. G. and Nyadjro, E. S.: Intraseasonal sea surface warming in the western Indian Ocean by oceanic equatorial Rossby waves, Geophys. Res. Lett., 44(9), 4224–4232, doi:10.1002/2017GL073331, 2017.

Sabeerali, C. T., Ramu Dandi, A., Dhakate, A., Salunke, K., Mahapatra, S. and Rao, S. A.: Simulation of boreal summer intraseasonal oscillations in the latest CMIP5 coupled GCMs, J. Geophys. Res. Atmos., 118(10), 4401–4420, doi:10.1002/jgrd.50403, 2013.

Saji, N. H., Goswami, B. N., Vinayachandran, P. N. and Yamagata, T.: A dipole mode in the tropical Indian Ocean, Nature, 401(6751), 360–363, doi:10.1038/43854, 1999.

2940 Sanchez-Franks, A., Webber, B. G. M., King, B. A., Vinayachandran, P. N., Matthews, A. J., Sheehan, P. M. F., Behara,
2941 A. and Neema, C. P.: The railroad switch effect of seasonally reversing currents on the Bay of Bengal high salinity core,
2942 Geophys. Res. Lett., doi:10.1029/2019gl082208, 2019.

2943 Sanchez-Franks, A., Kent, E. C., Matthews, A. J., Webber, B. G. M., Peatman, S. C. and Vinayachandran, P. N.:
2944 Intraseasonal variability of air-sea fluxes over the Bay of Bengal during the Southwest Monsoon, J. Clim.,
2945 doi:10.1175/JCLI-D-17-0652.1, 2018.

2946 Sarkar, S., H.T. Pham, S. Ramachandran, J.D. Nash, A. Tandon, J. Buckley, A.A. Lotliker, and M.M. Omand: The
2947 interplay between submesoscale instabilities and turbulence in the surface layer of the Bay of Bengal. Oceanography
2948 29(2):146–157, https://doi.org/10.5670/oceanog.2016.47, 2016.

2949 Sarma, V. V. and Aswanikumar, V.: Subsurface chlorophyll maxima in the north-western Bay of Bengal, J. Plankton
2950 Res., doi:10.1093/plankt/13.2.339, 1991.

2951 Sasamal, S. K., Panigrahy, R. C. and Misra, S.: Asterionella blooms in the northwestern Bay of Bengal during 2004, Int.
2952 J. Remote Sens., doi:10.1080/01431160500185391, 2005.

2953 Sawant, S. and Madhupratap, M.: Seasonally and composition of phytoplankton in the Arabian Sea, Curr. Sci., 1996.

2954 Schloesser, F.: A dynamical model for the Leeuwin Undercurrent, J. Phys. Oceanogr., 44, 1798-1810,
2955 https://doi.org/10.1175/JPO-D-13-0226.1, 2014.

2956 Schott, F. A. and McCreary, J. P.: The monsoon circulation of the Indian Ocean, Progr. Oceanogr., 51, 1-123, 2001.

2957 Schott, F., Dengler, M., and Schoenefeldt, R.: The shallow overturning circulation of the Indian Ocean. Progress in
2958 Oceanography 53 (2002) 57–103, 2002.

2959 Schott, F. A., Xie, S.-P. and McCreary, J. P.: Indian Ocean circulation and climate variability, Rev. Geophys., 47,
2960 RG1002, https://doi.org/10.1029/2007RG000245, 2009.

2961 Schumann, E. H., Churchill, J. R. S. and Zaayman, H. J.: Oceanic variability in the western sector of Algoa Bay, South
2962 Africa, African J. Mar. Sci., doi:10.2989/18142320509504069, 2005.

2963 Sengupta, D., Senan, R. and Goswami, B. N.: Origin of intraseasonal variability of circulation in the tropical central
2964 Indian Ocean, Geophys. Res. Lett., doi:10.1029/2000GL012251, 2001.

2965 Sengupta, D., Bharath Raj, G. N. and Shenoi, S. S. C.: Surface freshwater from Bay of Bengal runoff and Indonesian
2966 Throughflow in the tropical Indian Ocean, Geophys. Res. Lett., doi:10.1029/2006GL027573, 2006.

2967 Sengupta, D., Goddalehundi, B. R. and Anitha, D. S.: Cyclone-induced mixing does not cool SST in the post-monsoon
2968 north Bay of Bengal, Atmos. Sci. Lett., doi:10.1002/asl.162, 2008.

2969 Sengupta, D., Senan, R., Goswami, B. N. and Vialard, J.: Intraseasonal variability of equatorial Indian Ocean zonal
2970 currents, in Journal of Climate., 2007.

2971 Shalapyonok, A., Olson, R. J. and Shalapyonok, L. S.: Arabian Sea phytoplankton during Southwest and Northeast
2972 Monsoons 1995: Composition, size structure and biomass from individual cell properties measured by flow cytometry,
2973 Deep. Res. Part II Top. Stud. Oceanogr., doi:10.1016/S0967-0645(00)00137-5, 2001.

2974 Shankar, D., Vinayachandran, P. N. and Unnikrishnan, A. S.: The monsoon currents in the north Indian Ocean, Prog.
2975 Oceanogr., 52(1), 63–120, doi:10.1016/S0079-6611(02)00024-1, 2002.

2976 Sharma, G. S.: Water characteristics and current structure at 65°E during the southwest monsoon, J. Oceanogr. Soc.
2977 Jpn., 32, 284–296, https://doi.org/10.1007/BF02107985, 1976.

2978 Sharma, G.S., Gouveia, A.D., and Satyendranath, S.: Incursion of the Pacific Ocean Water into the Indian Ocean. Proc.
2979 Indian Acad. Sci., A (E & P Sciences) 87, 29–45, https://doi.org/10.1007/BF02839383, 1978.

2980 Sharmila, S., Pillai, P. A., Joseph, S., Roxy, M., Krishna, R. P. M., Chattopadhyay, R., Abhilash, S., Sahai, A. K. and
2981 Goswami, B. N.: Role of ocean-atmosphere interaction on northward propagation of Indian summer monsoon intra-
2982 seasonal oscillations (MISO), Clim. Dyn., 41(5–6), 1651–1669, doi:10.1007/s00382-013-1854-1, 2013.

Sheehan, P. M. F., Webber, B. G. M., Sanchez-Franks, A., Matthews, A. J., Heywood, K. J. and Vinayachandran, P. N.: Injection of Oxygenated Persian Gulf Water Into the Southern Bay of Bengal, Geophys. Res. Lett., doi:10.1029/2020GL087773, 2020.

Shetye, S. R., Gouveia, A. D., Shankar, D., Shenoi, S. S. C., Vinayachandran, P. N., Sundar, D., Michael, G. S. and Nampoothiri, G.: Hydrography and circulation in the western Bay of Bengal during the northeast monsoon, J. Geophys. Res. C Ocean., doi:10.1029/95JC03307, 1996.

Shinoda, T., Hendon, H. H. and Glick, J.: Intraseasonal Variability of Surface Fluxes and Sea Surface Temperature in the Tropical Western Pacific and Indian Oceans, J. Clim., 11, 1685–1702, 1998.

Shinoda, T., Han, W., Joseph Metzger, E. and Hurlburt, H. E.: Seasonal variation of the Indonesian throughflow in Makassar Strait, J. Phys. Oceanogr., doi:10.1175/JPO-D-11-0120.1, 2012.

Shroyer, E., Rudnick, D., Farrar, J. T., Lim, B., Venayagamoorthy, S. K., St. Laurent, L., Garanaik, A. and Moum, J.: Modification of Upper-Ocean Temperature Structure by Subsurface Mixing in the Presence of Strong Salinity Stratification, Oceanography, 29(2), 62–71, doi:10.5670/oceanog.2016.39, 2016.

Siedler, G., Rouault, M., and Lutjeharms, J.: Structure and origin of the subtropical South Indian Ocean Countercurrent, Geophys. Res. Lett., 33, L24609, https://doi.org/10.1029/2006GL027399, 2006.

Siedler, G., Rouault, M., Biastoch, A., Backeberg, B. C., Reason, C. J. C., and Lutjeharms, J.: Modes of the southern extension of the East Madagascar Current, J. Geophys. Res., 114, C01005, https://doi.org/10.1029/2008JC004921, 2009.

Singh, A., Gandhi, N., Ramesh, R. and Prakash, S.: Role of cyclonic eddy in enhancing primary and new production in the Bay of Bengal, J. Sea Res., doi:10.1016/j.seares.2014.12.002, 2015a.

Singh, A. and Ramesh, R.: Environmental controls on new and primary production in the northern Indian Ocean, Prog. Oceanogr., doi:10.1016/j.pocean.2014.12.006, 2015b.

Singh, D., Tsiang, M., Rajaratnam, B. and Diffenbaugh, N. S.: Observed changes in extreme wet and dry spells during the south Asian summer monsoon season, Nat. Clim. Chang., doi:10.1038/nclimate2208, 2014.

Smith, R. L., Huyer, A., Godfrey, J. S., and Church, J. A.: The Leeuwin Current off Western Australia, 1986–1987, J. Phys. Oceanogr., 21, 323–345, https://doi.org/10.1175/1520-0485(1991)021<0323:TLCOWA>2.0.CO;2, 1991.

Sorokin, Y., Kopylov, A. and Mamaeva, N.: Abundance and dynamics of microplankton in the central tropical Indian Ocean, Mar. Ecol. Prog. Ser., doi:10.3354/meps024027, 1985.

Speich, S., Blanke, B. and Cai, W.: Atlantic meridional overturning circulation and the Southern Hemisphere supergyre, Geophys. Res. Lett., doi:10.1029/2007GL031583, 2007.

Sperber, K. R. and Annamalai, H.: Coupled model simulations of boreal summer intraseasonal (30-50 day) variability, Part 1: Systematic errors and caution on use of metrics, Clim. Dyn., 31(2–3), 345–372, doi:10.1007/s00382-008-0367-9, 2008.

Sprintall, J., Wijffels, S. E., Molcard, R. and Jaya, I.: Direct estimates of the indonesian throughflow entering the indian ocean: 2004-2006, J. Geophys. Res. Ocean., doi:10.1029/2008JC005257, 2009.

Sprintall, J., Gordon, A. L., Koch-Larrouy, A., Lee, T., Potemra, J. T., Pujiana, K. and Wijffels, S. E.: The Indonesian seas and their role in the coupled ocean-climate system, Nat. Geosci., doi:10.1038/ngeo2188, 2014a.

Sprintall, J. and Révelard, A.: The Indonesian Throughflow response to Indo-Pacific climate variability, J. Geophys. Res. Ocean., doi:10.1002/2013JC009533, 2014b.

Sprintall, J., Gordon, A. L., Wijffels, S. E., Feng, M., Hu, S., Koch-Larrouy, A., Phillips, H., Nugroho, D., Napitu, A., Pujiana, K., Dwi Susanto, R., Sloyan, B., Yuan, D., Riama, N. F., Siswanto, S., Kuswardani, A., Arifin, Z., Wahyudi, A. J., Zhou, H., Nagai, T., Ansong, J. K., Bourdalle-Badié, R., Chanut, J., Lyard, F., Arbic, B. K., Ramdhani, A. and Setiawan, A.: Detecting change in the Indonesian seas, Front. Mar. Sci., doi:10.3389/fmars.2019.00257, 2019.

Sree Lekha, J., Buckley, J. M., Tandon, A. and Sengupta, D.: Subseasonal Dispersal of Freshwater in the Northern Bay of Bengal in the 2013 Summer Monsoon Season, J. Geophys. Res. Ocean., doi:10.1029/2018JC014181, 2018.

Srinivasan, A., Garraffo, Z. and Iskandarani, M.: Abyssal circulation in the Indian Ocean from a 1 / 12° resolution global hindcast, Deep. Res. Part I Oceanogr. Res. Pap., doi:10.1016/j.dsr.2009.07.001, 2009.

Srokosz, M. A., Quartly, G. D. and Buck, J. J. H.: A possible plankton wave in the Indian Ocean, Geophys. Res. Lett., doi:10.1029/2004GL019738, 2004.

Srokosz, M. A. and Quartly, G. D.: The madagascar bloom: A serendipitous study, J. Geophys. Res. Ocean., doi:10.1029/2012JC008339, 2013.

Srokosz, M. A., Robinson, J., McGrain, H., Popova, E. E., and Yool, A.: Could the Madagascar bloom be fertilized by Madagascan iron?, J. Geophys. Res. Oceans, 120, 5790– 5803, https://doi.org/10.1002/2015JC011075, 2015.

Stramma, L., Bange, H. W., Czeschel, R., Lorenzo, A. and Frank, M.: On the role of mesoscale eddies for the biological productivity and biogeochemistry in the eastern tropical Pacific Ocean off Peru, Biogeosciences, doi:10.5194/bg-10-7293-2013, 2013.

Strutton, P. G., Coles, V. J., Hood, R. R., Matear, R. J., McPhaden, M. J. and Phillips, H. E.: Biogeochemical variability in the central equatorial Indian Ocean during the monsoon transition, Biogeosciences, doi:10.5194/bg-12-2367-2015, 2015.

Stuecker, M. F., Timmermann, A. , Jin, F. F., Chikamoto, Y. , Zhang, W., Wittenberg, A. T., Widiasih, E., and Zhao, S.: Revisiting ENSO/Indian Ocean Dipole phase relationships, Geophys. Res. Lett., 44, 2481–2492, 2017.

Suhas, E., Neena, J. M. and Goswami, B. N.: An Indian monsoon intraseasonal oscillations (MISO) index for real time monitoring and forecast verification, Clim. Dyn., 40(11–12), 2605–2616, doi:10.1007/s00382-012-1462-5, 2013.

Sun, S., Lan, J., Fang, Y., Tana, and Gao, X.: A triggering mechanism for the Indian Ocean dipoles independent of ENSO. J. Climate, 28, 5063-5076, https://doi.org/10.1175/JCLI-D-14-00580.1, 2015.

Susanto, R. D., Wei, Z., Adi, R. T., Fan, B., Li, S. and Fang, G.: Observations of the Karimata Strait throughflow from December 2007 to November 2008, Acta Oceanol. Sin., doi:10.1007/s13131-013-0307-3, 2013.

Suzuki, R., Behera, S. K., Iizuka, S. and Yamagata, T.: Indian Ocean subtropical dipole simulated using a coupled general circulation model, J. Geophys. Res. C Ocean., doi:10.1029/2003JC001974, 2004.

Swallow, J. C. and Pollard, R. T.: Flow of bottom water through the Madagascar Basin, Deep Sea Res. Part A, Oceanogr. Res. Pap., doi:10.1016/0198-0149(88)90095-7, 1988.

Takeuchi, K.: Numerical study of the Subtropical Front and the Subtropical Countercurrent. J. Oceanogr. Soc. Japan, 40, 371–381, https://doi.org/10.1007/BF02303341, 1984.

Talley, L. D., and Sprintall., J.: Deep expression of the Indonesian Throughflow: Indonesian Intermediate Water in the South Equatorial Current, Journal of Geophysical Research, Oceans, 110: doi:10.1029/2004JC002826, 2005.

Talley, L. D.: Freshwater transport estimates and the global overturning circulation: Shallow, deep and throughflow components. *Progress in Oceanography, 78*(4), 257-303. doi: 10.1016/j.pocean.2008.05.001, 2008.

Talley, L. D.: Closure of the global overturning circulation through the Indian, Pacific, and Southern Oceans: Schematics and transports. Oceanography 26 (1), 80-97. doi: 10.5670/oceanog.2013.07, 2013.

Talley, L. D., Pickard, G. L., Emery, W. J. and Swift, J. H.: Descriptive Physical Oceanography: An Introduction, 6th Edition. Academic Press, Elsevier Ltd. 983pp, 2011.

Talley, L. D., Feely, R. A., Sloyan, B. M., Wanninkhof, R., Baringer, M.O., Bullister, J. L., et al.: Changes in ocean heat, carbon content, and ventilation: A review of the first decade of GO-SHIP global repeat hydrography. Annu. Rev. Mar. Sci. 8, 185-215. doi: 10.1146/annurev-marine-052915-100829, 2016.

Talley, L., Johnson, G. C., Purkey, S., Feely, R. A. and Wanninkhof, R.: Global Ocean Ship-based Hydrographic Investigations Program (GO-SHIP) provides key climate-relevant deep ocean observations, US CLIVAR Variations, 15, 8-14, 2017.

Tarran, G. A., Burkill, P. H., Edwards, E. S. and Woodward, E. M. S.: Phytoplankton community structure in the Arabian Sea during and after the SW monsoon, 1994, Deep. Res. Part II Top. Stud. Oceanogr., doi:10.1016/S0967-0645(98)00122-2, 1999.

Taylor, B. M., Benkwitt, C. E., Choat, H., Clements, K. D., Graham, N. A., and Meekan, M. G.: Synchronous biological feedbacks in parrotfishes associated with pantropical coral bleaching, Global Change Biology, 26, 3, 1285-1294, https://doi.org/10.1111/gcb.14909, 2019.

Terray, P., Delecluse, P., Labattu, S. and Terray, L.: Sea surface temperature associations with the late Indian summer monsoon, Clim. Dyn., doi:10.1007/s00382-003-0354-0, 2003.

Thadathil, P., Muraleedharan, P. M., Rao, R. R., Somayajulu, Y. K., Reddy, G. V. and Revichandran, C.: Observed seasonal variability of barrier layer in the Bay of Bengal, J. Geophys. Res. Ocean., 112(2), doi:10.1029/2006JC003651, 2007.

Thadathil, P., Suresh, I., Gautham, S., Prasanna Kumar, S., Lengaigne, M., Rao, R. R., Neetu, S. and Hegde, A.: Surface layer temperature inversion in the Bay of Bengal: Main characteristics and related mechanisms, J. Geophys. Res. Ocean., doi:10.1002/2016JC011674, 2016.

Thangaprakash, V. P., Girishkumar, M. S., Suprit, K., Kumar, N. S., Chaudhuri, D., Dinesh, K., Kumar, A., Shivaprasad, S., Ravichandran, M., Farrar, J. T., Sundar, R. and Weller, R.: What Controls Seasonal Evolution of Sea Surface Temperature in the Bay of Bengal? Mixed Layer Heat Budget Analysis Using Moored Buoy Observations Along 90°E, Oceanography, 29(2), 202–213, doi:10.5670/oceanog.2016.52, 2016.

Thompson, P. A., Pesant, S. and Waite, A. M.: Contrasting the vertical differences in the phytoplankton biology of a dipole pair of eddies in the south-eastern Indian Ocean, Deep. Res. Part II Top. Stud. Oceanogr., doi:10.1016/j.dsr2.2006.12.009, 2007.

Thompson, R. O. R. Y.: Observations of the Leeuwin Current off Western Australia, J. Phys. Oceanogr., 14, 623–628, https://doi.org/10.1175/1520-0485(1984)014<0623:OOTLCO>2.0.CO;2, 1984.

Thompson, R. O. R. Y.: Continental-shelf-scale model of the Leeuwin Current, J. Mar. Res., 45(4), 813–827, https://doi.org/10.1357/002224087788327190, 1987.

Toole, J. M., and Warren, B. A.: A hydrographic section across the subtropical South Indian Ocean, Deep-Sea Res I, 40, 1973-2019, https://doi.org/10.1016/0967-0637(93)90042-2, 1993.

Tozuka, T., Kataoka, T., and Yamagata, T.: Locally and remotely forced atmospheric circulation anomalies of Ningaloo Niño/Niña, Clim. Dyn., 43, 2197–2205, https://doi.org/10.1007/s00382-013-2044-x, 2014.

Turner, A. G., Joshi, M., Robertson, E. S., and Woolnough, S. J.: The effect of Arabian Sea optical properties on SST biases and the South Asian summer monsoon in a coupled GCM, Clim. Dyn., 39(3), 811–826, https://doi.org/10.1007/s00382-011-1254-3, 2012.

Ummenhofer, C. C., Biastoch, A., and Böning, C. W.: Multidecadal Indian Ocean variability linked to the Pacific and implications for preconditioning Indian Ocean dipole events. J. Climate, 30, 1739–1751, 2017.

Uz, B. M.: What causes the sporadic phytoplankton bloom southeast of Madagascar?, J. Geophys. Res. Ocean., doi:10.1029/2006JC003685, 2007.

Van Sebille, E., Biastoch, A., Van Leeuwen, P. J. and De Ruijter, W. P. M.: A weaker Agulhas current leads to more Agulhas leakage, Geophys. Res. Lett., doi:10.1029/2008GL036614, 2009.

Van Sebille, E., Van Leeuwen, P. J., Biastoch, A. and De Ruijter, W. P. M.: On the fast decay of Agulhas rings, J. Geophys. Res. Ocean., doi:10.1029/2009JC005585, 2010a.

van Sebille, E., van Leeuwen, P. J., Biastoch, A. and de Ruijter, W. P. M.: Flux comparison of Eulerian and Lagrangian estimates of Agulhas leakage: A case study using a numerical model, Deep. Res. Part I Oceanogr. Res. Pap., doi:10.1016/j.dsr.2009.12.006, 2010b.

van Sebille, E., Beal, L. M. and Johns, W. E.: Advective Time Scales of Agulhas Leakage to the North Atlantic in Surface Drifter Observations and the 3D OFES Model, J. Phys. Oceanogr., doi:10.1175/2011jpo4602.1, 2011.

Van Sebille, E., Sprintall, J., Schwarzkopf, F. U., Sen Gupta, A., Santoso, A., England, M. H., Biastoch, A. and Böning, C. W.: Pacific-to-Indian Ocean connectivity: Tasman leakage, Indonesian Throughflow, and the role of ENSO, J. Geophys. Res. Ocean., doi:10.1002/2013JC009525, 2014.

Vecchi, G. A. and Soden, B. J.: Global warming and the weakening of the tropical circulation. J. Climate, 20, 4316–4340, 2007.

Vecchi, G. A. and Harrison, D. E.: Monsoon Breaks and Subseasonal Sea Surface Temperature Variability in the Bay of Bengal*, J. Clim., 15(12), 1485–1493, doi:10.1175/1520-0442(2002)015<1485:MBASSS>2.0.CO;2, 2002.

Venkatesan, R., Vedachalam, N., Arul Muthiah, M., Sundar, R., Kesavakumar, B., Ramasundaram, S. and Jossia Joseph, K.: Reliability metrics from two decades of Indian ocean moored buoy observation network, Mar. Technol. Soc. J., doi:10.4031/MTSJ.52.3.14, 2018.

Venrick, E. L.: Mid-ocean ridges and their influence on the large-scale patterns of chlorophyll and production in the North Pacific, Deep. Res. Part A, doi:10.1016/s0198-0149(12)80006-9, 1991.

Vialard, J., Foltz, G. R., McPhaden, M. J., Duvel, J. P. and de Boyer Montégut, C.: Strong Indian Ocean sea surface temperature signals associated with the Madden-Julian Oscillation in late 2007 and early 2008, Geophys. Res. Lett., 35(19), 1–5, doi:10.1029/2008GL035238, 2008.

Vialard, J., Duvel, J. P., Mcphaden, M. J., Bouruet-Aubertot, P., Ward, B., Key, E., Bourras, D., Weller, R., Minnett, P., Weill, A., Cassou, C., Eymard, L., Fristedt, T., Basdevant, C., Dandonneau, Y., Duteil, O., Izumo, T., de Boyer Montégut, C., Masson, S., Marsac, F., Menkes, C. and Kennan, S.: Cirene: Air-sea interactions in the seychelles-chagos thermocline ridge region, Bull. Am. Meteorol. Soc., doi:10.1175/2008BAMS2499.1, 2009a.

Vialard, J., Shenoi, S. S. C., McCreary, J. P., Shankar, D., Durand, F., Fernando, V. and Shetye, S. R.: Intraseasonal response of the northern Indian Ocean coastal waveguide to the Madden-Julian Oscillation, Geophys. Res. Lett., 36(14), 1–5, doi:10.1029/2009GL038450, 2009b.

Vialard, J., Jayakumar, A., Gnanaseelan, C., Lengaigne, M., Sengupta, D. and Goswami, B. N.: Processes of 30-90 days sea surface temperature variability in the northern Indian Ocean during boreal summer, Clim. Dyn., 38(9–10), 1901–1916, doi:10.1007/s00382-011-1015-3, 2012.

Vinayachandran, P. N., Matthews, A. J., Vijay KuMar, K., Sanchez-Franks, A., Thushara, V., George, J., Vijith, V., Webber, B. G. M., Queste, B. Y., Roy, R., Sarkar, A., Baranowski, D. B., Bhat, G. S., Klingaman, N. P., Peatman, S. C., Parida, C., Heywood, K. J., Hall, R., King, B., Kent, E. C., Nayak, A. A., Neema, C. P., Amol, P., Lotliker, A., Kankonkar, A., Gracias, D. G., Vernekar, S., D'Souza, A. C., Valluvan, G., Pargaonkar, S. M., Dinesh, K., Giddings, J. and Joshi, M.: Ocean–Atmosphere interaction and its impact on the south asian monsoon, Bull. Am. Meteorol. Soc., doi:10.1175/BAMS-D-16-0230.1, 2018.

Waite, A. M., Pesant, S., Griffin, D. A., Thompson, P. A. and Holl, C. M.: Oceanography, primary production and dissolved inorganic nitrogen uptake in two Leeuwin Current eddies, Deep. Res. Part II Top. Stud. Oceanogr., doi:10.1016/j.dsr2.2007.03.001, 2007a.

Waite, A. M., Thompson, P. A., Pesant, S., Feng, M., Beckley, L. E., Domingues, C. M., Gaughan, D., Hanson, C. E., Holl, C. M., Koslow, T., Meuleners, M., Montoya, J. P., Moore, T., Muhling, B. A., Paterson, H., Rennie, S., Strzelecki, J., and Twomey, L.: The Leeuwin Current and its eddies: An introductory overview, Deep Sea Res. II, 54(8–10), 789–796, https://doi.org/10.1016/j.dsr2.2006.12.008, 2007b.

Waite, A. M., Beckley, L. E., Guidi, L., Landrum, J. P., Holliday, D., Montoya, J., Paterson, H., Feng, M., Thompson, P. A. and Raes, E. J.: Cross-shelf transport, oxygen depletion, and nitrate release within a forming mesoscale eddy in the eastern Indian Ocean, Limnol. Oceanogr., doi:10.1002/lno.10218, 2016.

Waliser, D. E., Murtugudde, R. and Lucas, L. E.: Indo-Pacific Ocean response to atmospheric intraseasonal variability: 1. Austral summer and the Madden-Julian Oscillation, J. Geophys. Res., 108(C5), 3160, doi:10.1029/2002JC001620, 2003.

Wang, H., Kumar, A., Murtugudde, R., Narapusetty, B., and Selp, K. L.: Covariations between the Indian Ocean dipole and ENSO: a modeling study. Clim. Dyn., doi:10.1007/s00382-019-04895-x, 2019.

Warner, S. J., Becherer, J., Pujiana, K., Shroyer, E. L., Ravichandran, M., Thangaprakash, V. P. and Moum, J. N.: Monsoon mixing cycles in the Bay of Bengal: A year-long subsurface mixing record, Oceanography, doi:10.5670/oceanog.2016.48, 2016.

3163 Warren, B. A.: Deep flow in the Madagascar and Mascarene basins, Deep. Res. Oceanogr. Abstr., doi:10.1016/0011-
3164 7471(74)90015-1, 1974.

3165 Warren, B. A.: Bottom water transport through the Southwest Indian Ridge, Deep. Res., doi:10.1016/0146-
3166 6291(78)90596-9, 1978.

3167 Warren, B.A.: Transindian hydrographic section at Lat. 18°S: Property distributions and circulation in the South Indian
3168 Ocean. Deep-Sea Res A., 28, 759-788. doi: 10.1016/S0198-0149(81)80001-5, 1981.

3169 Warren, B.A. : Driving the meridional overturning in the Indian Ocean, Deep. Res. Part I, doi:10.1016/0967-
3170 0637(94)90101-5, 1994.

3171 Warren, B. A., Whitworth, T. and LaCasce, J. H.: Forced resonant undulation in the deep Mascarene Basin, Deep. Res.
3172 Part II Top. Stud. Oceanogr., doi:10.1016/S0967-0645(01)00151-5, 2002.

3173 Weaver, A. J., and Middleton, J. H.: On the dynamics of the Leeuwin Current, J. Phys. Oceanogr., 19, 626–648,
3174 https://doi.org/10.1175/1520-0485(1989)019<0626:OTDOTL>2.0.CO;2, 1989.

3175 Weaver, A.J., and Middleton, J.H.: An analytic model for the Leeuwin Current off western Australia, Cont. Shelf Res.,
3176 10(2), 105–122, https://doi.org/10.1016/0278-4343(90)90025-H, 1990.

3177 Webber, B. G. M., Matthews, A. J. and Heywood, K. J.: A dynamical ocean feedback mechanism for the Madden-Julian
3178 Oscillation, Q. J. R. Meteorol. Soc., 136(648), 740–754, doi:10.1002/qj.604, 2010.

3179 Webber, B. G. M., Stevens, D. P., Matthews, A. J. and Heywood, K. J.: Dynamical ocean forcing of the Madden-Julian
3180 oscillation at lead times of up to five months, J. Clim., 25(8), 2824–2842, doi:10.1175/JCLI-D-11-00268.1, 2012a.

3181 Webber, B. G. M., Matthews, A. J., Heywood, K. J. and Stevens, D. P.: Ocean Rossby waves as a triggering mechanism
3182 for primary Madden-Julian events, Q. J. R. Meteorol. Soc., 138(663), 514–527, doi:10.1002/qj.936, 2012b.

3183 Webber, B. G. M., Matthews, A. J., Heywood, K. J., Kaiser, J. and Schmidtko, S.: Seaglider observations of equatorial
3184 Indian Ocean Rossby waves associated with the Madden-Julian Oscillation, J. Geophys. Res. Ocean., 119(6), 3714–
3185 3731, doi:10.1002/2013JC009657, 2014.

3186 Webber, B. G. M., Matthews, A. J., Vinayachandran, P. N., Neema, C. P., Sanchez-Franks, A., Vijith, V., Amol, P. and
3187 Baranowski, D. B.: The Dynamics of the Southwest Monsoon Current in 2016 from High-Resolution In Situ
3188 Observations and Models, J. Phys. Oceanogr., 48(10), 2259–2282, doi:10.1175/JPO-D-17-0215.1, 2018.

3189 Webster, P. J., Moore, A., Loschnigg, J. P. and R., L. R.: Coupled oceanic-atmoshperic dynamics in the Indian Ocean
3190 during 1997-1998, Nature, 401(September), 356–360, 1999.

3191 Weijer, W. and van Sebille, E.: Impact of Agulhas leakage on the Atlantic overturning circulation in the CCSM4, J.
3192 Clim., doi:10.1175/JCLI-D-12-00714.1, 2014.

3193 Weller, R. A., Farrar, J. T., Buckley, J., Mathew, S., Venkatesan, R., Lekha, J. S., Chaudhuri, D., Suresh Kumar, N. and
3194 Praveen Kumar, B.: Air-sea interaction in the Bay of Bengal, Oceanography, doi:10.5670/oceanog.2016.36, 2016.

3195 Wiggert, J. D., Jones, B. H., Dickey, T. D., Brink, K. H., Weller, R. A., Marra, J. and Codispoti, L. A.: The Northeast
3196 Monsoon's impact on mixing, phytoplankton biomass and nutrient cycling in the Arabian Sea, Deep. Res. Part II Top.
3197 Stud. Oceanogr., doi:10.1016/S0967-0645(99)00147-2, 2000.

3198 Wiggert, J. D., Hood, R. R., Banse, K. and Kindle, J. C.: Monsoon-driven biogeochemical processes in the Arabian Sea,
3199 Prog. Oceanogr., doi:10.1016/j.pocean.2005.03.008, 2005.

3200 Wiggert, J. D., Murtugudde, R. G. and Christian, J. R.: Annual ecosystem variability in the tropical Indian Ocean:
3201 Results of a coupled bio-physical ocean general circulation model, Deep. Res. Part II Top. Stud. Oceanogr., 53(5–7),
3202 644–676, doi:10.1016/j.dsr2.2006.01.027, 2006.

3203 Wiggert, J. D., Vialard, J., and Behrenfeld, M. J.: Basin-wide modification of dynamical and biogeochemical processes
3204 by the positive phase of the Indian Ocean Dipole during the SeaWiFS era. In: Indian Ocean biogeochemical Processes
3205 and Ecological Variability, Geophysical Monograph Series, 185, 385-407, https://doi.org/10.1029/2008GM000776,
3206 2009.

Wijesekera, H. W., Jensen, T. G., Jarosz, E., Teague, W. J., Metzger, E. J., Wang, D. W., Jinadasa, S. U. P., Arulananthan, K., Centurioni, L. R. and Fernando, H. J. S.: Southern Bay of Bengal currents and salinity intrusions during the northeast monsoon, J. Geophys. Res. Ocean., doi:10.1002/2015JC010744, 2015.

Wijesekera, H. W., Shroyer, E., Tandon, A., Ravichandran, M., Sengupta, D., Jinadasa, S. U. P., Fernando, H. J. S., Agrawal, N., Arulananthan, K., Bhat, G. S., Baumgartner, M., Buckley, J., Centurioni, L., Conry, P., Thomas Farrar, J., Gordon, A. L., Hormann, V., Jarosz, E., Jensen, T. G., Johnston, S., Lankhorst, M., Lee, C. M., Leo, L. S., Lozovatsky, I., Lucas, A. J., MacKinnon, J., Mahadevan, A., Nash, J., Omand, M. M., Pham, H., Pinkel, R., Rainville, L., Ramachandran, S., Rudnick, D. L., Sarkar, S., Send, U., Sharma, R., Simmons, H., Stafford, K. M., Laurent, L. S., Venayagamoorthy, K., Venkatesan, R., Teague, W. J., Wang, D. W., Waterhouse, A. F., Weller, R. and Whalen, C. B.: ASIRI: An ocean-atmosphere initiative for bay of Bengal, Bull. Am. Meteorol. Soc., doi:10.1175/BAMS-D-14-00197.1, 2016a.

Wijesekera, H., Teague, W., Jarosz, E., Wang, D., Jensen, T., Jinadasa, S. U. P., Fernando, H., Centurioni, L., Hallock, Z., Shroyer, E. and Moum, J.: Observations of Currents Over the Deep Southern Bay of Bengal—With a Little Luck, Oceanography, 29(2), 112–123, doi:10.5670/oceanog.2016.44, 2016b.

Wijesekera, H. W., Teague, W. J., Wang, D. W., Jarosz, E., Jensen, T. G., Jinadasa, S. U. P., Fernando, H. J. S. and Hallock, Z. R.: Low-frequency currents from deep moorings in the southern bay of Bengal, J. Phys. Oceanogr., doi:10.1175/JPO-D-16-0113.1, 2016c.

Wijffels, S., Roemmich, D., Monselesan, D., Church, J. and Gilson, J.: Ocean temperatures chronicle the ongoing warming of Earth. *Nature Clim Change* 6, 116–118 https://doi.org/10.1038/nclimate2924, 2016.

Williams, A. P. and C. Funk, C.: A westward extension of the warm pool leads to a westward extension of the Walker circulation, drying eastern Africa. Clim. Dyn., 37, 2417-2435, 2011.

Wilson, C. and Qiu, X.: Global distribution of summer chlorophyll blooms in the oligotrophic gyres, Prog. Oceanogr., doi:10.1016/j.pocean.2008.05.002, 2008.

Woo, M., Pattiaratchi, C. and Schroeder, W.: Summer surface circulation along the Gascoyne continental shelf, Western Australia. *Cont Shelf Res* **26**, 132–152, 2006.

Woo, L. M., Pattiaratchi, C. B.: Hydrography and water masses off the western Australian coast, Deep Sea Res. I, 55(9), 1090–1104, https://doi.org/10.1016/j.dsr.2008.05.005, 2008.

Wyrtki, K.: An equatorial jet in the Indian Ocean, Science (80-.)., doi:10.1126/science.181.4096.262, 1973.

Xie, S.-P., Annamalai, H., Schott, F. A., and McCreary, J. P.: Structure and mechanisms of South Indian Ocean climate variability, J. Clim., 15, 864–878, 2002.

Xie, S.-P., Du, Y., Huang, G., Zheng, X.-T., Tokinaga, H., Hu, K. M., and Liu, Q. Y.: Decadal shift in El Niño influences on Indo–Western Pacific and East Asian climate in the 1970s. J. Climate, 23, 3352–3368, 2010.

Yamagami, Y. and Tozuka, T.: Interdecadal changes of the Indian Ocean subtropical dipole mode, Clim. Dyn., doi:10.1007/s00382-014-2202-9, 2015.

Yang, J., Liu, Q., Xie,S.-P., Liu, Z. and Wu, L.: Impact of the Indian Ocean SST basin mode on the Asian summer monsoon. Geophys. Res. Lett., 34, L02708. doi:10.1029/2006GL028571, 2007.

Yang, Y., Xie, S.-P ., Wu, L., Kosaka, Y., Lau, N. C., and Vecchi, G. A.: Seasonality and predictability of the Indian Ocean dipole mode: ENSO forcing and internal variability, J. Clim., 28, 8021–8036, 2015.

Yit Sen Bull, C., and van Sebille, E.: Sources, fate, and pathways of Leeuwin Current water in the Indian Ocean and Great Australian Bight: A Lagrangian study in an eddy-resolving ocean model, J. Geophys. Res. Oceans, 121, 1626–1639, https://doi.org/10.1002/2015JC011486, 2016.

Yoshida, K., and Kidokoro, T.: A subtropical countercurrent II: A prediction of eastward flows at lower subtropical latitudes, J. Oceanogr. Soc. Japan, 23(5), 231–246, 1967.

Yu, L., Jin, X. and Weller, R. A.: Annual, seasonal, and interannual variability of air-sea heat fluxes in the Indian Ocean, in Journal of Climate., 2007.

3252   Yu, L.: Sea Surface Exchanges of Momentum, Heat, and Fresh Water Determined by Satellite Remote Sensing, in

3253   Encyclopedia of Ocean Sciences, 1, pp. 15–23, Elsevier, https://doi.org/

3254